博士論文

Quantum information-theoretic study of complexity in chaotic many-body dynamics

(多体カオスのダイナミクスにおける複雑性の量子情報理論的研究)

金子 和哉

Abstract

Bridging the gap between macroscopic thermodynamics and microscopic quantum dynamics is one of the most fundamental problems in statistical physics, dating back to von Neumann. Recently, nonequilibrium dynamics of isolated quantum many-body systems have been observed in highly controllable quantum systems, such as ultracold atoms, superconducting qubits, and trapped ions. Both theoretical and experimental studies have revealed that isolated many-body systems thermalize under the unitary time evolution. These studies triggered progress in understanding mechanisms of thermalization. A widely accepted mechanism of thermalization is based on a conjecture called the eigenstate thermalization hypothesis (ETH). The ETH is a counterpart of ergodicity in quantum systems and states that all the energy eigenstates of a chaotic Hamiltonian are indistinguishable from the thermal states. The ETH has been numerically confirmed for many nonintegrable systems, while it is violated in integrable systems and localized systems.

Another essential concept of thermodynamics is the second law, which is formulated in several ways, such as the entropy increase and the impossibility of the perpetual motion of the second kind. The second law in quantum systems has been studied based on quantum information theory, while it has not yet been much studied in light of chaos of many-body dynamics. Correspondingly, our understanding of the second law in quantum systems is not as established as that of thermalization for isolated many-body quantum systems.

More recently, high-energy physics has provided new insights into quantum chaotic dynamics. In the context of the black hole information problem, the notion of information scrambling is proposed as a new characterization of quantum many-body chaos. Information scrambling represents the spreading of localized quantum information over the entire system. Moreover, information scrambling is closely related to quantum pseudorandomness, which is an important resource of quantum information tasks.

The present thesis is devoted to two issues regarding chaotic quantum many-body dynamics. First, we consider the second law at the level of individual energy eigenstates, which is a crucial ingredient of thermodynamics of isolated quantum many-body systems. Specifically, we investigate both numerically and analytically the possibility of work extraction by

cyclic Hamiltonian dynamics. We propose a second-law analog of the ETH from numerical results, which we name the eigenstate second law, and rigorously prove a weaker version of the eigenstate second law. Second, we focus on another aspect of chaotic quantum systems beyond conventional thermodynamics, especially the universal structure of entanglement and information scrambling. We propose a generalization of the ETH to characterize the higher-order complexity of quantum chaos at the level of a single energy eigenstate. In addition, we attempt to bridge the gap between chaotic many-body dynamics and intrinsically random unitary dynamics by introducing a new quantum information-theoretic concept regarding partial pseudorandomness.

The first issue of this thesis is the possibility of work extraction from quantum many-body systems. The concept of work is crucially important in thermodynamics, as one cannot extract positive work from a single heat bath by any cyclic operation, which is manifestation of the second law in the version of the Kelvin-Planck statement. Establishing the second law from microscopic dynamics is one of the central issues in statistical physics. Motivated by researches on designing quantum heat engines, this problem has been actively investigated for isolated quantum systems. Theoretical progress also has been made, and, for example, an important notion called passivity has been introduced. For a given Hamiltonian, a quantum state is said to be passive, if its energy cannot be decreased by any cyclic unitary operations. It has been proved that the Gibbs states are exactly passive, while pure states are not passive in general. However, such characterization of passive states is not enough to conclude that the second law is already established based on quantum mechanics, especially given that a pure state also describes thermal equilibrium.

Since one has only limited controllability of large-scale systems, a natural question is whether one can extract positive work by a limited class of unitary operations. In this thesis, we numerically investigate this question and show that integrability plays an important role. We numerically calculate the extracted work from individual energy eigenstates by quench protocols of the mixed-field Ising model with changing its integrability. We show that one cannot extract positive work from any energy eigenstate, if the initial Hamiltonian or the protocol has nonintegrability. This result brings us to an analogy between thermalization and the second law. We thus conjecture the eigenstate second law, which states that all the energy eigenstates satisfy the second law under experimentally realistic quench protocols. In fact, we show that the eigenstate second law follows from the ETH for a nonlocal operator corresponding to the energy of the final state. On the other hand, we numerically show the violation of the eigenstate second law in an integrable system, which is the counterpart of the violation of the ETH in integrable systems. In addition, we prove that for arbitrary fixed unitary operation, one cannot extract positive work from almost all energy eigenstates. This claim is regarded as a weaker version of the eigenstate second law and holds even in integrable

systems as long as the Boltzmann's formula is true. This weaker version of the second law is analogous to the weaker version of the ETH.

The second issue of this thesis is how to characterize complexity and randomness of quantum chaotic dynamics. The complexity of a quantum state increases in time until it saturates at the maximum value. Thermalization and information scrambling are related to the growth of complexity under Hamiltonian time evolutions. Characterization of the complexity of chaotic many-body dynamics is expected to provide a unified description of thermalization and information scrambling. Moreover, quantum chaos has attracted attention in high-energy physics and quantum information theory. In the context of the blackhole information paradox, the out-of-time-ordered correlator (OTOC) has been proposed as an indicator of information scrambling, and the decay of the OTOC characterizes quantum chaos. Furthermore, it has been argued that blackholes are quantum chaotic and the most powerful information scrambler. These researches suggest that quantum chaotic dynamics are closely related to random unitary dynamics, which is well known as a good scrambler. Random unitaries are also important in quantum information theory, while we need a large number of quantum gates to realize exact random unitaries. This fact has brought up the research of quantum pseudorandomness that approximates random unitaries. Quantum pseudorandomness is formulated as a unitary k-design, which simulates the kth moment of random unitaries. However, the relationship between chaotic Hamiltonian dynamics and unitary k-designs has not been fully addressed in previous studies.

Combining the notions of the ETH and unitary k-designs, we introduce a higher-order generalization of the ETH, named the k-ETH ($k = 1, 2, \dots$). The lowest order ETH (i.e., the 1-ETH) reproduces the conventional ETH. The higher-order ETH is its higher-order counterpart and characterizes the higher-order randomness. The k-ETH is formulated by considering the k-replicated system in the same way as the definition of unitary k-designs. The k-ETH ($k \geq 2$) also implies that the kth Renyi entanglement entropy of an energy eigenstate follows a universal system-size dependence, called the Page curve. The volume law of the eigenstate entanglement can be explained by the conventional ETH, while the Page correction intrinsically originates from the higher-order ETH. In addition, we numerically verified that the 2-ETH approximately holds for a nonintegrable spin model, but does not hold for an integrable model.

In order to clarify the connection between the k-ETH and unitary k-designs, we introduce a new information-theoretic concept named a partial unitary k-design (PU k-design). A PU k-design is an approximation of random unitaries in which one focuses only on a limited number of observables. A conventional unitary k-design is a special case of a PU k-design where all the observables are accessible. The k-ETH is also a special case of a PU k-design where the ensemble is given by the random-time sampling of Hamiltonian time evolution operators. On the other hand, we found that its relationship to information scrambling is not straightforward

as follows. The exact scrambling, (i.e., the exact agreement of the late-time OTOC with its random-unitary average), requires the exact 2-ETH, but the approximate decay of the OTOC in the thermodynamic limit follows only from the approximate 1-ETH.

Our results shed new light on the foundation of statistical mechanics and characterization of chaos in quantum many-body systems. Moreover, we expect that our approach would contribute not only to statistical mechanics but also to various fields related to quantum many-body dynamics, including high-energy physics and quantum information theory. Investigating the possibility of experimental verification of our results with quantum simulators is an important future issue.

Publication list

This thesis is based on the following two publications:

1. K. Kaneko, E. Iyoda, and T. Sagawa, *Work extraction from a single energy eigenstate*, Phys. Rev. E **99**, 032128 (2019).
2. K. Kaneko, E. Iyoda, and T. Sagawa, *Characterizing complexity of many-body quantum dynamics by higher-order eigenstate thermalization*, arXiv:1911.10755.

The following two publications are not directly related to this thesis.

3. E. Iyoda, K. Kaneko, and T. Sagawa, *Fluctuation theorem for many-body pure quantum states*, Phys.Rev.Lett. **119**, 100601 (2017).
4. K. Kaneko, E. Iyoda, and T. Sagawa, *Saturation of entropy production in quantum many-body systems*, Phys. Rev. E **96**, 062148 (2017).

Contents

Part I Review

Chapter 1

Introduction

As an introduction, we give an overview of three different backgrounds of our studies. In Sec. 1.1, we consider a longstanding problem in statistical physics dates back to Boltzmann: how statistical mechanics emerges in isolated systems. In Sec. 1.2, we introduce the notion of quantum chaos, which is not only important in the context of the foundation of statistical mechanics but also has recently attracted interest in high-energy physics. In Sec. 1.3, we provide an overview of recent experiments in isolated quantum systems, which has shed new light on the foundation of statistical mechanics. In Sec. 1.4, we give a summary of our results.

1.1 Foundations of statistical mechanics

Thermodynamics is a phenomenology of macroscopic thermal behaviors, while statistical mechanics predicts thermodynamic properties from microscopic mechanics, as originally established by Maxwell, Boltzmann, and Gibbs in the nineteenth century. The gap between the macroscopic theory at the phenomenology level and its microscopic foundation is the central issue of this thesis.

1.1.1 Principles of statistical mechanics

Statistical mechanics consists of the following two principles [1]. One is *the principle of equal probability*, which states that the thermal equilibrium value of a mechanical quantity is given by the average in the microcanonical ensemble. The microcanonical ensemble is a mixed

state in which all the microstates in a given energy shell appear with equal probabilities. We emphasize that the principle of equal probability is a working hypothesis to calculate the thermal value. A real microstate of the thermal equilibrium is not necessarily given by the microcanonical ensemble even in thermal equilibrium from the macroscopic point of view.

The second principle is *the Boltzmann's formula* stating that the thermodynamics entropy $S(E)$ is given by

$$S(E) = k_{\mathrm{B}} \log W(E), \tag{1.1}$$

where $W(E)$ is the number of microstates in the system in the energy shell around energy E, and k_{B} is the Boltzmann's constant. Because $W(E)$ grows exponentially with the system size, $S(E)$ becomes an extensive quantity. The Boltzmann's formula connects a microscopic quantity to a macroscopic thermodynamic quantity, the entropy, which cannot be represented as any mechanical quantity.

Although there is no doubt on the empirical validity of the above two principles, their foundation from microscopic physics has not yet been established. In the early days, Boltzmann addressed this problem based on classical mechanics while, as is well known, he did not succeed in establishing the connection between statistical mechanics and classical mechanics. After that, many researchers also challenged this problem. In particular, von Neumann [2, 3] investigated the relaxation to thermal equilibrium on the basis of quantum mechanics and an idea that is nowadays known as typicality. While his seminal study had been not fully appreciated during the last century, today, his work attracts renewed attention because it is now realized that many important ideas were already there in his papers.

1.1.2 Ergodicity and typicality

There is a long history of studies regarding the principle of equal probability. A most famous attempt addressing this issue is an approach from *ergodicity* [4]. Ergodicity is a property of classical systems stating that a dynamical trajectory uniformly covers a surface of constant energy in the phase space. This immediately implies that the long-time average equals the microcanonical average. Thus, many researchers have considered that the principle of equal probability is justified if the system satisfies ergodicity. Nonintegrable systems, such as the Sinai's billiard [5], are known to satisfy ergodicity, while integrable systems never show ergodicity because conserved quantities restrict a trajectory on a small subspace. Even in nonintegrable systems, there are some counterexamples of ergodicity[*1]. For example, in 1955, Fermi, Pasta, and Ulam [7] performed a numerical simulation of one-dimensional anharmonic oscillators, and found that ergodicity is violated in this model.

[*1] As for classical Hamiltonian dynamical systems, almost all systems are neither integrable nor ergodic [6].

A concept of *typicality* [8–11] gives another route to the understanding of the foundation of statistical mechanics. The typicality of microstates argues that almost all microstates are indistinguishable from the thermal equilibrium as long as one observes a restricted class of physical quantities such as few-body observables like the total momentum and the total magnetization. In this picture, the principle of equal probability is regarded as a prescription to obtain common properties of typical microstates.

Some researchers argue that typicality is more reasonable than ergodicity as a foundation of statistical mechanics. However, it is far from obvious whether typicality really accounts for the thermalization mechanism, because the typicality argument apparently applies to non-thermalizing systems as well. We note that such non-thermalizing systems have recently been realized experimentally, where one can observe the breakdown of thermalization in real laboratories. To achieve a complete understanding of thermalization, we need to consider more detailed properties of the many-body system, such as the nonintegrability and chaos, rather than simply relying on the typicality argument. That is to say, the foundation of statistical mechanics is still a fundamental unsolved question of modern physics.

1.1.3 Eigenstate thermalization hypothesis (ETH)

In this thesis, we focus on isolated quantum systems, in which the time evolution is described by the Schrödinger equation:

$$i\frac{d}{dt}\left|\psi(t)\right\rangle = H\left|\psi(t)\right\rangle . \tag{1.2}$$

Throughout this thesis, we set $\hbar = 1$. If we denote an energy eigenstate of H by $|E_i\rangle$ $(i = 1, \dots, d)$ and the corresponding eigenenergy by E_i, the solution of the Schrödinger equation (1.2) is given by

$$\left|\psi(t)\right\rangle = \sum_{i=1}^{d} c_i e^{-iE_i t}\left|E_i\right\rangle , \tag{1.3}$$

where $c_i \in \mathbb{C}$ is determined from the initial condition. Equation (1.3) implies that a pure state remains pure during the time evolution, and the steady state cannot be described by statistical ensembles that are mixed states. Thus, a natural question about thermalization is whether the expectation value $\langle\psi(t)|O|\psi(t)\rangle$ approximately equals the microcanonical average $\langle O\rangle_{\mathrm{MC}}$ for a given observable O or a restricted class of observables such as few-body observables. If $\langle\psi(t)|O|\psi(t)\rangle \approx \langle O\rangle_{\mathrm{MC}}$ holds for large t, we can say that O approaches the thermal equilibrium value.

Recently, quantum many-body systems isolated from environments have been realized by real experiments [12–17]. In fact, as we review in Sec. 1.3 in more detail, thermalization (i.e., the approach to thermal equilibrium) under the unitary time evolution has been observed in

recent experiments [18–22]. These experimental systems are nonintegrable systems, which do not have an extensive number of local conserved quantities.

Moreover, many numerical simulations have demonstrated that thermalization of few-body observables occurs in generic nonintegrable systems, such as the Bose-Hubbard model [23–27] and the hard-core boson models [28–31]. These numerical studies have investigated relaxation dynamics after a quench: The system is initially prepared in a product state or the ground state of the initial Hamiltonian. Then, the parameters of the Hamiltonian, such as the magnetic field and the depth of optical lattice, are suddenly quenched to different values. Because the initial state is not an eigenstate of the post-quench Hamiltonian, the initial state is not stationary and evolves according to the post-quench Hamiltonian. The numerical studies have focused on the time-dependence of the expectation values of few-body observables and have reported that they relax to stationary values near the thermal average. Moreover, from the finite-size scaling, it has been argued that the deviation between the stationary value and the microcanonical average converges to zero in the thermodynamic limit.

Let us briefly see the mechanism of thermalization in nonintegrable systems. We divide $\langle\psi(t)|O|\psi(t)\rangle$ into the time-independent part and the time-dependent part:

$$\langle\psi(t)|O|\psi(t)\rangle = \sum_{i=1}^{d} |c_i|^2 \langle E_i|O|E_i\rangle + \sum_{i\neq j} e^{i(E_i-E_j)t} c_i^* c_j \langle E_i|O|E_j\rangle . \tag{1.4}$$

We naively expect that the second term on the right-hand side is negligible for large t because it rapidly oscillates. As shown in Chapter 2, this naive expectation can be mathematically justified for specific quantum states. Thus, for achieving $\langle\psi(t)|O|\psi(t)\rangle \approx \langle O\rangle_{\mathrm{MC}}$, it is sufficient that

$$\langle E_i|O|E_i\rangle \approx \langle O\rangle_{\mathrm{MC}} \tag{1.5}$$

holds for all the energy eigenstates. Here, the microcanonical average $\langle O\rangle_{\mathrm{MC}}$ is calculated as the uniform average over the energy eigenstate around energy E_i. Equation (1.5) implies that the energy eigenstate $|E_i\rangle$ looks thermal as long as one focuses on O. This conjecture is called *the eigenstate thermalization hypothesis (ETH)*, which was first proposed by Srednicki [32–34] in the 1990s. If the ETH is true, the effective stationary value of $\langle\psi(t)|O|\psi(t)\rangle$ equals the microcanonical average for any initial state in the energy shell. Thus, the ETH can be regarded as a quantum counterpart of the ergodic hypothesis and is believed to be crucial for the thermalization in isolated quantum systems [28, 35].

As ergodicity is related to classical chaos, the ETH is also related to quantum chaos. In fact, Srednicki's studies [32–34] are based on Berry's conjecture [36] in quantum chaos, which states that energy eigenstates of a quantum particle system corresponding a classical chaotic system consist of random superpositions of plane waves. Berry's conjecture connects classical chaos or ergodicity to properties of energy eigenstates of quantum systems, and the ETH is an

extension of Berry's conjecture to generic quantum systems, including spin systems, atomic and atomic-molecular-and-optical (AMO) systems.

We note that essentially the same arguments as the ETH have been considered in earlier works [37–41]. We review the ETH in more detail in Chapter 2.

1.2 Quantum chaos

1.2.1 Classical chaos

Chaos is an important concept in the theory of dynamical systems [42]. The term of chaos was introduced by Li and Yorke [43] in 1975. Roughly speaking, chaos is a *pseudorandom behavior* arising from deterministic dynamics [44]. Although there is no accepted rigorous and general definition of chaos, many researchers believe that the exponential sensitivity to infinitesimal perturbations, so-called *the butterfly effect*, is an important feature of classical chaos. In this thesis, we adopt the rough definition of chaos by the butterfly effect and do not go deeply into the mathematical arguments.

To formulate chaos, we consider a classical system of N particles, and denote their positions by $\boldsymbol{x} := (x_1, \dots, x_N)$ and their momenta by $\boldsymbol{p} := (p_1, \dots, p_N)$. A classical state is described by a point of the phase space, denoted as $\boldsymbol{X} := (\boldsymbol{x}, \boldsymbol{p})$. We consider a single trajectory $\boldsymbol{X}(t)$ with an initial condition $\boldsymbol{X}(0) = \boldsymbol{X}_0$. A small perturbation to the initial condition $\boldsymbol{X}_0 \to \delta\boldsymbol{X}_0$ gives a new trajectory $\boldsymbol{X}(t) + \delta\boldsymbol{X}(t)$. Here, $\delta\boldsymbol{X}(t)$ is the deviation between the old trajectory and the new trajectory. If the system is chaotic, the deviation induced by the initial perturbation grows exponentially in time. This is represented as

$$\frac{\|\delta\boldsymbol{X}(t)\|}{\|\delta\boldsymbol{X}(0)\|} \propto e^{\lambda_{\mathrm{L}} t}, \tag{1.6}$$

where $\|\cdot\|$ is the Euclidean norm, and λ_{L} is a real constant called the Lyapunov exponent. The Lyapunov exponent characterizes the initial sensitivity to perturbation, and chaos is defined as the system which has a positive Lyapunov exponent. We note that this definition of chaos by the positivity of λ_{L} is not a fully rigorous definition of chaos; see Ref. [42] for more rigorous definitions.

1.2.2 Chaos in quantum systems

Let us move on to quantum systems. In the sense of the classical dynamical systems theory, any quantum system is said to be integrable and thus not chaotic, because the Schröringer equation (1.2) is just linear. In fact, $\langle E_1|\psi(t)\rangle, \dots, \langle E_d|\psi(t)\rangle$ do not depend on time, and thus they are conserved quantities of the Schrödinger equation. The existence of an extensive number of conserved quantities implies that the system is (Liouville) integrable. In other

words, small perturbations do not grow in quantum systems. This is also seen from the fact that the unitary dynamics $e^{-iHt/\hbar}$ preserves the norm of a vector, i.e.,

$$\frac{\|\delta\,|\psi(t)\rangle\,\|}{\|\delta\,|\psi(0)\rangle\,\|} = 1, \tag{1.7}$$

for all t. This fact raises a question: what is a quantum counterpart of classical chaos?

Although there is no straightforward extension of chaos to quantum systems as seen above, some "chaotic" properties have been discovered in quantum systems whose classical counterparts are chaotic [45, 46]. As mentioned before, Berry's conjecture [36] is one of the crucial signatures of quantum chaos. The ETH is an extension of Berry's conjecture for many-body systems with no direct classical counterpart and thus is a characteristic of quantum chaos.

Another important conjecture in quantum chaos is the Bohigas-Gianonni-Schimt (BGS) conjecture [47], which represents the relationship between quantum chaos and random matrix theory [48]. Let us focus on the unfolded energy spectrum $\{\lambda_i\}_{i=1}^d$, which is obtained by rescaling the energy spectrum $\{E_i\}_{i=1}^d$ so that mean level spacing is unity. We define a level-spacing distribution $P(s)$ as a distribution of spacings of neighboring energy levels, i.e., $s = \lambda_{i+1} - \lambda_i$. The BGS conjecture states that a level-spacing distribution for a chaotic quantum system shows a distribution predicted by the Wigner-Dyson random matrix ensemble. On the other hand, integrable systems do not obey the Wigner-Dyson distribution. In general, the level-spacing distribution in the integrable case obeys the Poisson distribution, which is known as the Berry-Tabor conjecture [49].

1.2.3 New perspective on quantum chaos

Recently, quantum chaos has been extensively investigated in the context of blackhole physics and holographic duality [50, 51]. Progress in studies of the black hole information problem based on quantum information theory [52–55] has led to another characterization of quantum chaos called *information scrambling*. Information scrambling indicates a spreading of localized quantum information. We expect that localized information spreads over the entire system as time increases, and becomes more nonlocal by chaotic dynamics than by nonchaotic dynamics. In fact, several numerical studies [56–59] have shown that information is almost maximally delocalized at late times in nonintegrable systems but not in integrable systems. The aforementioned features of quantum chaos, such as the ETH and the BGS conjecture, are related to properties of a Hamiltonian, whereas information scrambling focuses on a dynamical and information-theoretic aspect of quantum chaos.

There are several measures quantifying delocalized information. Here, we look at scrambling in a spin system through the growth of the number of involved elementary operators [50]. We consider the dynamics of a simple operator A acting on a single site in the Heisenberg picture. The time-evolved operator at time t is given by $A(t) := e^{iHt}Ae^{-iHt}$. Even if $A(0) = A$ is

local, $A(t)$ is not local for $t \neq 0$, which can be seen as follows. By expanding e^{-iHt} in t, we have

$$A(t) = \sum_{m=0}^{\infty} \frac{(it)^m}{m!}[H, [H, \dots, [H, A] \dots]], \tag{1.8}$$

where $[\cdot, \cdot]$ represents the commutator. If H is represented as a summation of n-body operators, $[H, A]$ becomes an n-body operator. In general, a deeply nested commutator $[H, [H, \dots, [H, A] \dots]]$ contains many-body operators acting nontrivially on all sites. At early times, such higher-order terms in the right-hand side of Eq. (1.8) are negligible. However, the higher-order terms become more dominant as time increases. This implies that $A(t)$ itself is a nonlocal and many-body operator.

We can quantify the nonlocality of $A(t)$ by considering the squared commutator with another local operator B:

$$C_{A,B}(t) := d^{-1}\mathrm{Tr}([A(t), B]^\dagger [A(t), B]). \tag{1.9}$$

If A does not have overlap with B, i.e., $[A, B] = 0$, the squared commutator $C_{A,B}(t)$ vanishes at $t = 0$. On the other hand, if $A(t)$ becomes nonlocal, $C_{A,B}(t)$ takes a nonzero value. In a typical case, A and B are set to Pauli operators. In that case, the squared commutator can be represented as

$$C_{A,B}(t) = 2 - 2\mathrm{Re}(F_{A,B}(t)) \tag{1.10}$$

with $F_{A,B}(t) := d^{-1}\mathrm{Tr}[A(t)BA(t)B]$. The four-point correlation function $F_{A,B}(t)$ is called the out-of-time-ordered correlator (OTOC), because it has the unusual time-ordering. The OTOC was first investigated by Larkin and Ovchinnikov [60] in a study of disordered superconductors and has received attention again as a measure of scrambling and also a quantum version of the butterfly effect [50, 51]. In particular, it has been conjectured that the rate of exponential decay of the OTOC is a quantum counterpart of the Lyapunov exponent, and the maximally chaotic quantum systems are related to gravity theories by the holographic duality [61, 62]. We review information scrambling and the OTOC in more detail in Chapter 2.

1.3 Experiments of isolated quantum systems

As mentioned above, the recent interest in nonequilibrium quantum dynamics has been motivated by experimental realizations of isolated quantum many-body systems. The development of experimental technologies has provided highly controllable quantum systems, such as ultracold atoms [12, 13], trapped ions [14, 15], and superconducting qubits [16, 17, 63]. These artificial quantum systems allow one to study various quantum many-body phenomena experimentally.

As a remarkable example, we review an experiment of thermalization by Trotzky *et al.* [18]. They observed relaxation to thermal equilibrium under unitary time evolution by using ultracold atoms. They trapped ^{87}Rb atoms in a one-dimensional optical lattice, which is described by the Bose-Hubbard model with a harmonic potential:

$$H_{\mathrm{BH}} := -J\sum_j (b_j^\dagger b_{j+1} + \mathrm{h.c.}) + \frac{U}{2}\sum_j n_j(n_j-1) + \frac{K}{2}\sum_j j^2 n_j, \tag{1.11}$$

where $b_j^\dagger$ and b_j are the creation and annihilation bosonic operators at site j, and $n_j := b_j^\dagger b_j$ is the particle-number operator. They initially prepared a nonequilibrium state where every even site is occupied by an atom, while every odd site is empty, giving the initial state $|\psi(0)\rangle = |0,1,0,1,\ldots\rangle$. Then, a quench is performed by changing the depth of the potential, and the system evolves following the Schrödinger equation. By changing the depth of the potential again, they measured the local density of atoms. They reported that the local density n_{odd} in the odd sites fluctuates in time, and eventually relaxes to a stationary value. In particular, the stationary value is $n_{\mathrm{odd}} \approx 0.5$, which implies that the system is in thermal equilibrium. They also performed numerical simulations by using the time-dependent density-matrix renormalization group (t-DMRG) [64], and confirmed that the experimental results agree with simulations of unitary dynamics generated by the Bose-Hubbard Hamiltonian (1.11). From this consistency, their experiment is regarded as a direct demonstration of thermalization in an isolated quantum system.

Non-ergodic quantum systems, which do not exhibit thermalization, have also been realized in experimental systems. For example, Kinoshita *et al.* [65] performed a cold-atom experiment showing the non-thermalizing behavior in a near-integrable system, known as the quantum Newton's cradle. A classical Newton's cradle is a system with a series of suspended balls and is often used to demonstrate the conservation of momentum. They made a quantum mechanical Newton's cradle consisting of around 40 to 250 ^{87}Rb atoms. The atoms are trapped in an anharmonic potential, and they measured the momentum distribution. They reported that the momentum distribution relaxes to a stationary distribution, but does not equal the thermal distribution. This is because their system is approximated by the integrable Lieb-Liniger model [66], and an integrable system never thermalizes because of the presence of local conserved quantities.

1.4 Organization of this thesis and the summary of the results

This thesis is organized as follows. Chapters 2, 3, and 4 are devoted to a review of fundamental concepts related to our study. In Chapters 5, 6, and 7, we describe our main results.

In Chapter 2, we review how thermalization can be formulated in quantum mechanics and how the ETH explains thermalization of isolated quantum systems. We also review the entan-

glement structure of random thermal pure states. In Chapter 3, we investigate the possibility of work extraction from a quantum state and introduce the concept of passivity, which is related to our study in Chapter 5. In Chapter 4, we review the details of information scrambling and the OTOC. Moreover, we introduce unitary k-designs, which describes pseudorandom unitary dynamics and gives an information-theoretic meaning of the OTOC. These concepts are related to our second study discussed in Chapters 6 and 7.

In Chapter 5, we address our first question: Is it possible to extract work from a single energy eigenstate of a quantum many-body system? This question is closely related to the validity of the second law of thermodynamics for individual eigenstates and the applicability of conventional thermodynamics and statistical mechanics for quantum many-body systems. As a reasonable analogy to the ETH, we expect that the second law is valid at the level of a single energy eigenstate. To confirm this expectation, we calculate the average work extracted from individual energy eigenstates by using numerical exact diagonalization and show that work extraction is impossible from *any* energy eigenstate of nonintegrable systems. This result brings us to a conjecture, named *the eigenstate second law*, stating that all the energy eigenstates satisfy the second law. Our numerical result implies that the eigenstate second law is true in nonintegrable systems, but not in integrable systems. We analytically show that these results can be derived from the ETH for a nonlocal operator describing the final energy after a quench. To complement our numerical result, we prove the weaker version of the eigenstate second law stating that work extraction is impossible from *most* energy eigenstates.

Chapter 6 is devoted to the second question: is it possible to explain various symptoms of quantum many-body chaos in a unified manner in terms of the ETH? We address this question by proposing the higher-order extension of the ETH named *the k-ETH*, where an integer k represents the order of the randomness. Roughly speaking, the k-ETH is the most natural extension of the ETH to operators acting on the k-replicated system. We show that the lowest-order ETH (1-ETH) reproduces the conventional ETH, and the second-order ETH (2-ETH) is related to the steady value of the OTOC, i.e., information scrambling. In addition, the k-ETH ($k \geq 2$) is related to the entanglement entropy of individual energy eigenstates. If the k-ETH is true, the kth Renyi entanglement entropy follows a universal system-size dependence similar to that of thermal pure states. Moreover, we numerically verified that the approximate 2-ETH for operators related to the OTOC and the entanglement entropy holds for a nonintegrable spin model, but does not hold for an integrable model.

In Chapter 7, we introduce a new information-theoretic notion of quantum pseudorandomness named *partial untiary k-designs* (PU k-designs) to bridge the k-ETH and unitary k-designs. Roughly speaking, PU k-designs are pseudo-unitary k-designs, in which one focuses on a limited number of operators of the k-replicated system, but not on all the operators. The k-ETH implies that an ensemble given by the random-time sampling of corresponding

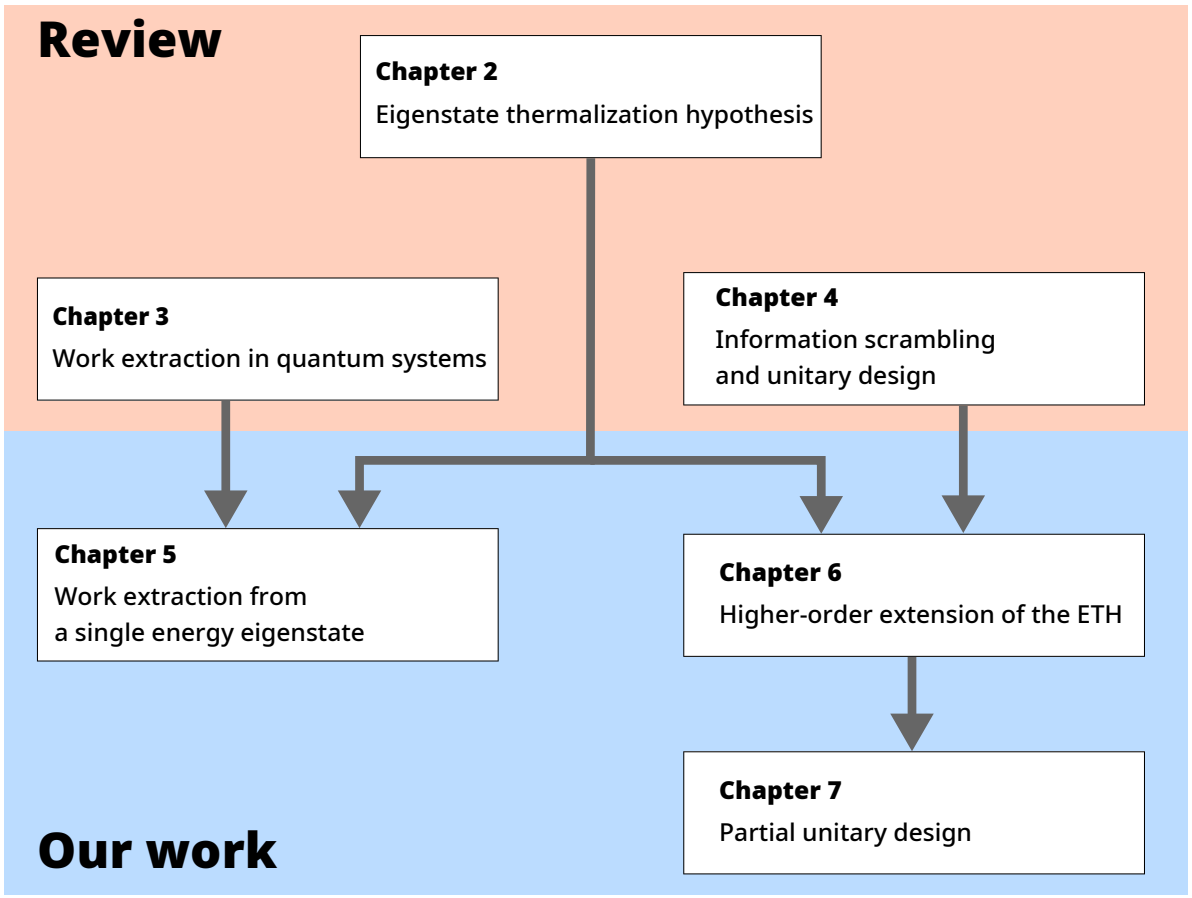

Fig. 1.1 The structure of this thesis.

time-evolution operators is a PU k-design. To comprehend PU k-designs, we provide special examples.

In Chapter 8, we summarize this thesis and give some remarks on future prospects. Figure 1.1 shows the relationship between the chapters of this thesis.

Chapter 2

Eigenstate thermalization hypothesis

In this chapter, we review the ETH and its relevance to thermalization. The ETH is a widely accepted mechanism of thermalization in isolated quantum systems and states that all the energy eigenstates represent thermal equilibrium. We first consider the definition of thermalization and introduce the ETH in Sec. 2.1. Then, we explain the technical details of the ETH in Sec. 2.2. The weaker version of the ETH is introduced in Sec. 2.3. We review recent numerical studies in Sec. 2.4. In Sec. 2.5, we focus on the entanglement entropy of thermal pure states.

2.1 Thermalization in isolated quantum system

First of all, we consider the definition of thermalization in isolated quantum systems and some theoretical results.

2.1.1 Definition of thermalization

Let us consider an isolated quantum system and denote its Hilbert space by $\mathcal{H}$. We assume that the dimension D of $\mathcal{H}$ is finite. We denote the Hamiltonian of the system by H. Its eigenenergy and eigenstate are denoted by E_i and $|E_i\rangle$, respectively. A typical example of the system is a local-interacting spin model on a finite-dimensional lattice, such as the Ising and XXZ models. We prepare an arbitrary pure state $|\psi_0\rangle$ as the initial state. $|\psi_0\rangle$ is often set as a product state or a ground state of some Hamiltonian both in numerical simulations [23, 28, 67, 68] and experiments [18, 20]. In a quench experiment, H corresponds to a post-quench

Hamiltonian. Then, the system evolves according to a unitary operator e^{-iHt}, and the state at time t is written as

$$|\psi(t)\rangle = e^{-iHt}\,|\psi_0\rangle = \sum_{i=1}^{D} e^{-iE_i t} c_i\,|E_i\rangle\,, \tag{2.1}$$

where we set $\hbar = 1$ and $c_i := \langle E_i|\psi_0\rangle$. As is seen from Eq. (2.1), $|\psi(t)\rangle$ is a quasi-periodic function of time, and it goes back to the initial state with an arbitrarily small error at infinitely many times during the time evolution. This phenomenon is known as recurrence. The occurrence of many recurrences in classical Hamiltonian dynamics was proved by Poincaré, and its quantum counterpart was established in Refs. [69, 70]. Although the recurrence time typically grows double-exponentially with respect to the system size, we need a careful treatment of recurrences in the definition of thermalization under unitary time evolution.

Besides, the limited accessibility to quantum many-body systems is a crucial point to understand thermalization. Since the quantum state itself is always changing with time, one can in principle track the time dependence of the state during the entire time evolution. However, the full tomography of quantum states requires to measure a large number of observables, including an exponentially large number of many-body observables. On the other hand, in practice we can only access few-body observables, which is a small subset of the whole set of observables of a many-body system. If one observes only a small number of observables, different quantum states might look the same, because these states might give almost the same expectation values as for measured observables. Correspondingly, as will be seen in the following, thermalization can occur under unitary dynamics as long as one measures a handful of observables.

Based on the above argument, we focus on an arbitrary fixed observable O and give a (non-rigorous) definition of thermalization for O (see Ref. [9, 71, 72] for more rigorous definitions). We say that O thermalizes starting from the initial state $|\psi_0\rangle$, if there exists a thermal equilibrium value $O_{\rm th}$ such that

$$\langle O(t)\rangle := \langle\psi(t)|O|\psi(t)\rangle \approx O_{\rm th} \tag{2.2}$$

holds for almost all $t \in (0, \infty)$. Strictly speaking, there are some ambiguities in the above definition, such as thermal equilibrium value and almost all. While the mathematically rigorous treatment of these terms is a difficult task, their physical meanings are as follows. First, $O_{\rm th}$ can be calculated by averaging in the microcanonical ensemble. If we restrict ourselves to the purely phenomenological level without relying on statistical mechanics, we can expect that $O_{\rm th}$ is determined only by some macroscopic parameters of the initial state (e.g., the average energy and the particle number) for systems consistent with thermodynamics. The term almost all aims at excluding the relaxation process at early times and recurrence times during which $\langle O(t)\rangle$ deviates from the thermal equilibrium value.

In this thesis, we do not go into the details of timescales of thermalization. To prove that relaxation time is not extremely long under physically reasonable assumptions is an important issue to establish the foundation of thermodynamics. This is still a challenging problem because the relaxation time strongly depends on the choice of observables and the initial state.

We divide the definition of thermalization (2.2) into the two parts for the convenience of the following investigation. The first part is the relaxation of the expected value to a certain stationary value O_∞:

$$\langle O(t)\rangle \approx O_\infty \quad \text{for almost all } t \in (0,\infty). \tag{2.3}$$

At this stage, we do note care about weather O_∞ equals the thermal equilibrium value or not. This part is called *equilibration*.

The second part is the equivalence of the stationary value and the thermal equilibrium value:

$$O_\infty \approx O_{\rm th}. \tag{2.4}$$

In general, the left-hand side depends on the details of the initial state, while the right-hand side is expected to depend only on macroscopic parameters. This cannot be proved only from quantum mechanics, because Eq. (2.4) is violated for several types of systems (e.g., integrable systems, localized systems, quantum many-body scar). Thus, we need some additional assumptions such as the nonintegrability of the Hamiltonian to justify Eq. (2.4).

2.1.2 Equilibration

We first consider equilibration. As we already mentioned, complete equilibration, implying that all the states approach a unique time-independent state in the limit of $t \to \infty$, is impossible because of recurrences. However, the expectation value of a given observable can relax to the effective stationary value between recurrences. Although this fact was already pointed out in the pioneering works of thermalization [32–34,37–41], more refined results were obtained in this century [73–78].

Here, we review a simple result about equilibration based on the arguments of Reimann [73] and Linden *et al.* [74]. For simplicity, we assume that the Hamiltonian has no degeneracy. This assumption is not essential and can be easily removed [76]. We also denote the matrix elements of O in the energy eigenbasis as $O_{ij} := \langle E_i|O|E_j\rangle$.

We first consider the long-time average of $\langle O(t)\rangle$ represented as $O_\infty := \overline{\langle O(t)\rangle}$, where the overline denotes the long-time average: $\overline{f(t)} := \lim_{\tau\to\infty} \tau^{-1}\int_0^\tau f(t)dt$. We can explicitly calculate

the long-time average as follows:

$$O_\infty = \sum_{i,j} \overline{\left[e^{i(E_i-E_j)t}\right]} c_i^* c_j O_{ij} = \sum_i |c_i|^2 O_{ii}, \tag{2.5}$$

where we used $\overline{\left[e^{i(E_i-E_j)t}\right]} = \delta_{ij}$. Moreover, we introduce the diagonal ensemble by

$$\rho_\infty := \sum_i |c_i|^2 |E_i\rangle \langle E_i| . \tag{2.6}$$

Then, O_∞ is rewritten as the average on the diagonal ensemble: $O_\infty = \mathrm{Tr}[O\rho_\infty]$. The diagonal ensemble is diagonal in the energy eigenbasis and describes the effective stationary state of a quantum system. We emphasize that the diagonal ensemble highly depends on the initial state. Indeed, the number of parameters in the diagonal ensemble equals the dimension of the Hilbert space d, which grows exponentially with the system size. This is contrastive to the microcanonical and Gibbs states, which has only a few parameters. In the next subsection, we investigate under which conditions one can identify the diagonal ensemble with thermal equilibrium.

We can derive an upper bound of the temporal fluctuation of $\langle O(t)\rangle$ around the stationary value. To obtain the bound, he made the following assumption regarding the spectrum of H.

Assumption 1 (Nonresonant condition)**.** *$E_i - E_j = E_k - E_l \neq 0$ if and only if $i = k$ and $j = l$.*

The nonresonant condition does not hold for noninteracting systems, while it is expected to hold in nonintegrable systems. Reimann [73] and Linden *et al.* [74] proved the following bound.

Proposition 1 (Equilibration [73, 74])**.** *Under the nonresonant condition, the temporal fluctuation of O is bounded from above as*

$$\sigma(O)^2 := \overline{\left[\langle O(t)\rangle - O_\infty\right]^2} \leq \frac{\|O\|^2}{D_{\mathrm{eff}}}, \tag{2.7}$$

where $\|O\|$ is the operator norm of O, and D_{eff} is the effective dimension of $|\psi_0\rangle$ defined by

$$D_{\mathrm{eff}} := \frac{1}{\sum_i |c_i|^4}. \tag{2.8}$$

The effective dimension represents the effective number of energy eigenstates contained in the initial state, and is a measure of coherence in the energy eigenbasis. The effective dimension takes the minimum value $D_{\mathrm{eff}} = 1$ for a single energy eigenstate and the maximum value $D_{\mathrm{eff}} = d$ for the uniform superposition of the energy eigenstates : $|\psi_{\max}\rangle := \sum_i |i\rangle / \sqrt{d}$.

When O is a local observable, the operator norm of O does not scale with the system size. Thus, the temporal fluctuation of a local observable vanishes if the effective dimension diverges in the thermodynamic limit.

Proof. From the nonresonant condition, the temporal fluctuation is written as

$$\sigma(O)^2 = \sum_{i \neq j} |c_i|^2 |c_j|^2 |O_{ij}|^2 , \tag{2.9}$$

which is bounded as

$$\begin{aligned} \sigma(O)^2 &\leq \frac{1}{2} \sum_{i \neq j} |c_i|^4 |O_{ij}|^2 + \frac{1}{2} \sum_{i \neq j} |c_j|^4 |O_{ij}|^2 && (2.10) \\ &\leq \sum_{i,j} |c_i|^4 |O_{ij}|^2 && (2.11) \\ &= \sum_{i} |c_i|^4 (O^\dagger O)_{ii} && (2.12) \\ &\leq \frac{\|O\|^2}{D_{\text{eff}}}, && (2.13) \end{aligned}$$

where we used $|c_i|^2 |c_j|^2 \leq (|c_i|^4 + |c_j|^4)/2$ and $(O^\dagger O)_{ii} \leq \left\|O^\dagger O\right\| \leq \|O\|^2$. □

We note that there are several improvements to inequality (2.7) [75–78]. For example, Short and Farrelly [77] have removed the nonresonant condition.

2.1.3 Thermality of stationary values

The foregoing theory of equilibration does not answer whether the diagonal ensemble is thermal or not. We next address this question and derive the explicit condition of the Hamiltonian satisfying $O_\infty \approx O_{\text{th}}$. In the following analysis, we make two additional postulations for the consistency with the phenomenological observation of thermodynamics.

We first assume that the initial state does not have *macroscopic coherence* with respect to the energy eigenbasis. This implies that the initial state has a macroscopically definitive value of the post-quench Hamiltonian, and its energy fluctuation is negligible. This postulation originates from the fact that generating macroscopic superpositions is very difficult. Because the ground states do not have macroscopic coherence in general [79–83], the standard setup of quench experiments satisfies this postulation. Moreover, if the initial state does not have a long-range order, the standard deviation of the the post-quench Hamiltonian is estimated as $\Delta E \sim \sqrt{N}$ [28]. If the above postulation is true, the initial state can be approximated as

$$|\psi_0\rangle \approx |\tilde{\psi}_0\rangle := \sum_{E_i \in I_{E,\Delta E}} c_i |E_i\rangle , \tag{2.14}$$

where $I_{E,\Delta E} := [E - \Delta E, E]$ is the energy shell.

The second postulation is the stability of thermal equilibrium. It is believed that a small perturbation to the initial state changes a microstate, but does not change the macroscopic properties of thermal equilibrium. Let us consider a small perturbation to $|\tilde{\psi}_0\rangle$. The perturbed

state is denoted as $|\tilde{\psi}_0'\rangle := \sum_{E_i \in I_{E,\Delta E}} c_i' |E_i\rangle$, where $c_i' = c_i + \delta c_i$, and δc_i is an infinitesimal complex number. From the normalization condition, δc_i must satisfy $\sum_{E_i \in I_{E,\Delta E}} (c_i \delta c_i^* + c_i^* \delta c_i) = 0$. The stationary value of O for the perturbed state is given by

$$O'_\infty := \sum_{E_i \in I_{E,\Delta E}} |c_i'|^2 O_{ii} = \sum_{E_i \in I_{E,\Delta E}} (|c_{ii}|^2 + c_i \delta c_i^* + c_i^* \delta c_i) O_{ii} + \mathcal{O}(\delta^2). \tag{2.15}$$

From the second postulation, we expect that $O_\infty \approx O'_\infty \approx O_{\rm th}$. We thus have the following two relations:

$$\sum_{E_i \in I_{E,\Delta E}} |c_i|^2 (O_{ii} - O_{\rm th}) \approx 0, \tag{2.16}$$

$$\sum_{E_i \in I_{E,\Delta E}} (c_i \delta c_i^* + c_i^* \delta c_i) O_{ii} \approx 0. \tag{2.17}$$

Since we can choose arbitrary $\{\delta c_i\}$ under the normalization condition, O_{ii} must be independent of i from the second relation. From the first relation, we obtain

$$O_{ii} \approx O_{\rm th} \tag{2.18}$$

for all i. This implies that all the energy eigenstates give almost the same expectation value of O as the thermal value. This condition of the energy eigenstates is called the ETH, as introduced in Sec 1.1. We will explain a more precise statement of the ETH in Sec. 2.2.

We can immediately derive the principle of equal probability from the ETH as follows. The microcanonical ensemble average of O is defined as

$$\langle O \rangle_{\rm MC} := \frac{1}{d_{E,\Delta E}} \sum_{E_i \in I_{E,\Delta E}} O_{ii}, \tag{2.19}$$

where $d_{E,\Delta E}$ represents the number of the energy eigenstates in $I_{E,\Delta E}$. Then, the ETH (2.18) leads

$$\langle O \rangle_{\rm MC} \approx O_{\rm th}, \tag{2.20}$$

which is identical to the principle of equal probability. In summary, the principle of equal probability is derived from the combination of the Schrödinger equation and the two postulates argued above. Hereafter, we totally identify the thermal equilibrium value to the microcanonical average. Thus, the ETH (2.18) is rewritten as

$$O_{ii} \approx \langle O \rangle_{\rm MC}, \tag{2.21}$$

which states that the eigenstate expectation value equals the microcanonical average for all the energy eigenstates.

2.2 Diagonal ETH and off-diagonal ETH

In this section, we consider a more precise statement of the ETH and its generalization to the off-diagonal elements.

2.2.1 Diagonal ETH

The important point for precisely formulating the ETH is to consider the system-size scaling. We denote the number of sites of the lattice by N, and the thermodynamic limit is given by the limit of $N \to \infty$ while keeping the lattice structure. Roughly speaking, the ETH states that $O_{ii} = \langle O \rangle_{\mathrm{MC}}$ holds for all the energy eigenstates in the thermodynamic limit. We now make this statement more rigorous by introducing a measure quantifying the deviation of the eigenstate expectation value from the microcanonical average.

We focus on the following quantity:

$$I(O) := \max_{E_i \in I_{uN,\Delta E}} |O_{ii} - \langle O \rangle_{\mathrm{MC}}| , \tag{2.22}$$

where $I_{uN,\Delta E} := [uN - \Delta E, uN]$, u is the energy density, and ΔE is the width of the energy shell. Here, u and ΔE are the parameters specifying the energy shell and do not depend on N. $I(O)$ is a direct measure quantifying the deviation, and it was also used in numerical studies [84]. By using the above measure, the ETH is formalized as follows. We say that the ETH for O holds (with respect to the energy shell $I_{uN,\Delta E}$) if

$$\lim_{N \to \infty} I(O) = 0. \tag{2.23}$$

This is the precise formulation of Eq. (2.21). We note that Eq. (2.23) is sometimes called the diagonal-ETH to avoid confusion with the off-diagonal ETH. In this thesis, however, we simply say the ETH to refer to the diagonal-ETH (2.23).

Although the mathematical proof of Eq. (2.23) is not known, the ETH is believed to hold in generic nonintegrable systems. In fact, there exists a large amount of numerical evidence that the ETH is true for few-body observables, at least in the middle of the spectrum of nonintegrable systems [28, 35]. We note that nonintegrable systems can have a few conserved quantities, such as the total magnetization and the total number of the particles. For such systems, the ETH is valid only within each sector separated by the conserved quantities. We explain the details of the numerical studies of the ETH in Sec. 2.4.

The ETH does not hold in integrable systems because of the existence of an extensive number of few-body conserved quantities. However, Birol *et al.* [85] has shown that a weaker version of the ETH holds even in integrable systems, which will be discussed in Sec. 2.3.

2.2.2 Off-diagonal ETH

The (diagonal) ETH states that the diagonal matrix elements in the energy shell take almost the same value. Another natural question is whether the off-diagonal matrix elements have some common properties in thermalizing systems. Such universal behavior of the off-diagonal matrix elements is known as the *off-diagonal ETH* [35, 72]. The off-diagonal ETH is not related to the stationary value of an observable, but is related to the fluctuations and correlation functions.

In order to derive the off-diagonal ETH, let us consider the diagonal matrix elements of the square of a local observable O. From the completeness of the energy eigenbasis, we have

$$(O^2)_{ii} = \sum_{j=1}^{D} |O_{ij}|^2 . \tag{2.24}$$

If the diagonal ETH is true for both O and O^2, we have

$$\sum_{j(\neq i)} |O_{ij}|^2 = (O^2)_{ii} - O_{ii}^2 \approx \langle O^2 \rangle_{\mathrm{MC}} - \langle O \rangle_{\mathrm{MC}}^2 . \tag{2.25}$$

The left-hand side of Eq. (2.25) is the summation of the off-diagonal matrix elements of O, and the right-hand side represents the thermal fluctuation of O. It is well known and also rigorously provable that the thermal fluctuation of a local observable vanishes in the thermodynamic limit [86, 87]. Thus, we have

$$\lim_{N\to\infty} |O_{ij}|^2 = 0 \quad \text{for } i \neq j, \tag{2.26}$$

which implies that the off-diagonal matrix elements vanish in the thermodynamic limit. Equation (2.26) is a representation of the off-diagonal ETH.

We can see that the off-diagonal ETH (2.26) ensures that the temporal fluctuation of O vanishes in the thermodynamic limit. The temporal fluctuation of O is bounded from above as

$$\sigma(O)^2 \leq \max_{i\neq j} |O_{ij}|^2 \sum_{i\neq j} |c_i|^2 |c_j|^2 \tag{2.27}$$

$$\leq \max_{i\neq j} |O_{ij}|^2 . \tag{2.28}$$

If the off-diagonal ETH is true, the right-hand side of this inequality converges to zero in the thermodynamic limit. That is, the off-diagonal ETH justifies that equilibration occurs for any initial state, and the large effective dimension is not necessary for equilibration in this case.

2.2.3 Srednicki's ansatz

On the basis of the random matrix theory, Srednicki [33, 34] conjectured a universal form of matrix elements in chaotic systems, which is known as the Srednicki's ansatz. The Srednicki's

ansatz states that matrix elements of O in the energy eigenbasis takes the following form[*1]:

$$O_{ij} = O(\bar{E})\delta_{ij} + d(\bar{E})^{-1/2} f_O(\bar{E}, \omega) R_{ij}. \tag{2.29}$$

Here, $\bar{E} := (E_i + E_j)/2$, $\omega := E_i - E_j$, and $d(\bar{E})$ is the number of the energy eigenstates in the energy shell around energy $\bar{E}$. $O(\bar{E})$ is a smooth function depend only on $\bar{E}$, $f_O(\bar{E}, \omega)$ is a smooth function of $\bar{E}$ and ω, and R_{ij} is a random complex variable distributed according to the Gaussian probability with zero mean and unit variance. In most cases, there exists $\omega_* > 0$ independent of N such that the function $f_O(\bar{E}, \omega)$ is almost constant for $\omega < \omega_*$ and decays exponentially for $\omega > \omega_*$.

The Srednicki's ansatz (2.29) includes the diagonal ETH and the off-diagonal ETH. If Eq. (2.29) holds, the microcanonical average of O at energy $\bar{E}$ can be rewritten as

$$\langle O \rangle_{\mathrm{MC}} = \frac{1}{d(\bar{E})} \sum_{E_i \in I_{\bar{E}, \Delta E}} O(E_i) \approx O(\bar{E}), \tag{2.30}$$

where we used the smoothness of $O(\bar{E})$. Thus, Eq. (2.29) implies that $O_{ii} \approx \langle O \rangle_{\mathrm{MC}}$, i.e., the diagonal-ETH. Because the factor $d(\bar{E})^{-1/2}$ decays exponentially with the system size, Eq. (2.29) implies that the off-diagonal elements vanish in the thermodynamic limit, which is equivalent to the off-diagonal ETH in the aforementioned form.

2.3 Weak ETH

Although integrable systems do not satisfy the ETH, Biroli *et al.* [85] found that a weaker version of the ETH holds in these systems. The weaker version of the ETH states that *most* of the energy eigenstates represent thermal equilibrium. This is often referred to as the *weak ETH*. Although the original ETH (2.23) prohibits the existence of any non-thermal energy eigenstate, the weak ETH allows the existence of a small number of non-thermal energy eigenstates whose ratio against the number of all eigenstates vanishes in the thermodynamic limit.

To give the precise statement of the weak ETH, we consider the variance of diagonal matrix elements in the energy shell:

$$\Delta(O)^2 := \frac{1}{d_{uN, \Delta E}} \sum_{E_i \in I_{uN, \Delta E}} (O_{ii} - \langle O \rangle_{\mathrm{MC}})^2. \tag{2.31}$$

We say that the weak ETH for O holds if

$$\lim_{N \to \infty} \Delta(O) = 0. \tag{2.32}$$

[*1] The Srednicki's ansatz (2.29) is not a mathematically rigorous statement, because the left-hand side of Eq. (2.29) is not a stochastic variable, while the right-hand side is a stochastic variable.

By applying the Chebyshev inequality to Eq. (2.32), we can show that most of the energy eigenstates satisfy $\langle E_i|O|E_i\rangle \approx \langle O\rangle_{\rm MC}$. Alba [88] has numerically shown that $\Delta(O)$ decays polynomially with the system size for integrable systems: in particular, $\Delta(O) \propto N^{-1/2}$ for integrable one-dimensional XXZ model. Moreover, the weak ETH has been proved for general translational invariant systems including integrable systems in Ref. [89], and a later work [87] proved that the following tighter bound

$$\Delta(O)^2 \leq cN^{-1+\delta} \tag{2.33}$$

holds for sufficiently large N, where c and δ are arbitrary positive constants.

Furthermore, Mori [90] proved the upper bound of the ratio of athermal eigenstates based on the large deviation analysis [9, 91]. The large deviation analysis is a more direct approach than considering the variance (2.31) to investigate the weak ETH. To formulate it, let us consider the number of the athermal eigenstates

$$d_\epsilon^{\rm out} := \sum_{E_i \in I_{uN,\Delta E}} \theta(|O_{ii} - \langle O\rangle_{\rm MC}| > \epsilon), \tag{2.34}$$

where θ is the step function and $\epsilon > 0$ is an arbitrary threshold. The ETH implies that $d_\epsilon^{\rm out} \to 0$ as $N \to \infty$, while the weak ETH is expressed as $d_\epsilon^{\rm out}/d_{uN,\Delta E} \to 0$. Mori [90] proved the following bound

$$\frac{d_\epsilon^{\rm out}}{d_{uN,\Delta E}} \leq e^{-\gamma(\epsilon)N} \tag{2.35}$$

with $\gamma(\epsilon) > 0$ for any local operator. This bound implies that the ratio of athermal eigenstates decays at least exponentially with N.

2.4 Numerical studies of the ETH

In this section, we review previous studies of numerical verification of the ETH. Rigol *et al.* [28] reported the first clear evidence of the ETH in a model related to an ultracold atomic system. They investigated hardcore bosons on an asymmetric two-dimensional lattice with 21 sites and calculated the momentum distribution by using exact numerical diagonalization. They showed that the eigenstate expectation value of the zero momentum occupation number does not change much with the label of the energy eigenstate in the nonintegrable case. In particular, the expectation values are almost identical to the microcanonical average. Thus, they concluded that the ETH holds for their model, and the ETH is the most plausible scenario for thermalization in ultracold atomic systems. After their seminal work, the ETH has been verified in the various nonintegrable models listed below.

Spin system

- 1d Ising model with transverse and longitudinal fields [38, 92–94]
- 2d Ising model with transverse field [95–97]
- 1d XXZ model with next-nearest-neighbor interaction [98–101]
- 1d XXZ model with (weak) random magnetic field [102, 103]
- 1d XXZ model with harmonic potential [104]
- 1d XXZ-ladder model [104–106]
- Rokhsar-Kivelson model (quantum dimer model) [107]

Fermionic system

- 1d Fermi-Hubbard model [108, 109]
- 1d spinless fermions with nearest and next-nearest hopping and repulsion [110–112]
- Holstein polaron model (electron-phonon coupling model) [113]
- Sachdev-Ye-Kitaev (SYK) model (Majorana fermions with disordered, long-range, and four-body interactions) [114, 115]
- Supersymmetric SYK model [116]

Bosonic system

- 1d Bose-Hubbard model [27, 104, 117]
- 1d hardcore bosons with nearest and next-nearest hopping and repulsion [84, 92, 118]
- 1d hard-core bosons with dipolar interaction trapped in a harmonic potential [119]
- 2d hardcore bosons with nearest-neighbour repulsion [28]

2.4.1 Finite-size scaling

Beugeling *et al.* [104] have numerically examined the system-size dependence of the deviation from the exact ETH in integrable and nonintegrable models. They calculated the variance $\Delta(O)^2$ of the eigenstate expectation values defined by Eq. (2.31) for three one-dimensional models: the spin-1/2 XXZ ladder model, the spin-1/2 XXZ model in a harmonic potential, and the Bose-Hubbard model. These models allow one to tune the integrability and do not have any local conserved quantity except for the total energy and the total magnetization (the number of bosons) in the nonintegrable cases. The authors found that the variance decays as $\Delta(O)^2 \propto d^{-1}$ with the dimension of the energy shell d for several few-body observables in the case of nonintegrable parameters far from the integrable point. The d^{-1} behavior is consistent with the prediction of random matrix theory and the Srednicki's ansatz (2.29). On the other hand, the polynomial decay rate α of $\Delta(O)^2 \propto d^{-\alpha}$ is very small near the integrable point.

Alba [88] investigated the system-size dependence of $\Delta(O)^2$ in an integrable system and showed the validity of the weak ETH (2.32). He focused on the one-dimensional spin-1/2 XXX

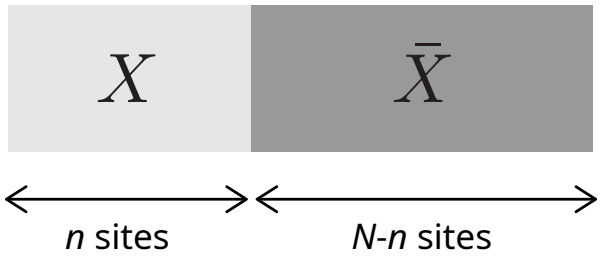

Fig. 2.1 Bipartition of the system into subsystems X and $\bar{X}$.

model, which is exactly solvable by the Bethe ansatz. The energy eigenstates were numerically constructed by using the Bethe ansatz solution for the chain sizes $N = 20, 40, 80, 160$, which is much larger than the accessible size of the exact numerical diagonalization. He calculated reduced density operators of energy eigenstates on a local region and showed that the variance of reduced density operators decays as N^{-1}. This is the same behavior as noninteracting models [85], but is contrastive to the d^{-1} behavior observed in nonintegrable systems.

2.5 Entanglement entropy

In the previous sections, we focused on observables represented as Hermitian operators acting on the Hilbert space. Here, we focus on entanglement, which is not straightforwardly represented by Hermitian operators. Entanglement is a resource of quantum information processing when operations are restricted to local quantum operations and classical communication (LOCC) [120].

Entanglement entropy is a standard measure of bipartite entanglement, which is defined as follows. Let divide the entire system into two subsystems X and $\bar{X}$ as illustrated in Fig. 2.1. We denote the reduced state of a pure state $|\psi\rangle$ on the subsystem X by $\rho_X := \mathrm{Tr}_{\bar{X}}[|\psi\rangle\langle\psi|]$. Then, entanglement entropy on X is defined as the von Neumann entropy of the reduced state

$$S(X) := -\mathrm{Tr}[\rho_X \log \rho_X], \tag{2.36}$$

and $S(\bar{X})$ is defined in the same manner. We note that $S(X) = S(\bar{X})$ holds for any bipartition, and $0 \leq S(\bar{X}) \leq \log d_X$, where d_X is the dimension of the Hilbert space on X. Over the last two decades, entanglement entropy has been widely used to study quantum many-body systems in various fields of physics, ranging from condensed matter physics [121] to high-energy physics [122].

2.5.1 Entanglement in quantum many-body systems

In condensed matter physics, entanglement entropy of the ground state has been studied to characterize non-trivial quantum phases and quantum criticality [121]. It is well known that

the entanglement entropy of the ground state of a gapped local Hamiltonian obeys the area law [123]. The (strict) area law states that the entanglement entropy scales with the size of the boundary region of X. If we take X as an m-dimensional hyper-square region with length $\ell := n^{1/m}$, the area law is represented as

$$S(X) = a_1 \ell^{m-1} + a_2 \ell^{m-2} + \cdots . \tag{2.37}$$

The area law of the gapped ground state is a consequence of the locality of Hamiltonian. The rigorous proof of the area law of the gapped ground state (and low energy eigenstates) has been established for general one-dimensional systems [124, 125]

On the other hand, one-dimensional critical systems show a logarithmic violation of the area law[*2]. The (1+1)-conformal field theory (CFT) describes the effective theory of one-dimensional critical systems. From this fact, Calabrese and Cardy [127, 128] showed that the entanglement entropy of the ground state follows the following universal scaling:

$$S(X) = \frac{c}{3} \log \frac{\ell}{a} + c', \tag{2.38}$$

where c is the central charge of the CFT, a is the short-distance cutoff, and c' is a non-universal constant which cannot be determined by the CFT.

In contrast to the ground state, excited states (except for low-lying states) generally obey the volume law instead of the area law [121].

2.5.2 Page curve

Random pure states are highly entangled because they do not have any local structure. Correspondingly, the entanglement entropy of a random pure state takes an almost maximum value. Page [129] calculated the entanglement entropy of a random pure state drawn from the uniform measure, and conjectured that the averaged entanglement entropy is given by

$$S_{\mathrm{Page}}(X) = \sum_{k=d_{\bar{X}}+1}^{d_X d_{\bar{X}}} \frac{1}{k} - \frac{d_X - 1}{2d_{\bar{X}}} \tag{2.39}$$

$$\approx \log d_X - \frac{d_X}{2d_{\bar{X}}}. \tag{2.40}$$

Equation (2.39) was proved later by several authors [130, 131]. When the system consists of N qubits, Eq. (2.40) can be rewritten as

$$S_{\mathrm{Page}}(X) \approx n \log 2 - 2^{-N+2n-1}, \tag{2.41}$$

[*2] Although it had been believed that the area law could be violated by at most $\log \ell$ even in critical systems, Movassagh and Shor [126] showed its counterexample by constructing an exactly solvable one-dimensional spin model which violates the area law by $\sqrt{\ell}$.

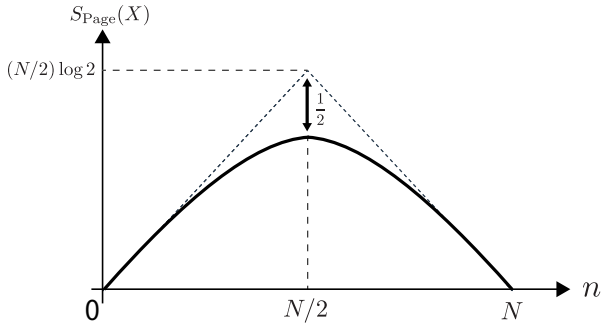

Fig. 2.2 The subsystem-size dependence of entangle entropy averaged over uniform random states. When n is small, $S_{\rm Page}(X)$ follows the volume law and takes almost the maximum value. On the other hand, it deviates from the maximum value at $n = N/2$.

where n is the number of qubits in X. Thus, random pure states obey the volume law. This result also implies that the deviation of the entanglement entropy from the maximum value is negligible for $n \ll N/2$, but becomes non-negligible value $1/2$ at $n = N/2$. Equation (2.41) as a function of n is called the Page curve.

From the viewpoint of statistical physics, uniform random states of the entire Hilbert space are regarded as random states at infinite temperature. This is one of the manifestations of the typicality in statistical mechanics [132, 133]. Thus, the Page's result is interpreted as the typical structure of entanglement at infinite temperature. This raises a question: how is the Page curve at infinite temperature ($\beta = 0$) connected to the low-entanglement structure of the ground state ($\beta = \infty$)? In other words, what is the structure of the entanglement of finite-temperature pure states? Recently, some groups [134–136] answered this question by using random pure states describing thermal equilibrium at finite temperature.

Nakagawa *et al.* [134, 135] derived an analytic formula of the entanglement entropy of thermal pure states. They focused on canonical-type random states introduced by Sugiura and Shimizu [137]. It is parameterized by inverse temperature $\beta \in (-\infty, \infty)$ and defined as

$$|\psi(\beta)\rangle := \mathcal{N}^{-1} e^{-\beta H/2} |\psi\rangle \,, \tag{2.42}$$

where $|\psi\rangle$ is a uniform random state, and $\mathcal{N}^2 := \langle\psi|e^{-\beta H}|\psi\rangle$ is a normalized constant. At $\beta = 0$, it reproduces a random state investigated by Page, and it becomes the ground state of H in $\beta \to \infty$. It was shown that these states reproduce the expectation value of the canonical ensemble with a probability close to one.

Then, Nakagawa *et al.* obtained the following formula of the average entanglement entropy of $|\psi(\beta)\rangle$:

$$S_\beta(X) = S_{\rm TD}(X) - \gamma_X. \tag{2.43}$$

Here, $S_{\mathrm{TD}}(X)$ is the thermodynamic entropy of subsystem X given by

$$S_{\mathrm{TD}}(X) := \beta(\langle H_X \rangle_\beta - F_X(\beta)), \tag{2.44}$$

where H_X is the local Hamiltonian on subsystem X, and $F_X(\beta) := \beta^{-1} \log \mathrm{Tr}[e^{-\beta H_X}]$ is the free energy on X. γ_X is a complicated function which depends on the partition functions of X and $\bar{X}$, and also depends on the interaction Hamiltonian between X and $\bar{X}$. Although the Page curve does not depend on the Hamiltonian, Eq. (2.43) depends on the Hamiltonian, where the leading contribution comes through the partition function. The existence of the term $S_{\mathrm{TD}}(X)$ is very natural, because $|\psi(\beta)\rangle$ is locally indistinguishable from thermal equilibrium. The second term on the right-hand side of Eq. (2.43) is a finite-temperature counterpart of the Page correction. In the limit of $\beta \to 0$, Eq. (2.43) reproduces the Page curve (2.41). In this sense, Eq. (2.43) is an extension of the Page curve to finite temperature.

In addition, a similar formula to Eq (2.43) was obtained by Lu and Grover [136]. They focused on another class of thermal pure states, called *ergodic bipartite (EB) states* [138]. The EB state is parameterized by total energy E and is defined as

$$|\psi_E\rangle := \sum_{E_i(X)+E_j(\bar{X})\in(E-\delta,E+\delta)} c_{ij} \, |E_i(X)\rangle \, |E_j(\bar{X})\rangle \, , \tag{2.45}$$

where $|E_i(X)\rangle$ and $|E_j(\bar{X})\rangle$ are the energy eigenstates of subsystem X and $\bar{X}$, respectively, $\delta > 0$ is the width of energy range, and c_{ij} is a random complex number drawn uniformly from a unit hypersphere. The EB state can be regarded as a thermal state in the sense that it reproduces the microcanonical average for local observables. We remark that Refs. [134–136] also investigated the kth Rényi entanglement entropy and derived the corresponding extension of the Page curve.

Chapter 3

Work extraction in quantum systems

In this chapter, we consider work extraction from quantum systems and explain the seminal results obtained by Pusz, Woronowicz, and Lenard. They obtained the complete characterization of work-extractable quantum states. As a preliminary, we review the second law and work extraction in conventional thermodynamics in Sec. 3.1. We present the standard setup for work extraction in quantum mechanics in Sec. 3.2. We review the notion of passivity and some related results in Sec 3.3, which is the main part of this chapter.

3.1 Second law and work extraction in thermodynamics

In the previous chapter, we investigated the relaxation process toward thermal equilibrium in isolated quantum systems. Relaxation to thermal equilibrium is one of the fundamental principles of thermodynamics. On the other hand, the second law is another fundamental principle and is closely related to the irreversibility of macroscopic phenomena. The second law characterizes transitions between different thermal equilibrium and determines whether a given thermodynamic transition is possible by a macroscopic operation. There exist several different ways to express the second law [139]. For example, Clausius's principle states that heat never flows spontaneously from a colder bath to a hotter one, and Carnot's principle states that all heat engines between two heat baths are equal or less efficient than the Carnot engine. Although these formulations of the second law seem very different at a glance, these are equivalent under reasonable assumptions made in thermodynamics. Establishing these principles and their equivalence based only on microscopic dynamics is still a central issue in

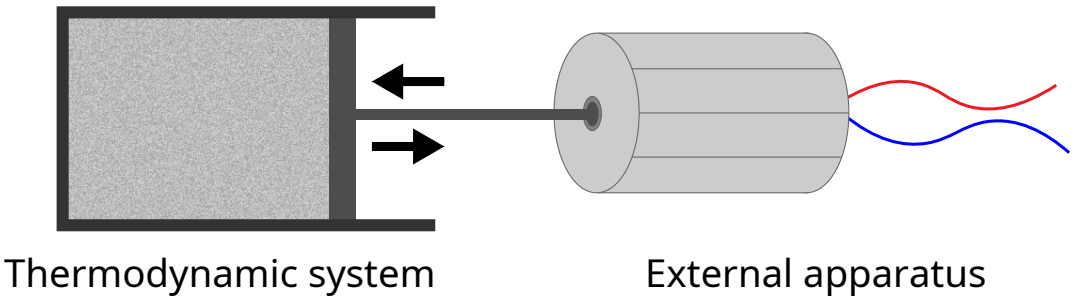

Fig. 3.1 A typical example of work extraction in thermodynamics. The total system consists of a thermodynamic system and a mechanical apparatus. Although the system couples to some environments in general, we assume that the system is surrounded by adiabatic walls and exchanges the energy only with the apparatus.

statistical physics.

Here, we review a thermodynamic description of work extraction. Let us consider a single thermodynamic system, such as gas confined in a container with a movable piston (see Fig. 3.1) and assume that gas is in its thermal equilibrium. Then, there is an external apparatus that can control the macroscopic parameters of the system, such as the position of the piston. In conventional thermodynamics, work is defined as the energy transfer between the system and the apparatus. If the system is not in contact with any environment, extracted work equals the energy change in the system. The second law can be expressed only with the use of work as follows: *No work can be extracted from thermal equilibrium during any cyclic operation by the external apparatus.* This formulation of the second law is often called the Kelvin-Planck principle or Thomson's principle (Thomson is the birth name of Kelvin). In contrast to heat and entropy, work is relatively easy to deal with in microscopic physics because it can be defined as a purely mechanical quantity. The Kelvin-Planck formulation only uses work, whose simplicity is an advantage over other formulations of the second law.

3.2 Quantum mechanical setup for work extraction

We formulate work extraction based on quantum mechanics. As in Chapter 2, we consider an isolated quantum system, where the time evolution is described by the Scrödinger equation. In contrast to Chapter 2, we now consider a time-dependent Hamiltonian to deal with the effect of an external apparatus.

We regard the thermodynamic system as a quantum system and denote its Hamiltonian by $H = \sum_{i=1}^{d} E_i \left|E_i\right\rangle \left\langle E_i\right|$. For simplicity, we assume that the Hamiltonian has no degeneracy. The system is thermally isolated while exchanges mechanical energy with an external apparatus. The apparatus controls an external time-dependent potential $V(t)$. As we only consider

cyclic processes in the present setup, we assume that the potential vanishes before $t = 0$ and after $t = \tau$. Thus, the total Hamiltonian is given by

$$H(t) = H + V(t), \tag{3.1}$$

which satisfies $H(0) = H(\tau) = H$. We consider an arbitrary initial state that can be a mixed state, which is denoted as ρ. The time evolution of the system is described by a unitary operator $U := \mathcal{T} \exp(-\int_0^\tau H(t)dt)$, where $\mathcal{T}$ is the time-ordering operator.

Let us formulate work extracted from the system. Since we assumed that there is no other object than the system and the apparatus, the energy decrease of the system equals the energy gain of the apparatus. Accordingly, we define the (average) extracted work $W(\rho, U)$ from the system as the change in the average energy:

$$W(\rho, U) := \mathrm{Tr}[H\rho] - \mathrm{Tr}[HU\rho U^\dagger]. \tag{3.2}$$

Here, $W = 0$ means that work is not extracted, while $W > 0$ means that a positive amount of work is extracted. Our question is whether the extracted work can be positive by some unitary operations, in other words, whether the average energy of the system can be lowered by some unitaries.

Finally, we remark a small problem of the above formulation. The above formulation of work in quantum systems is very common in the community of statistical mechanics [140]. For example, the generalization of the Jarzynski equality [142] to quantum systems is studied with this formulation [143,144]. However, this conventional formulation is sometimes regarded as not fully quantum and called semi-classical because the apparatus is implicitly treated as a classical object. To overcome this problem, we need to treat quantum mechanically both of the system and the apparatus [145, 146]. In the fully quantum formulation, the composite system evolves according to a time-independent Hamiltonian composed of the individual free Hamiltonians of the system and the apparatus and the interaction Hamiltonian between them. In this formulation, the dynamics of the system itself is not necessarily unitary and is described by a completely positive and trace-preserving (CPTP) map in general. Recently, Hayashi and Tajima [145] have established a precise formulation of the fully quantum work extraction based on quantum measurement theory, where the semi-classical formulation is realized as an approximation of the fully quantum formulation.

3.3 Passivity

Let us move to review the seminal works by Pusz, Woronowicz, and Lenard [147, 148]. They introduced a notion of *passivity* in the studies of deriving the Gibbs state from the first principles. A passive state is a quantum state which does not allow one to extract positive work by any cyclic unitary operation. The formal definition is as follows.

Definition 3.1 Passive state [147, 148]

A quantum state ρ is passive for a given Hamiltonian H, if $W(\rho, U) \leq 0$ holds for any unitary operator U.

By denoting the maximum extractable work by $W_{\max}(\rho) := \max_U W(\rho, U)$, the definition of the passive state can be rephrased as $W_{\max}(\rho) = 0$. We note that $W_{\max}(\rho)$ is sometimes called *ergotropy* [149, 150] ("ergo" means "work", and "tropy" means "transformation"). The ground state is passive, which is obvious from its definition as the minimum energy state. Moreover, the passive states contain a much broader class of quantum states. Passivity was first introduced by Pusz and Woronowicz in the context of mathematical physics, and their formulation is based on C^*-algebras. Afterward, it was translated into the standard notation of statistical mechanics by Lenard. The concepts of passivity and ergotropy play a key role in recent studies of quantum thermodynamics [151] and quantum communication [152].

We next consider the explicit form of the passive states. Pusz, Woronowicz, and Lenard obtained the necessary and sufficient condition of the passivity. Their results are represented as follows.

Theorem 3.1 Complete characterization of the passive states [147, 148]

A quantum state ρ is passive with respect to H, if and only if it satisfies the following two conditions:

1. ρ is diagonal in the energy eigenbasis of H, i.e., $\rho = \sum_i p_i |E_i\rangle \langle E_i|$.
2. The population of the energy eigenstate decreases with the eigenenergy, i.e.,

$$E_i > E_j \Rightarrow p_i \leq p_j \quad \text{for all } i \text{ and } j. \tag{3.3}$$

The first condition suggests that a passive state is a diagonal ensemble (2.6). Moreover, the first condition implies that any non-zero coherence in the energy eigenbasis becomes a resource of work. The second condition is shown schematically in Fig. 3.2.

The Gibbs state $\gamma_\beta := e^{-\beta H}/Z(\beta)$ with non-negative inverse temperature $\beta \geq 0$ is passive because it obviously satisfies the above two conditions. This fact also can be proved from the non-negativity of the relative entropy [141]. On the other hand, the microcanonical state is not passive unless one takes the energy shell as $I_E := \{E_i \leq E\}$. In that case, the corresponding microcanonical state

$$\rho_{\mathrm{GMC}}(E) := \frac{1}{d_E} \sum_{E_i \leq E} |E_i\rangle \langle E_i| \,. \tag{3.4}$$

is called the generalized microcanonical state or the θ-ensemble. The generalized microcanonical state is also a special case of the most energetic passive states [153], which is defined

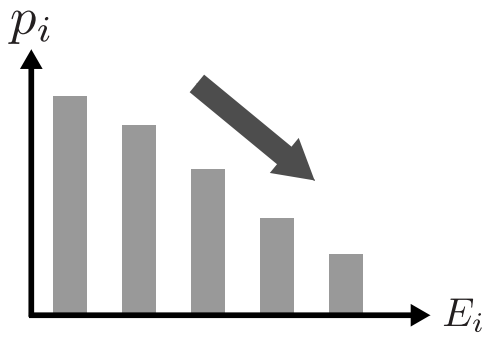

Fig. 3.2 Schematic representation of the second condition of Theorem 3.1.

by

$$\rho_{(k,l)}(\lambda) := \frac{\lambda}{k}\sum_{i=0}^{k} |E_i\rangle\langle E_i| + \frac{1-\lambda}{k}\sum_{i=0}^{l} |E_i\rangle\langle E_i| \tag{3.5}$$

with $0 \leq \lambda \leq 1$. That is, the most energetic passive state is a mixture of two generalized microcanonical states. An important property of the most energetic passive state is that it is the unique passive state that has the maximum energy with a fixed von Neumann entropy. More generally, any passive state can be represented as a mixture of generalized microcanonical states.

The notion of passivity is very similar to the second law in the Kelvin-Planck formulation. In this sense, theorem 3.1 is often regarded as a quantum mechanical derivation of the second law. However, passivity and the second law are different in the following two points:

1. The second law focuses on only macroscopic cyclic operations, while all microscopic operation is considered in the definition of passive states. Thus, passivity is a stronger constraint than the second law.
2. The second law is formulated for only thermal equilibrium, while passive states contain more general states but do not contain all the thermal states like thermal pure states.

These differences are indeed starting points of our main study in Chapter 5.

3.3.1 Proof of theorem 3.1

As mentioned above, Theorem 3.1 was first proved by Pusz and Woronowicz [147] by using the techniques of C^*-algebras. Later, Lenard [148] obtained an elementary proof.

Here, we follow Lenard's proof. The main part of the proof is to derive the explicit representation of ergotropy. Let the spectral decomposition of ρ be given by $\rho = \sum_{i=1}^{d} p_i |\psi_i\rangle\langle\psi_i|$

with $p_1 \geq \cdots \geq p_d$. For a given unitary operator U, the final energy can be written as

$$\mathrm{Tr}[HU\rho U^\dagger] = \sum_{i,j=1}^{d} E_i p_j \left|\langle E_i|U|\psi_j\rangle\right|^2. \tag{3.6}$$

We note that $|\langle E_i|U|\psi_j\rangle|^2$ is doubly stochastic, i.e., $\sum_i |\langle E_i|U|\psi_j\rangle|^2 = \sum_j |\langle E_i|U|\psi_j\rangle|^2 = 1$. The key of the proof is the Birkhoff-von Neumann theorem [154], which states that any doubly stochastic matrix is a convex combination of permutation matrices. From the Birkhoff-von Neumann theorem, we have

$$\mathrm{Tr}[HU\rho U^\dagger] = \sum_{\pi\in S_d} c_\pi \sum_{i=1}^{d} E_i p_{\pi(i)}, \tag{3.7}$$

where S_d is the permutation group of d elements, and c_π is a non-negative variable satisfying $\sum_{\pi\in S_d} c_\pi = 1$. The minimum of $\sum_{i=1}^d E_i p_{\pi(i)}$ as a function of $\pi \in S_d$ is achieved, when π satisfies $p_{\pi(1)} \geq \cdots \geq p_{\pi(d)}$ for $E_1 \leq \cdots \leq E_d$ [155]. Therefore, we have the following lower bound:

$$\mathrm{Tr}[HU\rho U^\dagger] \geq \sum_{i=1}^{d} E_i p_i. \tag{3.8}$$

The equality of the above bound can be achieved by $U_{\max} := \sum_i |E_i\rangle\langle\psi_i|$. Therefore, ergotropy of ρ is given by

$$W_{\max}(\rho) = \mathrm{Tr}[H\rho] - \sum_{i=1}^{d} p_i E_i \tag{3.9}$$

$$= \sum_{i=1}^{d} E_i p_j \left|\langle E_i|\psi_j\rangle\right|^2 - \sum_{i=1}^{d} E_i p_i. \tag{3.10}$$

We now derive the necessary and sufficient condition of $W_{\max}(\rho) = 0$. If ρ satisfies two conditions of Theorem 3.1, we can easily show that $W_{\max}(\rho) = 0$. We next show the converse below. Since work is invariant under the shift of the energy spectrum, we can assume $E_i > 0$ without loss of generality. Thus, $W_{\max}(\rho) = 0$ is equivalent to the following condition:

$$\sum_{j=1}^{d} \left|\langle E_i|\psi_j\rangle\right|^2 p_j = p_i \tag{3.11}$$

for all i. This equality implies that we can take $|\psi_i\rangle$ as $|\langle E_i|\psi_j\rangle|^2 = \delta_{ij}$, or equivalently, $|\psi_i\rangle = |E_i\rangle$ for all i. Therefore, we obtain $\rho = \sum_i p_i |E_i\rangle\langle E_i|$ with $p_1 \geq \cdots \geq p_d$. This concludes the proof of Theorem 3.1.

Chapter 4

Information scrambling and unitary design

In this chapter, we review three information-theoretical concepts related to quantum chaos: out-of-time-ordered correlator (OTOC), information scrambling, and quantum pseudorandomness. In Sec. 4.1, we introduce the OTOC, which characterizes the quantum butterfly effect. In Sec. 4.2, we discuss information scrambling, which is also a new characterization of chaos in quantum many-body systems. Moreover, information scrambling is closely related to the randomness of dynamics. Random unitary dynamics are also important in quantum information theory, and approximation of random unitary dynamics is formulated as unitary k-design, as explained in Sec. 4.3.

4.1 Out-of-time-ordered correlator (OTOC)

Recently, quantum chaos has attracted renewed attention in both gravity physics and statistical physics [50, 51]. The key is a new indicator called the out-of-time-ordered correlator (OTOC), which is a four-point correlation function with unusual time-ordering. Although quantum systems do not have the sensitivity to a small perturbation in the classical sense as mentioned in Sec. 1.2, the OTOC provides another route to quantify the butterfly effect in quantum systems. Roughly speaking, the OTOC is obtained by quantizing the definition of the classical Lyapunov exponent (1.6). The OTOC was first proposed by Larkin and Ovchinnikov

half a century ago [60]. They investigated the OTOC to describe the semi-classical behavior of superconductivity. Recently, the OTOC was reexamined through a series of studies by Shenker, Stanford, and Roberts [156–160].

For given Hermitian operators A and B, the (4-point) OTOC is defined as

$$F_{A,B}(t) := \mathrm{Tr}[A(t)B(0)A(t)B(0)\rho], \tag{4.1}$$

where $A(t) := e^{iHt}Ae^{-iHt}$ is the operator in the Heisenberg picture. The fast decay of the OTOC characterizes the quantum butterfly effect, and the relaxation of the OTOC to a small value is related to information scrambling. In the context of gravity physics, the OTOC has been used to investigate the holographic duality [51, 161, 162]. In the context of statistical physics, it was shown that the OTOC detects equilibrium and dynamical quantum phase transitions [163–166]

To understand how the OTOC is related to chaos, let us consider a single particle in a one-dimensional system. As in Sec. 1.2, we denote classical particle's position and momentum by x and p, respectively, and focus on the trajectory $(x(t), p(t))$ with the initial condition $(x(0), p(0)) = (x_0, p_0)$. If the system is chaotic, $\partial x(t)/\partial x_0$ is expected to increase exponentially with time:

$$\frac{\partial x(t)}{\partial x_0} \sim e^{\lambda_{\mathrm{L}} t}. \tag{4.2}$$

By use of the Poisson bracket $\{f(x_0, p_0), g(x_0, p_0)\} := (\partial f/\partial x_0)(\partial g/\partial p_0) - (\partial f/\partial p_0)(\partial g/\partial x_0)$, the left-hand side of Eq. (4.2) is rewritten as $\partial x(t)/\partial x_0 = \{x(t), p_0\}$. To obtain its quantum counterpart, we replace the Poisson bracket with the commutator according to $\{x(t), p_0\} \to -i[\hat{x}(t), \hat{p}(0)]$. If the semiclassical picture holds, the squared commutator grows as

$$\mathrm{Tr}\left(-[\hat{x}(t), \hat{p}(0)]^2\rho\right) \sim \{x(t), p_0\}^2 \sim e^{2\lambda_{\mathrm{L}} t}. \tag{4.3}$$

Thus, the early-time growth of the squared commutator characterizes the quantum butterfly effect.

To consider more general quantum systems, we replace $\hat{x}$ and $\hat{p}$ by arbitrary Hermitian operators A and B: We consider the following squared commutator

$$C_{A,B}(t) := \mathrm{Tr}\left(-[A(t), B(0)]^2\rho\right), \tag{4.4}$$

which characterizes the commutativity between $A(t)$ and $B(0)$. We note that $C_{A,B}(t) = 0$ if $A(t)$ and $B(0)$ are commutative $[A(t), B(0)] = 0$. Roughly speaking, the squared commutator quantifies how the initial perturbation induced by B affects the later measurement of A. The squared commutator is related to the OTOC (4.1) as follows. Expanding the commutator, we

have

$$C_{A,B}(t) = \mathrm{Tr}[A(t)B(0)^2A(t)\rho] + \mathrm{Tr}[B(0)A(t)^2B(0)\rho] - \mathrm{Tr}[A(t)B(0)A(t)B(0)\rho] - \mathrm{Tr}[B(0)A(t)B(0)A(t)\rho]. \tag{4.5}$$

If A and B are unitary (e.g., if they are Pauli matrices), the first and second terms on the right-hand side of the above equality become one, and $C_{A,B}(t)$ can be written as

$$C_{A,B}(t) = 2 - 2\mathrm{Re}[F_{A,B}(t)]. \tag{4.6}$$

This equality implies that the decay of the OTOC leads to the growth of the squared commutator. Thus, we conclude that the fast decay of the OTOC characterizes the quantum butterfly effect.

The OTOC plays an essential role in studies of gravity theory. From the semi-classical description, one naively expects that the OTOC at early times scales as

$$F_{A,B}(t) = 1 - \epsilon e^{\tilde{\lambda}_{\mathrm{L}} t} + \cdots \tag{4.7}$$

with $\epsilon > 0$ and $\tilde{\lambda}_{\mathrm{L}} > 0$. Indeed, this description is correct for several field theories, and $\tilde{\lambda}_{\mathrm{L}}$ is regarded as the quantum Lyapunov exponent. The time t_* , at which the OTOC deviates from one, is called the scrambling time [156]. If Eq. (4.7) is true, scrambling time is given by $t_* = \tilde{\lambda}_{\mathrm{L}}^{-1} \log \epsilon$. In addition, Maldacena, Shenker, and Stanford [61] have conjectured an upper bound on the quantum Lyapunov exponent:

$$\tilde{\lambda}_{\mathrm{L}} \leq 2\pi/\beta, \tag{4.8}$$

where β is the inverse temperature of the initial Gibbs state. This bound is called the Maldacena-Shenker-Stanford (MSS) bound. Notably, the CFTs, which are holographically dual to some gravity theories, saturate the MSS bound [61, 62].

4.2 Information scrambling

In strongly-interacting systems, locally encoded quantum information spreads out by the time evolution. After a certain time interval, information becomes nonlocal and cannot be accessed by any local measurements. Such delocalization process of quantum information is referred to as *information scrambling*, and a system that gives rise to information scrambling is called a scrambler [50]. Information scrambling has been originally studied in the context of the black hole information paradox [52–55], and has recently been discussed in condensed matter physics as a new feature of chaotic quantum systems [59, 167].

A general and rigorous mathematical definition of information scrambling has not been fully established. In fact, there are several definitions of information scrambling. For example, the

authors of Ref. [54] call the system scrambled, if the final state has the maximum amount of entanglement for any subsystem smaller than the half of the entire system. Other studies [56, 57, 168] have used the tripartite mutual information to quantify delocalized information. Yet other studies [167, 169] have defined information scrambling by the decay of the OTOC. These definitions are different at a glance, while they are related to each other, as shown below.

4.2.1 OTOC

In order to analyze more details of information scrambling, let us consider an operator A acting on a single qubit in an N qubits system. Even if $A(0) = A$ is a local operator at the initial time, $A(t)$ will become a nonlocal operator acting on many qubits at later times. In other words, $A(t)$ is not supported on local qubits but spreads over the entire system. This spreading of the support represents the delocalization of the local operator.

We can quantify this delocalization by using the OTOC as follows. As a reference, we take another local operator $B(0) = B$ whose support does not overlap with that of $A(0)$. Once $A(t)$ is delocalized, the support of $A(t)$ overlaps with that of $B(0)$. To quantify this overlap of the supports, we consider the commutator of $A(t)$ and $B(0)$. The commutator $[A(t), B(0)]$ is zero at $t = 0$ by setting, it would become nonzero at later times. Thus, the squared commutator $C_{A,B}(t)$ is a natural measure of the delocalization of $A(t)$, i.e., $C_{A,B}(t) \approx 0$ if $A(t)$ is localized, and $C_{A,B}(t) \gg 0$ if $A(t)$ is delocalized. If A and B are Hermitian and unitary, the time-dependent part of the squared commutator $C_{A,B}(t)$ is equivalent to the OTOC as seen in Eq. (4.6). This is the reason why the OTOC is often used to quantify the delocalization of the operator.

From a different point of view, however, the OTOC does not perfectly characterize scrambled information, because its definition is not directly related to any information-theoretic quantity, such as entanglement and entropy. In addition, the OTOC depends on the choices of operators A and B. From these viewpoints, the relaxation of the OTOC to the small value, (or equivalently, the saturation of the squared commutator at the significant value) is called *operator scrambling* [170], *operator spreading* [171], or *operator growth* [172] rather than information scrambling.

4.2.2 Tripartite mutual information

We next consider information scrambling from an information-theoretic viewpoint. Following Ref. [168], we introduce N ancilla qubits, and set the initial state as the maximally entangled state between target qubits and ancilla qubits, i.e., N EPR pairs:

$$|\psi(0)\rangle = |\mathrm{EPR}\rangle^{\otimes N} := \left(\frac{|0\rangle_{\mathrm{t}} |0\rangle_{\mathrm{a}} + |1\rangle_{\mathrm{t}} |1\rangle_{\mathrm{a}}}{\sqrt{2}} \right)^{\otimes N}. \tag{4.9}$$

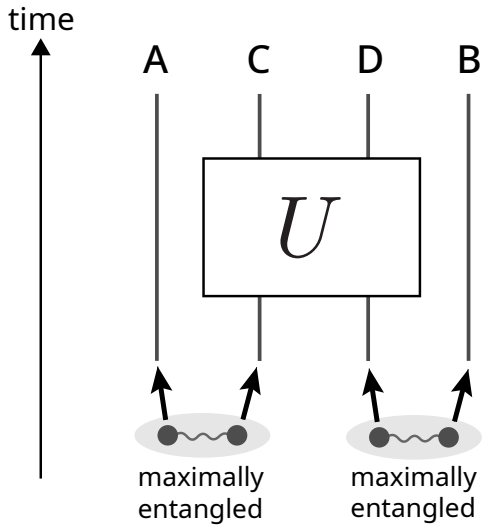

Fig. 4.1 Setup of Ref. [168]. There are N target qubits and additional N ancilla qubits. The ancilla (target) qubits are partitioned into two regions A and B (C and D). The vertical lines represent collections of qubits in individual regions, and U represents the time evolution of the system.

In this setup, we can say that information is initially localized in individual EPR pairs. The unitary operator U acts only on the target qubits, and the finial state is represented as $|\psi(t)\rangle = (U \otimes I)\,|\psi(0)\rangle$. The ancilla qubits are partitioned into two groups A and B, and the target qubits are partitioned into C and D, as shown in Fig. 4.1. The numbers of qubits on $\mathrm{A}, \mathrm{B}, \mathrm{C}, \mathrm{D}$ are denoted as a, b, c, d, respectively ($a < c, b > d, a + b = c + d = N$).

Our aim is to quantify how much initial information is delocalized by U. We use mutual information to quantify the correlation between the two regions. For example, the mutual information between A and C is defined by

$$I(\mathrm{A} : \mathrm{C}) := S(\mathrm{A}) + S(\mathrm{C}) - S(\mathrm{AC}), \tag{4.10}$$

where $S(\mathrm{A}), S(\mathrm{C}), S(\mathrm{AC})$ are the entanglement entropies of $\mathrm{A}, \mathrm{C}, \mathrm{AC}$, respectively. In this setup, $I(\mathrm{A} : \mathrm{B}) = I(\mathrm{C} : \mathrm{D}) = 0$ holds regardless of the choice of U. Information scrambling states that one cannot extract information of the initial state by any local measurements on the final state. This implies that the mutual information between A and C is small $I(\mathrm{A} : \mathrm{C}) \approx 0$, when U is a scrambler. Similarly, we have $I(\mathrm{A} : \mathrm{D}) \approx 0$. On the other hand, the mutual information between A and CD represents the total information, which becomes $I(\mathrm{A} : \mathrm{CD}) = 2a \log 2$ because unitary dynamics preserve the total information. To quantify delocalized information between C and D, we consider the following quantity:

$$I_3(\mathrm{A} : \mathrm{C} : \mathrm{D}) := I(\mathrm{A} : \mathrm{C}) + I(\mathrm{A} : \mathrm{D}) - I(\mathrm{A} : \mathrm{CD}), \tag{4.11}$$

which is the tripartite mutual information. If the system is scrambled, the tripartite mutual information takes a highly negative value: $I_3(\mathrm{A}:\mathrm{C}:\mathrm{D}) \approx -a\log 2$. On the other hand, it vanishes if the system is not scrambled. In fact, $I_3(\mathrm{A}:\mathrm{C}:\mathrm{D}) = 0$ holds for $U = I$ because $I(\mathrm{A}:\mathrm{C}) = 2a\log 2$ and $I(\mathrm{A}:\mathrm{D}) = 0$ for EPR pairs (4.9). Therefore, the tripartite mutual information (4.11) is a natural measure of information scrambling. We note that several numerical studies [56, 57] showed that the tripartite mutual information saturates at around the minimum value in nonintegrable systems. These results suggest that information scrambling is also a characteristic of chaotic dynamics.

Finally, we remark on the relationship between the tripartite mutual information and the OTOC. We go back to the N qubit system and consider the OTOC at infinite temperature. In particular, we consider the following operator-averaged OTOC:

$$\tilde{F}_{\mathrm{A,D}}(t) := \frac{1}{4^{a+d}} \sum_{i,j} \langle D_i(t) A_j(0) D_i(t) A_j(0) \rangle \,, \tag{4.12}$$

where the summation is taken over a complete basis of operators acting on A and that on D. In Ref. [168], it has been proved that a small value of the averaged OTOC implies that the tripartite mutual information is highly negative. More precisely, by defining $\delta := (\tilde{F}_{\mathrm{A,D}}(t) - \tilde{F}_{\min})/\tilde{F}_{\min}$ with $\tilde{F}_{\min}$ being the minimum value of the averaged OTOC, the tripartite mutual information is bounded as

$$I_3(\mathrm{A}:\mathrm{C}:\mathrm{D}) \leq -2a\log 2 + 2\log(1+\delta). \tag{4.13}$$

This result implies that a small value of the averaged OTOC is a sufficient condition of information scrambling.

4.3 Unitary design

Randomness is a fundamental concept in various fields of physics. For example, quantum chaotic systems are believed to have universal features described by random matrix theory [48,173], and randomness is a key resource of quantum information protocols and computation [174,175]. In quantum information theory, there are two types of randomness, i.e., a random state and a random operation. Here, we focus on the latter.

4.3.1 Haar random unitary (HRU)

We present a mathematical definition of a uniformly random unitary operator. The uniform measure on the unitary group is known as the Haar measure. Formally, the Haar measure is defined as the unique measure satisfying

$$\int dU = 1, \quad \int f(VU)dU = \int f(UV)dU = \int f(U)dU, \tag{4.14}$$

for all continuous functions f and for all unitary operators V. We refer to random unitaries drawn according to the Haar measure as the Haar random unitary (HRU), and denote the ensemble of the HRU by H. The HRU plays key roles in studies of quantum information [176, 177], thermalization [178–182] and information scrambling [53, 55, 168].

4.3.2 Unitary k-design

In spite of the importance of the HRU, it is very hard to generate the HRU in quantum circuits. In fact, the number of quantum gates to implement the HRU grows exponentially with the number of qubits [183]. Thus, it is more convenient to use pseudorandom unitary operations, which efficiently simulate the HRU up to a certain order of the moment. From this point of view, Dankert *et al.* [184] introduced the notion of a *unitary k-design*[*1], which is an ensemble of unitaries reproducing the HRU up to the kth moment[*2].

We now formulate unitary k-designs and use the following notation: $\mathcal{H}$ is a d-dimensional Hilbert space, $\mathcal{B}(\mathcal{H})$ is the set of linear operators on $\mathcal{H}$, $\mathcal{U}(\mathcal{H})$ is the set of unitary operators on $\mathcal{H}$, and ν is an arbitrary ensemble of unitaries sampled from $\mathcal{U}(\mathcal{H})$. We denote the ensemble average of a function f on $\mathcal{U}(\mathcal{H})$ over ν by $\mathbb{E}_{U\sim\nu}[f(U)]$. It is explicitly written as

$$\mathbb{E}_{U\sim\nu}[f(U)] := \sum_i p_i f(U_i) \tag{4.15}$$

for a discrete ensemble $\nu = \{p_i, U_i\}$, where $U_i \in \mathcal{U}(\mathcal{H})$ is sampled with probability p_i. More generally, we can consider a continuous ensemble $\nu = \{p(U), U\}$, where $p(U)$ is a probability measure on $\mathcal{U}(\mathcal{H})$. In the continuous case, the average of f is given by

$$\mathbb{E}_{U\sim\nu}[f(U)] := \int p(U) f(U) dU. \tag{4.16}$$

Then, unitary k-designs are formally defined as follows [184]. An ensemble ν is a unitary k-design, if ν satisfies

$$\mathbb{E}_{U\sim\nu}\left[U_{i_1 j_1}\cdots U_{i_k j_k} U^*_{i'_1 j'_1}\cdots U^*_{i'_k j'_k}\right] = \mathbb{E}_{U\sim\mathsf{H}}\left[U_{i_1 j_1}\cdots U_{i_k j_k} U^*_{i'_1 j'_1}\cdots U^*_{i'_k j'_k}\right] \tag{4.17}$$

for all the indices running from 1 to d. As seen clearly from this definition, a unitary k-design is a unitary $(k-1)$-design, while its converse is not true in general.

[*1] In the literature of quantum information theory, unitary k-designs are often referred to as unitary t-designs. In this thesis, we use k instead of t to avoid confusion with the notation of time.

[*2] A unitary k-design is a *statistical* notion of quantum pseudorandomness and can be regarded as a quantum analog of k-wise independent variables in classical computation theory [185]. Recently, Ji, Liu, and Song [186] proposed a *computational* notion of quantum pseudorandom unitary that is computationally indistinguishable from the HRU. Here, the computational indistinguishability means that no efficient quantum algorithm can distinguish pseudorandom unitary operations from the HRU. More recently, the computational pseudorandomness has been investigated in the context of the holographic duality [187, 188]

In addition, we introduce the k-fold channel [189], which is a useful tool to treat the kth moment of ν. Here, we consider the system $\mathcal{H}^{\otimes k}$ consisting of k-replicas of $\mathcal{H}$. The k-fold channel of ν is a super-operator (channel) whose action is given by

$$\Phi_{\nu}^{(k)}(O) := \mathbb{E}_{U\sim\nu}\left[U^{\dagger\otimes k} O U^{\otimes k}\right], \tag{4.18}$$

for all $O \in \mathcal{B}(\mathcal{H}^{\otimes k})$. There is a one-to-one correspondence between the k-fold channel of ν and the kth moment of ν, as can be seen by considering $O = |i_1,\dots,i_k\rangle\langle j_1,\dots,j_k|$. Thus, by using the k-fold channel, the definition of unitary k-design is rewritten as the following simple form.

Definition 4.1 Unitary k-design

An ensemble ν is a unitary k-design, if ν satisfies

$$\Phi_{\nu}^{(k)}(O) = \Phi_{\mathsf{H}}^{(k)}(O) \tag{4.19}$$

for all $O \in \mathcal{B}(\mathcal{H}^{\otimes k})$.

This form is more convenient than the definition by Eq. (4.17). Other equivalent definitions of unitary k-designs are summarized in Ref. [190].

Finally, we remark exact and approximate constructions of unitary designs. We can easily show that the Pauli group is an exact unitary 1-design. The Clifford group is known to be an exact unitary 3-design [191, 192]. On the other hand, it has been proved that, for $k \geq 4$ and $d \geq 5$, there is no subgroup of $\mathcal{U}(\mathcal{H})$ that is an exact unitary k-design [193, 194]. Instead, there are several approximate constructions of unitary k-designs [195–198]. We also note that the depth (i.e., the number of time steps) of an approximate unitary k-design is lower-bounded by $\mathcal{O}(kN/\log N)$, where N is the number of qubits [189, 197].

4.3.3 Relationship with information scrambling

The HRU describes the most random dynamics and can be regarded as a strong scrambler in the following sense. Let us consider the OTOC averaged over the HRU:

$$F_{\mathsf{H}}(A,B) := \mathbb{E}_{U\sim\mathsf{H}}\left[d^{-1}\mathrm{Tr}\{(U^{\dagger}AU)B(U^{\dagger}AU)B\}\right], \tag{4.20}$$

where we set the initial state as the infinite temperature state $\rho = I/d$ for simplicity. It is known that $F_{\mathsf{H}}(A,B)$ decreases exponentially with the system size if A and B are traceless [199]. Consequently, the OTOC becomes almost zero in a large system. The HRU is also a strong scrambler in terms of the tripartite mutual information. In fact, the HRU average of the tripartite mutual information takes a highly negative value [168].

Moreover, if dynamics is a unitary 2-design, the OTOC takes the same value as the HRU [199]. More explicitly, if ν is a unitary 2-design,

$$F_\nu(A,B) = F_{\mathsf{H}}(A,B) \tag{4.21}$$

holds for all $A, B \in \mathcal{B}(\mathcal{H})$, where we write $F_\nu(A,B) := \mathbb{E}_{U\sim\nu}\left[d^{-1}\mathrm{Tr}\{(U^\dagger AU)B(U^\dagger AU)B\}\right]$. This result is a consequence of the fact that the OTOC contains only two pairs of U and $U^\dagger$. In this sense, a unitary 2-design is sufficient for information scrambling.

The relationship between the OTOC and unitary 2-designs can be extended to the general case of unitary k-designs as follows. We define the $2k$-points OTOC for $U \in \mathcal{U}(\mathcal{H})$ by

$$d^{-1}\mathrm{Tr}\left[(U^\dagger A_k U)B_k \cdots (U^\dagger A_1 U)B_1\right] \tag{4.22}$$

with $A_1, \ldots, A_k, B_1, \ldots, B_k \in \mathcal{B}(\mathcal{H})$ and its average over ensemble ν by

$$F_\nu^{(2k)}(\boldsymbol{A},\boldsymbol{B}) := \mathbb{E}_{U\sim\nu}\left[d^{-1}\mathrm{Tr}\left\{(U^\dagger A_k U)B_k \cdots (U^\dagger A_1 U)B_1\right\}\right], \tag{4.23}$$

where we write $\boldsymbol{A} := (A_1, \ldots, A_k)$ and $\boldsymbol{B} := (B_1, \ldots, B_k)$. The conventional OTOC (4.1) is a special case of the $2k$-point OTOC, where $k = 2$, $A_1 = A_2 = A$, and $B_1 = B_2 = B$. As a higher-order extension of Eq. (4.21), we can easily prove that

$$F_\nu^{(2k)}(\boldsymbol{A},\boldsymbol{B}) = F_{\mathsf{H}}^{(2k)}(\boldsymbol{A},\boldsymbol{B}) \tag{4.24}$$

holds if ν is a unitary k-design [199].

Furthermore, Roberts and Yoshida [199] have provided a necessary and sufficient condition of a unitary k-design in terms of the $2k$-point OTOC. They considered the frame potential [189] as a measure of the randomness of an ensemble. The kth frame potential of an ensemble ν is defined as

$$\mathcal{F}_\nu^{(2k)} := \mathbb{E}_{U,V\sim\nu}\left[\mathrm{Tr}(U^\dagger V)\right]. \tag{4.25}$$

The kth frame potential is related to the 2-norm distance between the k-fold channels of ν and H. In fact, for any ensemble ν, the kth frame potential is bounded from below as

$$\mathcal{F}_\nu^{(2k)} \geq \mathcal{F}_{\mathsf{H}}^{(2k)} = k!, \tag{4.26}$$

where the equality holds if and only if ν is a unitary k-design [200]. The kth frame potential is related to the the $2k$-point OTOC by the following equality

$$\frac{1}{d^{4k}}\sum_{\boldsymbol{A},\boldsymbol{B}}\left|F_\nu^{(2k)}(\boldsymbol{A},\boldsymbol{B})\right|^2 = \frac{1}{d^{2(k+1)}}\mathcal{F}_\nu^{(2k)}, \tag{4.27}$$

where the summation $\sum_{\boldsymbol{A},\boldsymbol{B}} := \sum_{A_1}\cdots\sum_{A_k}\sum_{B_1}\cdots\sum_{B_k}$ is taken over a complete basis of $\mathcal{B}(\mathcal{H})$. The left-hand side of Eq. (4.27) is the average of the square of the $2k$-point OTOC over

all operators, which does not equal Eq. (4.12). By combining inequality (4.26) and Eq. (4.27), we can conclude that an ensemble ν becomes a unitary k-design if and only if the operator average of the square of the $2k$-point OTOC takes the minimum value. This is a crucial connection between the OTOC and unitary designs.

Part II Results

Chapter 5

Work extraction from a single energy eigenstate

In this chapter, we investigate the possibility of extracting work from a single energy eigenstate based on our paper [201]. In Sec. 5.1, we propose a conjecture called *the eigenstate second law*. This is a generalization of the ETH to the second law-like setup and states that anyone cannot extract a macroscopic amount of work from any energy eigenstate by simple cyclic operations. In Sec. 5.2, we numerically confirm the eigenstate second law for a nonintegrable spin model and clarify the role of the integrability for work extraction. In Sec. 5.3, we argue that the eigenstate second law can be understood from the ETH for a nonlocal many-body observable. In Sec. 5.4, we prove a weaker version of the eigenstate second law, which holds regardless of the integrability of the Hamiltonian and is a generalization of the weak ETH (2.35).

5.1 Eigenstate second law

5.1.1 Motivation

In the review part of this thesis, we have reviewed two streams of research on the foundation of statistical mechanics. One is the eigenstate thermalization, and the other is passivity. As reviewed in Chapter 2, the ETH is the most likely scenario behind thermalization in isolated

quantum many-body systems. The nonintegrability of the system is crucial for the validity of the ETH. On the other hand, passivity is related to the second law as reviewed in Chapter 3. Because the statement of passivity is very similar to the Kelvin-Planck formulation of the second law, passivity gives a microscopic foundation of the second law.

However, thermal equilibrium is not always described by statistical ensembles. Even a single energy eigenstate can describe thermal equilibrium, as the ETH states. In fact, considering the thermal nature of energy eigenstates will be the core of establishing the foundation of statistical mechanics. In this spirit, it is crucial for understanding the microscopic foundation of the second law to ask whether the second law is valid at the level of individual energy eigenstates. This question leads us to the eigenstate second law formulated below.

There are several studies [89,202–209] related to the second law for pure states. For example, Refs. [207, 208] addressed the validity of the Jarzynski equality [210, 211] for pure states of nonintegrable spin models on the basis of the ETH. However, the role of the integrability in work extraction is still unknown.

In addition, we remark on our previous studies [89, 209] showing the non-negativity of the entropy production and the validity of the fluctuation theorem for a special class of pure states. In those studies, the entire system consists of a working system and a large heat bath, and the initial state of the bath is a thermal energy eigenstate. On the other hand, the results in Refs. [89, 209] cannot be applied to the energy eigenstate of the composite system because the initial state of the entire system is assumed to be a product state of the system and the bath. For these reasons, we here consider the second law for a single energy eigenstate.

5.1.2 Formulation of the eigenstate second law

We now formulate the eigenstate second law. Because a pure state is not passive in general as shown in Sec. 3.3, a positive amount of work can be extracted from a single energy eigenstate if one can perform any unitary operation. In fact, we can easily construct a unitary operator $U_i := |E_i\rangle\langle E_0| + |E_0\rangle\langle E_i|$ with $|E_0\rangle$ being the ground state, by which one can extract work $E_i - E_0$ from an energy eigenstate $|E_i\rangle$. However, such a unitary operator is highly nonlocal and contains all N-body interactions in general. We thus ask whether work extraction is possible under a practical constraint on operations, such as the locality [212] and the symmetry [213, 214]. The number of unitary operations exponentially increases with the system-size because the dimension of the Hilbert space dimension does so. On the other hand, the number of feasible operations under practical constraints is expected to increase moderately with the system-size, not exponentially. It is reasonable to expect that there is a trade-off relation between the number of practically available operations and the number of quantum states that prohibit work extraction by the available operations (see Fig. 5.1). From the above observation, we expect that one cannot extract work from a thermal energy eigenstate by a

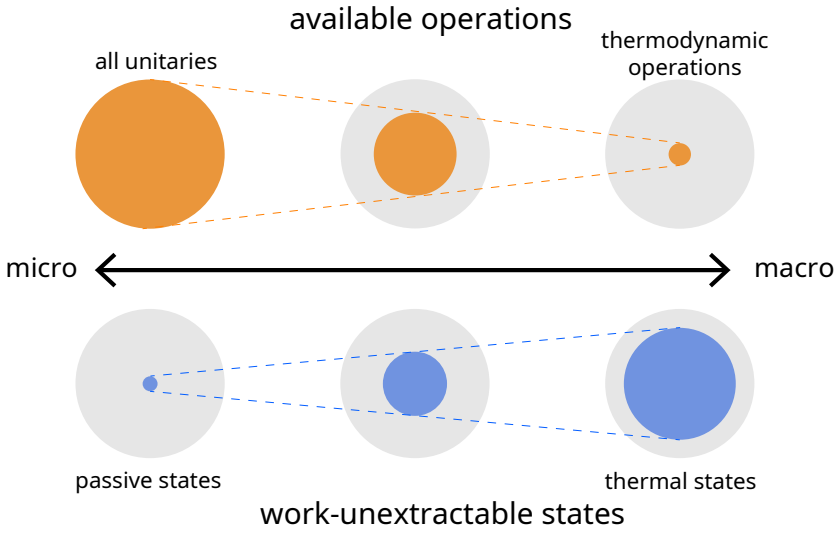

Fig. 5.1 Schematic illustration showing a trade-off between available operations and work-unextractable states. We expect that the number of work-unextractable quantum states increases with decreasing the number of available operations.

simple cyclic operation. In other words, protocols of work extraction from a thermal energy eigenstate will be complicated and highly time-dependent.

To formulate the eigenstate second law, we introduce the effective inverse temperature of an energy eigenstate [29]. Let H be an initial Hamiltonian and $|E_i\rangle$ be its eigenstate. We define the effective inverse temperature β_i of $|E_i\rangle$ through

$$E_i = \mathrm{Tr}[H\gamma_{\beta_i}], \tag{5.1}$$

where γ_{β_i} is the Gibbs state of the Hamiltonian H at inverse temperature β_i. The effective inverse temperature is a decreasing function of E_i, and $\beta_i > 0$ ($\beta_i < 0$) corresponds to the positive (negative) temperature. The Gibbs state at a positive temperature is passive, but that at a negative temperature is not passive. Correspondingly, the second law is only valid for positive-temperature states, and we focus on the eigenstates at $\beta_i > 0$. We remark that negative-temperature states are thermodynamically unstable while they have been created in experiments with ultracold atoms [215, 216].

Because the ETH depends on the choice of the observable, we define the eigenstate second law as an operation-dependent property as follows: For a given unitary operation U, we say that the eigenstate second law holds, if one cannot extract $\mathcal{O}(N)$ amount of work from any energy eigenstate whose effective inverse temperature is positive. That is, for sufficiently large N,

$$W_i(U) := W(|E_i\rangle\langle E_i|, U) \leq N\delta \tag{5.2}$$

holds for any $\delta > 0$ and energy eigenstate at $\beta_i > 0$. Here, $W_i(U) \leq N\delta$ represents the failure of work extraction at the macroscopic level. We expect that the eigenstate second law (5.2) holds for generic nonintegrable systems, as is the case for the ETH, as long as we only consider simple cyclic operations generated by local Hamiltonians.

We note the case that the state is given by a mixture of positive-temperature eigenstates $\rho := \sum_{i:\beta_i>0} p_i \left|E_i\right\rangle \left\langle E_i\right|$. The average work extraction from ρ is given by

$$W(\rho, U) = \sum_{i:\beta_i>0} p_i W_i(U). \tag{5.3}$$

If the eigenstate second law (5.2) holds for U, we have $W(\rho, U) \leq N\delta$, which implies that one cannot extract a macroscopic amount of work from the diagonal ensemble by U. This result is reasonable because the diagonal ensemble describes the effective stationary state, as seen in Sec. 2.1, for which we can expect that work cannot be extracted. In this sense, the eigenstate second law can be regarded as a manifestation of the second law for thermal states that is not necessarily described by conventional statistical ensembles.

We remark on coherence between the energy eigenbasis. In the conventional standard measurement scheme of work extraction [210,211], the measurement of energy is performed at the beginning and at the end of the protocol. In this case, the coherence in the initial state is destroyed by the first measurement, which changes the initial state into a diagonal ensemble. In this sense, the above argument for diagonal ensembles is applicable even in the presence of initial coherence.

5.2 Numerical verification of eigenstate second law

In this section, we numerically validate the eigenstate second law for a specific spin model with a cyclic quench protocol. Our numerical results show that the eigenstate second law is valid if at least one of the initial and quenched Hamiltonians is nonintegrable.

5.2.1 Setup

We study the one-dimensional Ising model with the next-nearest-neighbor interactions and the magnetic fields. This model is a typical example of exhibiting thermalization under unitary dynamics [92–94] and can be realized in experiments with ultracold atomic gases [217, 218]. The Hamiltonian is given by

$$H = \sum_{i=1}^{N} (gX_i + hZ_i + JZ_iZ_{i+1} + J'Z_iZ_{i+2}), \tag{5.4}$$

where X_i and Z_i denote the Pauli X and Z operators at site i, respectively. Here, g is the transverse field, h is the longitudinal field, J is the nearest-neighbor coupling constant, J' is

the next-nearest-neighbor coupling constant, and N is the number of spins. We impose the periodic boundary condition, and thus this model has translational symmetry.

The Hamiltonian (5.4) is integrable only for $g = 0$ or $h = J' = 0$. Otherwise, in fact, the level spacing distribution is well fitted by the Wigner-Dyson distribution (see Appendix of Ref. [201]). The ETH (2.23) for few-body observables holds well in the nonintegrable parameter region of this model [92–94].

We focus on a quench protocol as a simplest cyclic operation. The system is initially prepared in an eigenstate $|E_i\rangle$ of the initial Hamiltonian $H_{\rm I}$. The initial values of the magnetic fields are denoted as $g_{\rm I}$ and $h_{\rm I}$. The coupling constants do not change during the protocol. Then, we carry out the following cyclic protocol consisting of two global quenches. (i) At the initial time $t = 0$, the longitudinal field and transverse field are suddenly changed ($h_{\rm I} \to h_{\rm Q}, g_{\rm I} \to g_{\rm Q}$). We denote the postquench Hamiltonian by $H_{\rm Q}$. (ii) The eigenstate of $H_{\rm I}$ evolves according to the postquench Hamiltonian during the waiting time, i.e., $U = e^{-iH_{\rm Q}\tau}$. (iii) At time $t = \tau$, the external fields are quenched back to the initial values ($h_{\rm Q} \to h_{\rm I}, g_{\rm Q} \to g_{\rm I}$), and the Hamiltonian is restored to the initial one.

The average work extraction in this protocol is given by

$$W_i = E_i - \langle E_i | e^{iH_{\rm Q}\tau} H_{\rm I} e^{-iH_{\rm Q}\tau} | E_i \rangle \,. \tag{5.5}$$

We calculate W_i for all the energy eigenstates by using exact numerical diagonalization and consider all of the four combinations of the integrability of Hamiltonians: (a) $H_{\rm I}$ is nonintegrable and $H_{\rm Q}$ is nonintegrable; (b) $H_{\rm I}$ is integrable and $H_{\rm Q}$ is nonintegrable; (c) $H_{\rm I}$ is nonintegrable and $H_{\rm Q}$ is integrable; (d) $H_{\rm I}$ is integrable and $H_{\rm Q}$ is integrable.

5.2.2 Distribution of work

We first investigate the distribution of the average work extraction W_i. The waiting time after the first quench is taken to be much longer than the relaxation time ($\tau = 10^4$). We show the τ-dependence of extracted work later.

In Fig. 5.2, we plot W_i/N for all the energy eigenstates in the full spectrum with respect to the eigenenergy density E_i/N for $N = 12$ and $N = 18$. We here divided the extensive quantities W_i and E_i by N to normalize them. For all the cases, W_i tends to be negative (positive) for the positive (negative) temperature eigenstate.

In the case of (a), (b), and (c), where $H_{\rm I}$ and/or $H_{\rm Q}$ are nonintegrable, the distribution of W_i/N tends to get narrower in the horizontal direction as N increases and seems to collapse to a single curve in the thermodynamic limit $N \to \infty$. This behavior is akin to the distribution of diagonal matrix elements in nonintegrable systems [28, 92, 96, 98, 104]. Moreover, in these cases, there exists no energy eigenstate with $W_i > 0$ in the positive-temperature region for $N = 18$. This suggests that the eigenstate second law is valid in these cases.

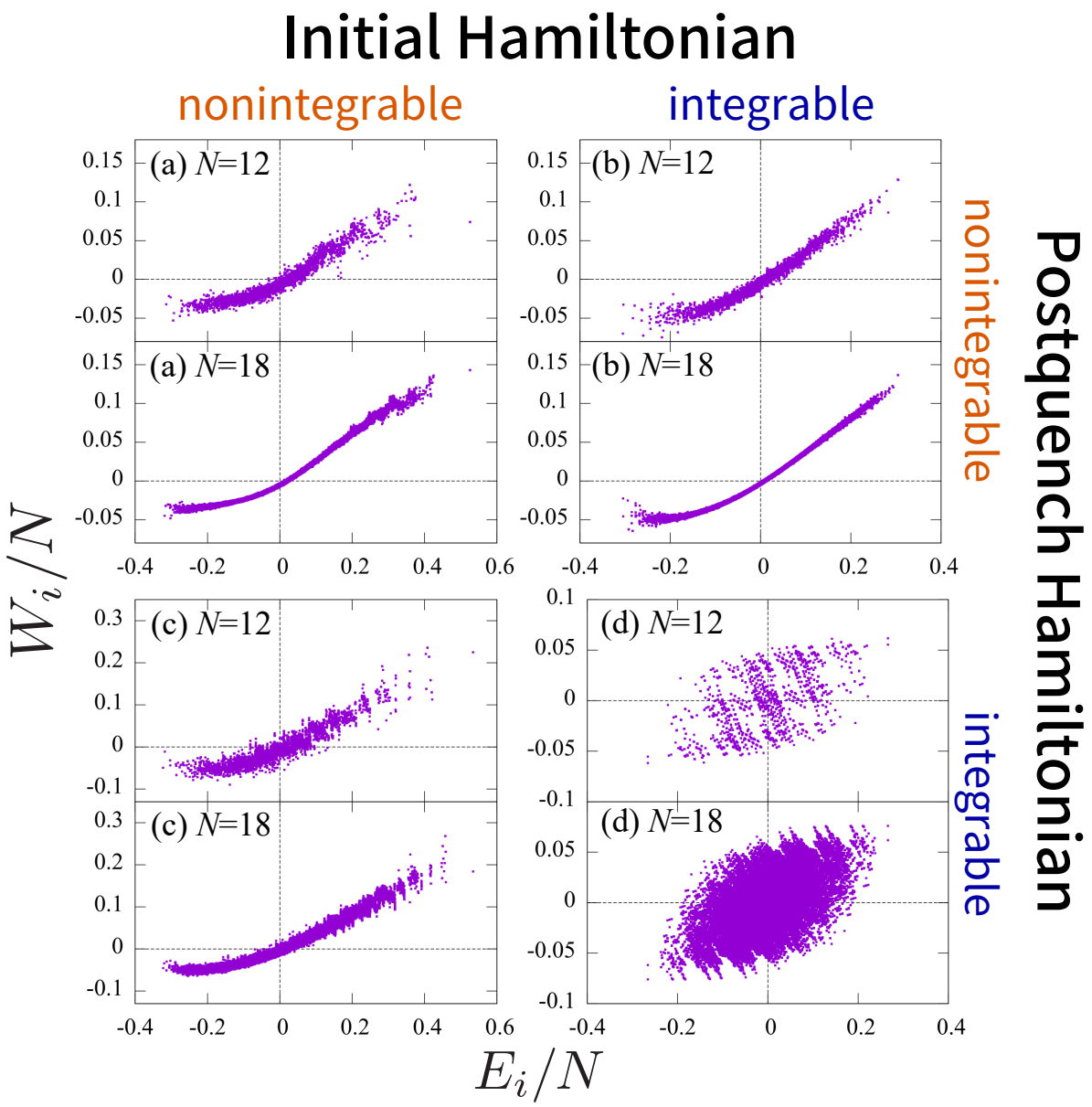

Fig. 5.2 The distribution of the average work extraction W_i/N for $N = 12$ (upper panels) and $N = 18$ (lower panels). Each point represents an energy eigenstate in the full spectrum. We set the nearest-neighbour interaction $J = 1$ and the waiting time $\tau = 10^4$. The vertical dashed line indicates the energy at infinite temperature, and the horizontal one indicates $W_i = 0$. The left (right) side of the vertical line corresponds to the positive-temperature (negative-temperature) region. Quench from (a) nonintegrable to nonintegrable ($J = J' = 1, g_{\rm I} = g_{\rm Q} = (\sqrt{5}+5)/8, h_{\rm I} = 0 \to h_{\rm Q} = 1.0$), (b) integrable to nonintegrable ($J = 1, J' = 0, g_{\rm I} = g_{\rm Q} = (\sqrt{5}+5)/8, h_{\rm I} = 0 \to h_{\rm Q} = 1.0$), (c) nonintegrable to integrable ($J = 1, J' = 0, g_{\rm I} = g_{\rm Q} = (\sqrt{5}+5)/8, h_{\rm I} = 1.0 \to h_{\rm Q} = 0$), and (d) integrable to integrable ($J = 1, J' = 0, h = 0, g_{\rm I} = 0.5 \to g_{\rm Q} = 1.5$). Reproduced from Fig. 1 of [201]. ©2019 American Physical Society.

On the other hand, in the case of (d), where both $H_{\rm I}$ and $H_{\rm Q}$ are integrable, the distribution is more scattered in the horizontal direction than the other cases. In this case, the distribution does not seem to collapse to a single curve, which is analogous to the distribution of diagonal matrix elements in integrable systems [28, 85, 88]. Contrary to the other cases, there are many eigenstates with $W_i > 0$ in the positive-temperature region, even for $N = 18$. Thus, the eigenstate second law is not valid in the case of (d). In the next subsection, we quantitatively check the above arguments of the validity of the eigenstate second law by investigating the scaling of the number of work-extractable energy eigenstates.

We next study the dependence of the distribution of W_i on the waiting time τ. Figure 5.3 shows the scatter plots of W_i/N for the waiting time $\tau = 10^{-1}, 10^0, 10^1, 10^2, 10^3, 10^4, 10^5$. When the waiting time is short ($\tau = 10^{-1}$), W_i/N is almost zero for all the energy eigenstates because the system remains close to the initial state. The average work begins to be a non-zero value at $\tau = 10^{-1}$ and does not vary significantly after $\tau = 10^2$. In particular, as for the cases of (a), (b), and (c), the distributions of W_i/N look the same for $\tau = 10^2, 10^3, 10^4, 10^5$ in each case. This suggests that the temporal fluctuations are negligible in these three cases. On the other hand, in the case of (d), the distributions of W_i/N are not the same for $\tau = 10^2, 10^3, 10^4, 10^5$. This is reasonable because integrable systems exhibit more significant temporal fluctuations than nonintegrable systems [35, 219].

5.2.3 Dependence on the size and integrability

To confirm the validity of the eigenstate second law, we investigate the dependence of the ratio of work-extractable eigenstates on the system-size. In the context of the foundation of statistical mechanics, negative-temperature states are not important because they are not thermodynamically stable for large systems. We thus count the number of work-extractable eigenstates in the positive-temperature region.

We note that the effective inverse temperature fluctuates due to the finite-size effect, and this fluctuation mixes positive-temperature eigenstates and negative-temperature eigenstates around $\beta_i = 0$. To overcome this problem, we set a threshold for the effective inverse temperature, denoted as $\beta_{\rm cut}$. Then, we consider all the energy eigenstates with $\beta_i \geq \beta_{\rm cut}$ and denote the number of them by $d_{\beta_{\rm cut}}$.

We count the number of energy eigenstates that violate the eigenstate second law. Let $d_\delta^{\rm out}$ be the number of eigenstates such that $\beta_i \geq \beta_{\rm cut}$ and $W_i/N \geq \delta$, where δ is a given positive constant. We calculate the ratio $d_\delta^{\rm out}/d_{\beta_{\rm cut}}$ with changing the system-size N and the integrability of the Hamiltonians.

Figure 5.4 shows the N-dependence of the ratio $d_\delta^{\rm out}/d_{\beta_{\rm cut}}$ for all the combinations of the integrability of the initial and post-quench Hamiltonians. In the case of (a), (b), and (c), where $H_{\rm I}$ and/or $H_{\rm Q}$ are nonintegrable, $d_\delta^{\rm out}/d_{\beta_{\rm cut}}$ decays more rapidly than an exponential

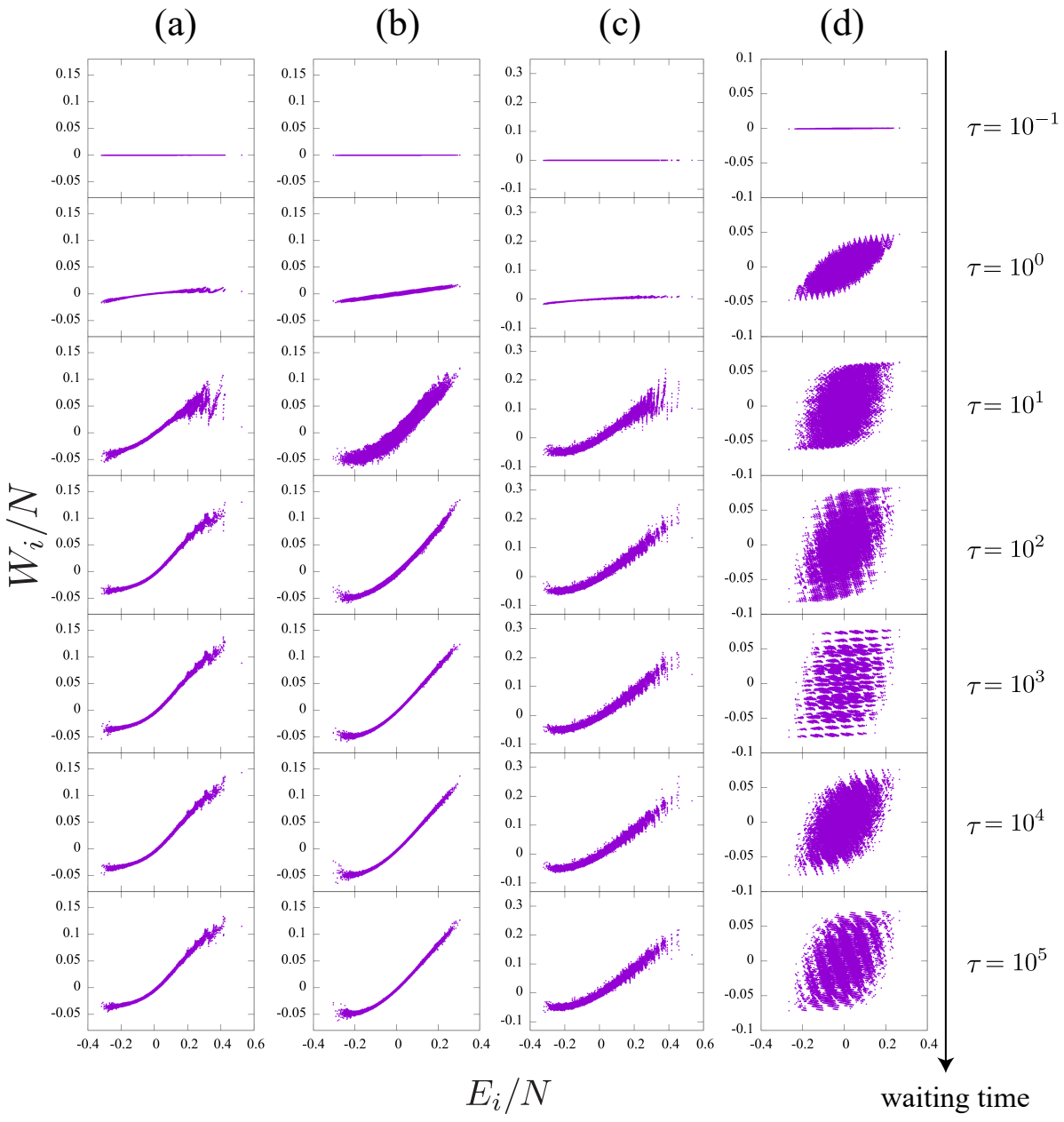

Fig. 5.3 The average work extraction W_i/N for $N = 18$ with the waiting time $\tau = 10^{-1}, 10^{0}, 10^{1}, 10^{2}, 10^{3}, 10^{4}, 10^{5}$ from top to bottom. The other parameters are the same as in Fig. 5.2. Reproduced from Fig. 5 of [201]. ©2019 American Physical Society.

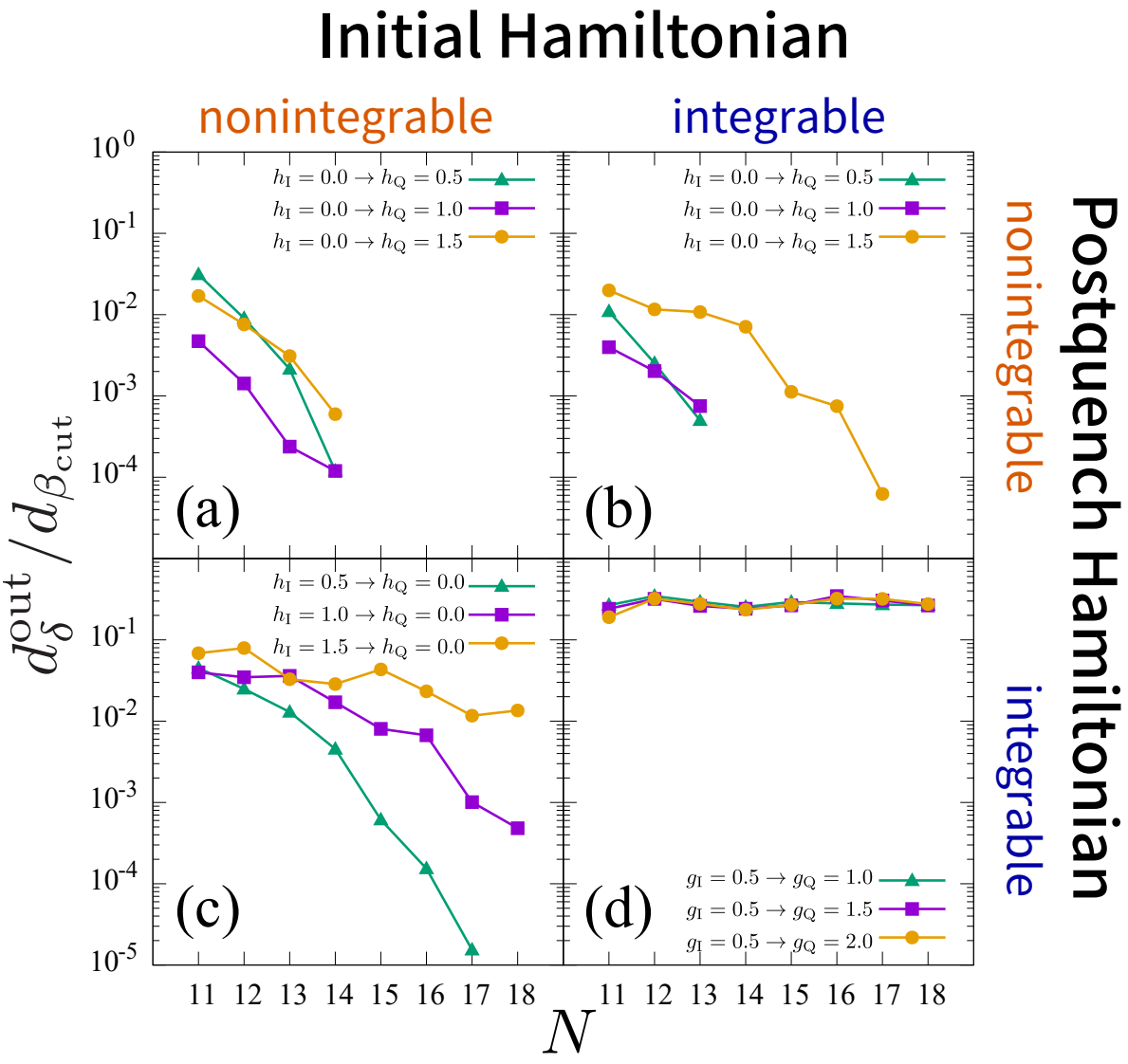

Fig. 5.4 The N-dependence of the ratio $d_\delta^{\rm out}/d_{\beta_{\rm cut}}$. The lack of data points indicates zero of $d_\delta^{\rm out}$. The parameters are set to $\tau = 10^4$, $\beta_{\rm cut} = 0.02$, and $\delta = 0.001$. Quench from (a) nonintegrable to nonintegrable ($J = J' = 1, g_{\rm I} = g_{\rm Q} = (\sqrt{5}+5)/8, h_{\rm I} = 0 \to h_{\rm Q} = 0.5, 1.0,$ and 1.5), (b) integrable to nonintegrable ($J = 1, J' = 0, g_{\rm I} = g_{\rm Q} = (\sqrt{5}+5)/8, h_{\rm I} = 0 \to h_{\rm Q} = 0.5, 1.0,$ and 1.5) , (c) nonintegrable to integrable ($J = 1, J' = 0, g_{\rm I} = g_{\rm Q} = (\sqrt{5}+5)/8, h_{\rm I} = 0.5, 1.0,$ and $1.5 \to h_{\rm Q} = 0$), and (d) integrable to integrable ($J = 1, J' = 0, h = 0, g_{\rm I} = 0.5 \to g_{\rm Q} = 1.0, 1.5,$ and 2.0). Reproduced from Fig. 2 of [201]. ©2019 American Physical Society.

Table 5.1 The validity of the eigenstate second law by our quench protocol for the four cases of the integrability. We remark that the validity of $d_\delta^{\rm out}/d_{\beta_{\rm cut}} = 0$ in the cases of (c) is not evident from Fig. 5.4 (c), while it is supported from an argument based on the ETH in Sec. 5.3 and Fig. 5.5 (c).

		Initial Hamiltonian $H_{\rm I}$	
		Nonintegrable	Integrable
Postquench	Nonintegrable	(a) True	(b) True
Hamiltonian $H_{\rm Q}$	Integrable	(c) True	(d) False

function, which implies the eigenstate second law. In particular, $d_\delta^{\rm out}$ itself becomes zero at finite N in the case of (a) and (b), where $H_{\rm Q}$ is nonintegrable. This result implies that work-extractable eigenstates vanish, and the eigenstate second law is valid even for small systems. The same argument is expected to be true in the case of (c), but that is not so evident from Figure 5.4 (c). However, our later analysis and an additional numerical result in Sec. 5.3 support that $d_\delta^{\rm out}/d_{\beta_{\rm cut}} = 0$ also holds in the case of (c).

In contrast to the cases of (a), (b), and (c), $d_\delta^{\rm out}$ itself increases exponentially with N in the case of (d). This can be seen from the fact that the number of states $d_{\beta_{\rm cut}}$ increases exponentially. This exponential growth of $d_\delta^{\rm out}$ is analogous to that of the number of athermal eigenstates in integrable systems [99]. Because integrable systems exhibit a large finite-size effect than nonintegrable systems, we cannot conclude that the ratio $d_\delta^{\rm out}/d_{\beta_{\rm cut}}$ does not decay in the case of (d).

Moreover, we mention a theoretical upper bound of $d_\delta^{\rm out}/d_{\beta_{\rm cut}}$, as will be shown in inequality (5.19). The bound predicts that $d_\delta^{\rm out}/d_{\beta_{\rm cut}}$ decreases at least exponentially with increasing the system-size, i.e., $e^{-\alpha N}$. However, in our numerical setup, the decay rate α is given by $\alpha = \beta_{\rm cut}\delta = 2 \times 10^{-5}$, which is too small to be observed in our numerical calculation.

Table 5.1 summarizes the validity of the eigenstate second law in our numerical calculations. The eigenstate second law is valid only for nonintegrable systems, which is analogous to the ETH.

5.3 Mechanism of the eigenstate second law

We next investigate the underlying mechanism of the eigenstate second law in a nonintegrable system.

5.3.1 Relationship to the ETH

The average energy after a protocol equals the expectation value of the time-evolved operator $H_{\rm I}(\tau) := UH_{\rm I}U^\dagger$ in the initial state. Correspondingly, we assume the ETH of the initial Hamiltonian for $H_{\rm I}(\tau)$ with respect to the energy eigenstates of $H_{\rm I}$, which is given by

$$\langle E_i|H_{\rm I}(\tau)|E_i\rangle \simeq \langle H_{\rm I}(\tau)\rangle_{\rm MC}\,. \tag{5.6}$$

Here, $\langle\cdots\rangle_{\rm MC}$ denotes the microcanonical average corresponding to the energy shell $I_{E,\Delta E} = [E-\Delta E, E]$, where E and ΔE are chosen as $E_i \in I_{E,\Delta E}$. As shown later, the ETH (5.6) holds true in our model (5.4) except for the case of (d).

From Eq. (5.6), the average work extraction can be written as

$$W_i \simeq E_i - \langle H_{\rm I}(\tau)\rangle_{\rm MC}\,. \tag{5.7}$$

This equality implies that the average work takes almost the same value for all the energy eigenstates in the energy shell. Because the eigenenergy E_i in the energy shell does not vary much with i, we have

$$W_i \simeq W_{\rm MC} \tag{5.8}$$

for all the eigenstate inside the energy shell, where $W_{\rm MC}$ is the average work extraction from the microcanonical state. This leads to a stronger eigenstate second law, which implies that the average work takes the thermal value (the microcanonical average) for all the energy eigenstates in the energy hell. This a stronger version of the eigenstate second law is equivalent to the ETH for $O_W := H_{\rm I} - H_{\rm I}(\tau)$.

We now show that $W_i \lesssim 0$ holds from Eq. (5.6). Let us consider the generalized microcanonical state, which is given by

$$\rho_{\rm GMC}(E) = \frac{1}{d_E}\sum_{E_i\le E} |E_i\rangle\langle E_i|\,, \tag{5.9}$$

where d_E is a normalization constant. We denote the average work extraction from the generalized microcanonical state by $W_{\rm GMC} := \langle H_{\rm I}(0)\rangle_{\rm GMC} - \langle H_{\rm I}(\tau)\rangle_{\rm GMC}$. The number of energy eigenstates in the energy shell is much larger than the number of eigenstates with energies lower than the shell, which implies that $d_{E,\Delta E}/d_E \simeq 1$. We thus have

$$\langle H_{\rm I}(0)\rangle_{\rm GMC} \simeq \langle H_{\rm I}(0)\rangle_{\rm MC}\,, \tag{5.10}$$

$$\langle H_{\rm I}(\tau)\rangle_{\rm GMC} \simeq \langle H_{\rm I}(\tau)\rangle_{\rm MC}\,. \tag{5.11}$$

From these relations and Eq. (5.8), the work extracted from $|E_i\rangle$ is approximated as

$$W_i \simeq W_{\rm GMC}. \tag{5.12}$$

As shown in Sec. 3.3, the generalized microcanonical state is passive, i.e., $W_{\rm GMC} \leq 0$, which leads to $W_i \lesssim 0$. Therefore, the eigenstate second law is justified from the ETH for $H_{\rm I}(\tau)$.

5.3.2 Numerical verification of the ETH for $H_{\rm I}(\tau)$

The validity of the ETH for $H_{\rm I}(\tau)$ is not obvious because $H_{\rm I}(\tau)$ is not a few-body operator, but contains N-body couplings in general. Here, we numerically verify the ETH for $H_{\rm I}(\tau)$ in nonintegrable systems.

To confirm the ETH (5.6), we calculate the eigenstate-to-eigenstate deviations

$$r_i := |\langle E_{i+1}|H_{\rm I}(\tau)|E_{i+1}\rangle - \langle E_i|H_{\rm I}(\tau)|E_i\rangle|\,, \tag{5.13}$$

which was introduced in Ref. [92]. If the ETH (5.6) holds, all of r_i converges to zero in $N \to \infty$. On the other hand, if there is an athermal eigenstate, the largest value of r_i remains at a non-zero value in $N \to \infty$. The decay of the average of r_i implies the weak ETH.

We consider the energy eigenstates at positive temperature as in Sec. 5.2. As in numerical verifications of the ETH [28], we remove the eigenstates locating around the edge of the spectrum, where the density of states is too low. Thus, our target states are eigenstates with $\beta_i > 0$ and $E_i \geq E_0/2$.

Figure 5.5 presents the N-dependence of the largest, the fifth largest, the tenth largest, and the average values of r_i. The average value of r_i decays exponentially with N in all the cases. This result implies that the weak ETH for $H_{\rm I}(\tau)$ holds true. The other values of r_i tends to zero only in the case of (a), (b), and (c), while does not decay in the case of (d). We thus conclude that the ETH for $H_{\rm I}(\tau)$ is valid for the case of (a), (b), and (c), where $H_{\rm I}$ and/or $H_{\rm Q}$ are nonintegrable. On the other hand, Fig. 5.5 implies that the ETH for $H_{\rm I}(\tau)$ is violated in the case of (d). These results are consistent with Table 5.1.

5.4 Weak eigenstate second law

We analytically derive the upper bound of the number of work-extractable eigenstates.

5.4.1 Assumption and the statement

In this section, we consider a general quantum system on a lattice with N sites in any spatial dimension. We denote the Hamiltonian by H and the number of its energy eigenstates whose energies are smaller than E by $d(E)$ and assume the following normal behavior of $d(E)$.

Assumption 2 (Existence of the entropy density)**.** *Let E_0 and E_∞ be the ground energy of H and the infinite-temperature energy (i.e., the average of the energy eigenvalues over all the eigenstates), respectively. Then, we assume that $u_0 := \lim_{N\to\infty} E_0/N$ and $u_\infty := \lim_{N\to\infty} E_\infty/N$*

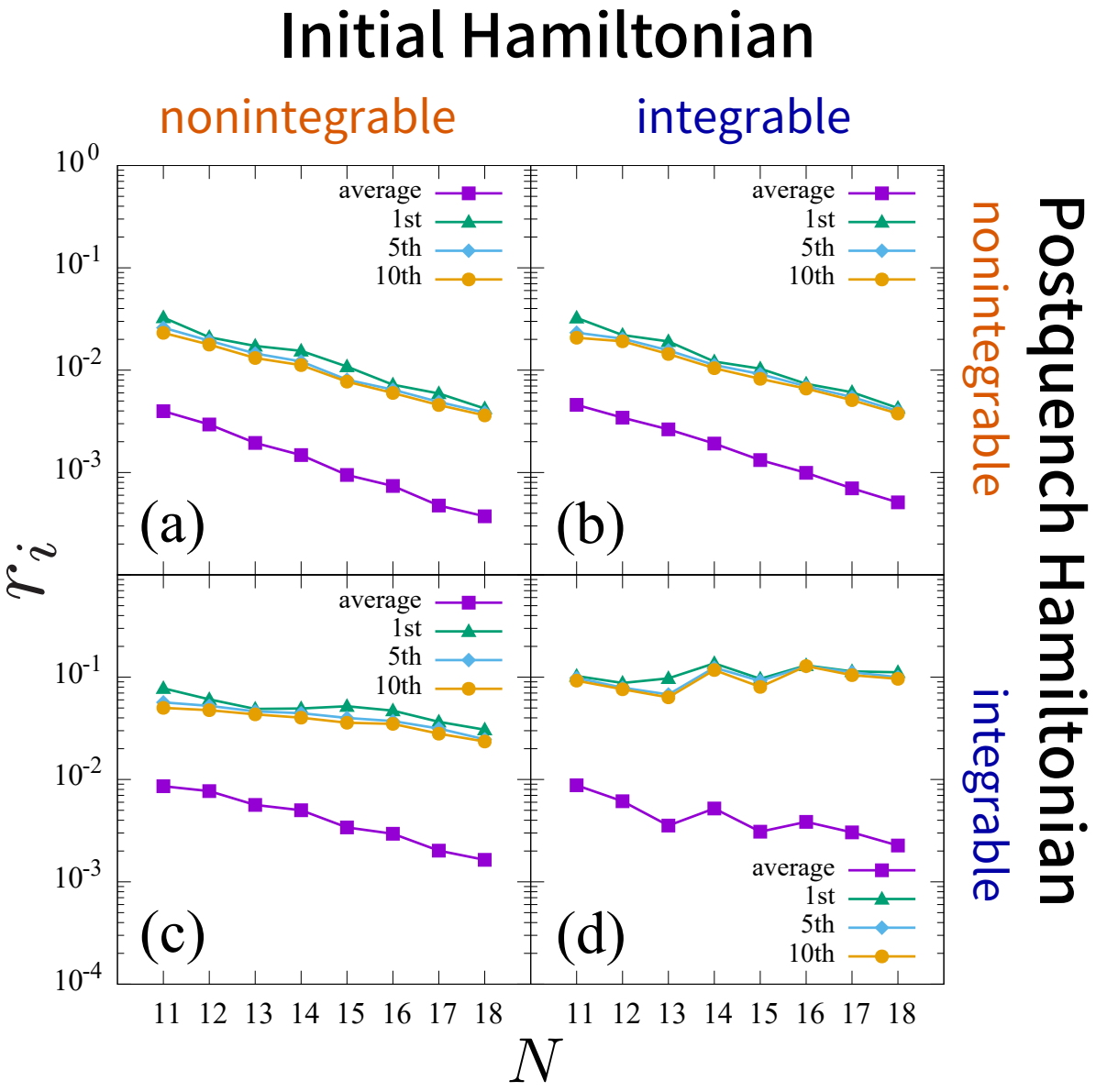

Fig. 5.5 The N-dependence of the eigenstate-to-eigenstate deviation r_i of $H_{\rm I}(\tau)$. In all the panels, the squares, triangles, diamonds, and circles represent the system-size dependence of the average, the largest, the fifth-largest, and the tenth-largest values of r_i, respectively. All the parameters are the same as in Fig. 5.2. These numerical results imply that the weak ETH for $H_{\rm I}(\tau)$ is valid for all the cases, while the ETH is valid only for the cases of (a), (b), and (c). Reproduced from Fig. 3 of [201]. ©2019 American Physical Society.

exist. For any $u \in (u_0, u_\infty)$*, we assume that*

$$\log d(uN) = N\sigma(u) + o(N), \tag{5.14}$$

where the entropy density $\sigma(u)$ *is a positive function independent of* N *and satisfies* $\beta(u) := \sigma'(u) > 0$ *and* $\sigma''(u) < 0$.

The interval (u_0, u_∞) corresponds to the positive-temperature region, and Eq. (5.14) is a standard definition of the entropy density in statistical mechanics, i.e., the Boltzmann formula. Assumption 2 is expected to be true in a large class of quantum systems and has been proved in locally interacting systems [86, 220]. We note that $d_{\beta_{\rm cut}}$ in Sec. 5.2 equals $d(E(\beta_{\rm cut}))$, where $E(\beta_{\rm cut})$ is the energy of the Gibbs state at $\beta = \beta_{\rm cut}$.

We fix an arbitrary unitary operator U, which does not necessarily represent a cyclic quench. The question here is whether the ratio of work-extractable eigenstates vanishes in the thermodynamic limit. We denote the number of energy eigenstates satisfying $W_i \geq N\delta$ with $\delta > 0$ by $d_\delta^{\rm out}(U)$:

$$d_\delta^{\rm out}(U) := \#\{E_i : E_i \leq uN \text{ and } W_i(U) \geq N\delta\}. \tag{5.15}$$

In this setup, we obtained the following upper bound of the ratio $d_\delta^{\rm out}(U)/d(uN)$. Under Assumption 2, for any $\delta > 0$, $u \in (u_0, u_\infty)$, and an arbitrary fixed unitary U, we have

$$\frac{d_\delta^{\rm out}(U)}{d(uN)} \leq e^{-N\beta(u)\delta/2 + o(N)}. \tag{5.16}$$

The derivation of this is presented in the next subsection. We note that this bound holds not only for nonintegrable systems but also for integrable systems if only Assumption 2 is satisfied.

Inequality (5.16) implies that the ratio of energy eigenstates breaking the second law vanishes in the thermodynamic limit. Thus, inequality (5.16) can be regarded as a weaker version of the eigenstate second law. Furthermore, the ratio must decrease at least exponentially with the system-size. This is similar to the large deviation-type bound of the weak ETH (2.35), which implies that the ratio of athermal eigenstates decreases at least exponentially as well. In spite of this apparent similarity, our proof of inequality (5.16) is essentially different from that of the weak ETH.

5.4.2 Derivation of inequality (5.16)

Let us prove inequality (5.16). We first prove an upper bound on a bit different quantity from $d^{\rm out}(U, N\delta)$, and the bound of $d^{\rm out}(U, N\delta)$ is derived as a corollary of it.

Although we have focused on the mean value of work so far, we here consider the stochastic work [210, 211] and its distribution. The stochastic work is defined through two projective measurements of the energy at the beginning and at the end of the protocol. For two outcomes

E_i and E_j of the energy measurements, the stochastic work extracted from the system is given by $w_{i\to j} := E_i - E_j$. For an initial state ρ and a cyclic protocol U, the work distribution $P_{(\rho,U)}(w)$ is given by

$$P_{(\rho,U)}(w) := \sum_{i,j} \delta(w_{i\to j} - w) \left|\langle E_j|U|E_i\rangle\right|^2 \langle E_i|\rho|E_i\rangle \,. \tag{5.17}$$

The cumulative distribution is denoted by $P_{(\rho,U)}(w \geq x) := \int_x^\infty P_{(\rho,U)}(w)dw$. For an energy eigenstate $|E_i\rangle$, we will also use a shorthand notation $P_{(i,U)}(w \geq x) := P_{(|E_i\rangle\langle E_i|,U)}(w \geq x)$. Specifically, we investigate the possibility of extracting a significant amount of work for large N, and thus set $x = N\delta$ with $\delta > 0$.

We focus on energy eigenstates with $E_i \leq uN$ for a given energy density u and denote the number of energy eigenstates with $P_{(i,U)}(w \geq N\delta)$ being larger than ϵ by $\tilde{d}^{\rm out}_{\epsilon,\delta}(U)$:

$$\tilde{d}^{\rm out}_{\epsilon,\delta}(U) := \#\{E_i : E_i \leq uN \text{ and } P_{(i,U)}(w \geq N\delta) \geq \epsilon\}. \tag{5.18}$$

If $P_{(i,U)}(w \geq N\delta)$ is negligibly small on a macroscopic scale, there is no chance to extract a macroscopic amount of work from $|E_i\rangle$, which is consistent with the second law. Therefore, $\tilde{d}^{\rm out}_{\epsilon,\delta}(U) \to 0$ implies the eigenstate second law, while $\tilde{d}^{\rm out}_{\epsilon,\delta}(U)/d(uN) \to 0$ implies the weak eigenstate second law.

We can obtain the following upper bound of $\tilde{d}^{\rm out}_{\epsilon,\delta}(U)$, which implies the weak eigenstate second law.

Proposition 2. *Under Assumption 2, for any $\delta > 0$, $u \in (u_0, u_\infty)$, $\epsilon \geq e^{-N\beta(u)\delta/2}$, and an arbitrary fixed unitary U, we have*

$$\frac{\tilde{d}^{\rm out}_{\epsilon,\delta}(U)}{d(uN)} \leq e^{-N\beta(u)\delta/2+o(N)}. \tag{5.19}$$

Inequality (5.19) implies that the probability of extracting macroscopic amount of work decays exponentially with N for most energy eigenstates. In other words, the energy distribution of the final state satisfies the large deviation principle [221]. The proof of inequality (5.19) is as follows.

Proof. From Markov's inequality, we have

$$\frac{\tilde{d}^{\rm out}_{\epsilon,\delta}(U)}{d(uN)} \leq \frac{1}{\epsilon d(uN)} \sum_{i:E_i\leq uN} P_{(i,U)}(w \geq N\delta). \tag{5.20}$$

By using the definition of the cumulative distribution, we can rewrite the summation in the right-hand side of the above as

$$\sum_{i:E_i\leq uN} P_{(i,U)}(w \geq N\delta) = \sum_{i:E_i\leq uN} \sum_{j:E_j\leq E_i-N\delta} \left|\langle E_j|U|E_i\rangle\right|^2 . \tag{5.21}$$

Then, the right-hand side is evaluated as

$$\sum_{i:E_i\le uN}\sum_{j:E_j\le E_i-N\delta}|\langle E_j|U|E_i\rangle|^2 \le \sum_{j:E_j\le uN-N\delta}\sum_{i:E_i\le uN}|\langle E_j|U|E_i\rangle|^2 \tag{5.22}$$

$$\le \sum_{j:E_j\le uN-N\delta}1 \tag{5.23}$$

$$= d((u-\delta)N), \tag{5.24}$$

where we used $\sum_{i:E_i\le uN}|\langle E_j|U|E_i\rangle|^2 \le 1$ to get the second line. We thus have

$$\frac{\tilde{d}^{\rm out}_{\epsilon,\delta}(U)}{d(uN)} \le \frac{d((u-\delta)N)}{\epsilon d(uN)}. \tag{5.25}$$

We next evaluate $d((u-\delta)N)/d(uN)$. By using Assumption 2, we have

$$\frac{d((u-\delta)N)}{d(uN)} = e^{-N\{\sigma(u)-\sigma(u-\delta)\}+o(N)}, \tag{5.26}$$

$$\le e^{-N\beta(u)\delta+o(N)}, \tag{5.27}$$

where we used $\sigma(u)\ge\sigma(u-\delta)+\beta(u)\delta$. Therefore, we have

$$\frac{\tilde{d}^{\rm out}_{\epsilon,\delta}(U)}{d(uN)} \le e^{-N\beta(u)\delta+o(N)}/\epsilon. \tag{5.28}$$

By setting $\epsilon = e^{-N\beta(u)\delta/2}$, we obtain the desired bound (5.19). □

We derive an upper bound of $d^{\rm out}_\delta(U)$ from inequality (5.19). If $P_{(i,U)}(w\ge N\delta)\le\epsilon$, the average work $W_i = \int wP_{(i,U)}(w)dw$ is upper bounded as

$$W_i = \int_{w_{\min}}^{N\delta} P_{(i,U)}(w)dw + \int_{N\delta}^{w_{\max}} P_{(i,U)}(w)dw \tag{5.29}$$

$$\le N\delta(1-\epsilon) + w_{\max}\epsilon, \tag{5.30}$$

where $w_{\min}$ and $w_{\max}$ are the minimum and maximum values of stochastic work, respectively. We note that $w_{\max}\le 2\|H\| = \mathcal{O}(N)$. By setting $\epsilon = e^{-N\beta(u)\delta/2}$, we can show that

$$W_i \le N\delta + o(1). \tag{5.31}$$

From this inequality, we obtain $d^{\rm out}_\delta(U)\le\tilde{d}^{\rm out}_{\epsilon,\delta}(U)$, which implies inequality (5.16).

5.4.3 Impossibility of work extraction from a pure state with large coherence

We next consider a pure state which has a large amount of coherence in the energy eigenbasis and prove the impossibility of work extraction from that state. Let $|\psi\rangle$ be a pure state in the Hilbert space of the positive-temperature region, i.e., $|\psi\rangle = \sum_{i:E_i\le uN} c_i|E_i\rangle$. The

corresponding density operator is written by $\rho = |\psi\rangle\langle\psi|$. We consider an arbitrary unitary operation U and show that $W(\rho, U) \lesssim N\delta$.

We apply the two-point measurement scheme described in Sec. 5.4.2. The cumulative distribution of the stochastic work for ρ can be written as

$$P_{(\rho,U)}(w \geq N\delta) = \sum_{i:E_i \leq uN} |c_i|^2 P_{(i,U)}(w \geq N\delta). \tag{5.32}$$

From this and the Cauchy-Schwartz inequality, we have

$$P_{(\rho,U)}(w \geq N\delta) \leq \sqrt{\left(\sum_{i:E_i \leq uN} P_{(i,U)}(w \geq N\delta)^2\right)\left(\sum_{i:E_i \leq uN} |c_i|^4\right)} \tag{5.33}$$

$$\leq \sqrt{\frac{\epsilon^2(d(uN) - \tilde{d}^{\mathrm{out}}_{\epsilon,\delta}(U)) + \tilde{d}^{\mathrm{out}}_{\epsilon,\delta}(U)}{d_{\mathrm{eff}}}}, \tag{5.34}$$

where we denoted the effective dimension by $d_{\mathrm{eff}} = 1/\sum_i |c_i|^4$. The effective dimension can be regarded as a measure of coherence of pure states; The large effective dimension implies a large amount of coherence. By setting $\epsilon = e^{-N\beta(u)\delta/2}$ and using inequality (5.19), we have

$$P_{(\rho,U)}(w \geq N\delta) \leq \sqrt{\frac{d(uN)e^{-N\beta(u)\delta/2+o(N)}}{d_{\mathrm{eff}}}}. \tag{5.35}$$

Then, we can bound the average work extraction as

$$W(\rho, U) = \int_{w_{\min}}^{N\delta} P_{(\rho,U)}(w)dw + \int_{N\delta}^{w_{\max}} P_{(\rho,U)}(w)dw \tag{5.36}$$

$$\leq N\delta(1 - P_{(\rho,U)}(w \geq N\delta)) + w_{\max}P_{(\rho,U)}(w \geq N\delta), \tag{5.37}$$

$$\leq N\delta + w_{\max}\sqrt{\frac{d(uN)e^{-N\beta(u)\delta/2+o(N)}}{d_{\mathrm{eff}}}}. \tag{5.38}$$

We assume that $d_{\mathrm{eff}} \gg d(uN)e^{-N\beta(u)\delta/2} = e^{N(\sigma(u)-\beta(u)\delta/2)+o(N)}$, which means that $\rho = |\psi\rangle\langle\psi|$ have a large amount of coherence in the energy eigenbasis. In particular, a typical pure state with respect to the Haar measure satisfies this assumption [74]. In this case, we have $W(\rho, U) \lesssim N\delta$ for any protocol U. We thus conclude that one cannot extract a macroscopic amount of work from $|\psi\rangle$.

5.5 Conclusion

In this chapter, we have investigated the possibility of extracting an extensive amount of work from individual energy eigenstates. Inspired by the eigenstate thermalization, we have proposed the eigenstate second law (5.2), which states that work extraction is impossible from

any energy eigenstate by a simple cyclic protocol. As the ETH leads to thermalization for generic initial states, the eigenstate second law ensures the second law in quantum many-body systems.

We have numerically investigated the validity of the eigenstate second law in the mixed-filed Ising model (5.4) for a cyclic quench protocol. Our numerical results are summarized in Table 5.1. We have found that the eigenstate second law is valid if at least one of the Hamiltonians is nonintegrable, while it does not hold in the integrable case. These results suggest that, in nonintegrable systems, the second law is applicable even to a single energy eigenstate, which is not a statistical mixture but also highly entangled. In addition, we proved the weaker version of the eigenstate second law (inequality (5.16)), which implies that work extraction is impossible from *almost all* energy eigenstates. This is valid regardless of the integrability and is analogous to the weak ETH.

We expect that the eigenstate second law holds for a much wider class of nonintegrable systems and protocols, as is the case for the ETH. In fact, we have shown that the eigenstate second law can be derived from the ETH for a nonlocal observable. Therefore, we can say that chaotic properties of eigenstates provide a consistent view of the microscopic origin of the second law and that of thermalization. Future studies would reveal a more comprehensive understanding of the relationship among quantum chaos, the ETH, and the second law.

Many-body localization (MBL) systems [102,222,223] do not satisfy the weak ETH, because they breaks translation symmetry and their energy eigenstates do not obey the volume law of entanglement entropy. Thus, it is reasonable to expect that the eigenstate second law is violated in MBL systems. If this observation is true, energy eigenstates of MBL systems can be used as an energy storage, i.e., quantum battery [150, 224, 225]. The validity of the eigenstate second law in MBL systems is a fascinating future issue.

Chapter 6

Higher-order extension of the ETH

In this chapter, we attempt to characterize complexity of quantum many-body dynamics by extending the ETH, which is based on our paper [226]. We first discuss the complexity of quantum chaotic dynamics and highlight the difficulty of quantifying the complexity in Sec. 6.1. On the basis of techniques of quantum information theory reviewed in Sec. 4.3, our extension of the ETH, termed the k-ETH, is formalized in Sec. 6.2. In Sec. 6.3, we discuss how the k-ETH is related to the value of the $2k$-point OTOC at late times. In Sec. 6.4, we derive the finite-temperature Page curve for the kth-Rényi entanglement entropy (k-REE) of individual energy eigenstates from the k-ETH. In Sec. 6.5, we introduce an extension of entanglement entropy to operator space called operator space entanglement entropy (OSEE), and derive the finite-temperature Page curve of the OSEE. These results suggest that the Page curve characterizes the high-order complexity of chaotic many-body systems. In Sec. 6.6, we numerically verify the 2-ETH by investigating the finite-size scaling analysis for a nonintegrable spin model.

6.1 Complexity of chaotic dynamics

Chaos in quantum many-body systems is expected to have hierarchical structure. Starting from a simple initial state, such as the product state $|\psi(0)\rangle = |00\cdots0\rangle$, a quantum state will become more and more chaotic as time goes by. Such a simple initial state will first relax to a thermal equilibrium, where any local observable equal its thermal equilibrium value. After that, $|\psi(t)\rangle$ will be scrambled, i.e., information is delocalized over the entire system. Even-

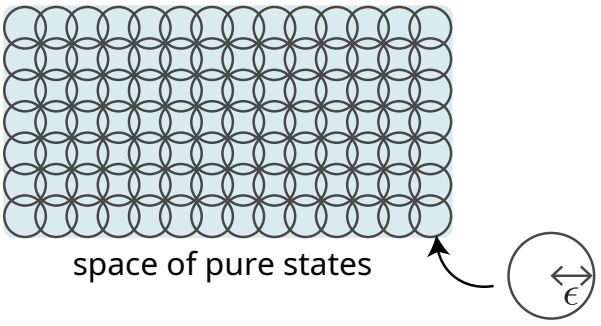

Fig. 6.1 Schematic of covering the space of pure quantum state with small round patches with radius ϵ. The number of patches is $e^{e^{\mathcal{O}(N)}}$.

tually, $|\psi(t)\rangle$ would reach a pseudorandom state, which is hardly distinguished from truly random states. These three phenomena are referred to as thermalization, information scrambling, and (pseudo)randomization, respectively. In this thesis, we have separately discussed these characteristics of quantum many-body chaos in Secs. 2.1, 4.2, and 4.3. Our fundamental question is how various chaotic phenomena emerge from local Hamiltonian dynamics. To address this question, we first reconsider quantum many-body dynamics from the viewpoint of *complexity*.

Complexity (or, more precisely, circuit complexity) is an essential concept in computation theory. The complexity of a quantum state, denoted by $\mathcal{C}$, is defined as the minimal number of quantum gates needed to generate it within a fixed small error ϵ from a product state [227]. Obviously, the initial product state in a quench experiment has the minimum complexity, i.e., $\mathcal{C}(0) = 0$. On the other hand, pseudorandom states at late times will have an exponentially large amount of complexity [183]. In fact, the complexity of a random pure state is exponentially large in the system size N, which can be seen as follows. An ϵ-net divides the space of quantum states into many small patches (see Fig. 6.1), and the number of these patches is doubly exponential in N. However, the number of quantum circuits constructed from t gates grows exponentially with t. From these two countings, we can conclude that most quantum states require an exponentially large number of gates to generate. Form the above argument, it is reasonable to expect that the complexity increases with time and saturates at almost the maximum value after a long time, i.e., $\mathcal{C}(t) \approx \mathcal{C}_{\max} = e^{\mathcal{O}(N)}$ [228]. This behavior is illustrated in Fig. 6.2 and would be regarded as an essence of quantum many-body chaos.

In a quantum circuit, the number of gates increases linearly with a time step. However, the complexity might not necessarily increase linearly, because the complexity is defined as the *minimum* number of gates needed to generate, and our circuit might be inefficient. If a more efficient preparation of the state existed, the complexity would be smaller than the number of gates in the circuit itself. For this reason, it is challenging to rigorously obtain the actual value of the complexity of a given quantum circuit and also of a Hamiltonian dynamics [228].

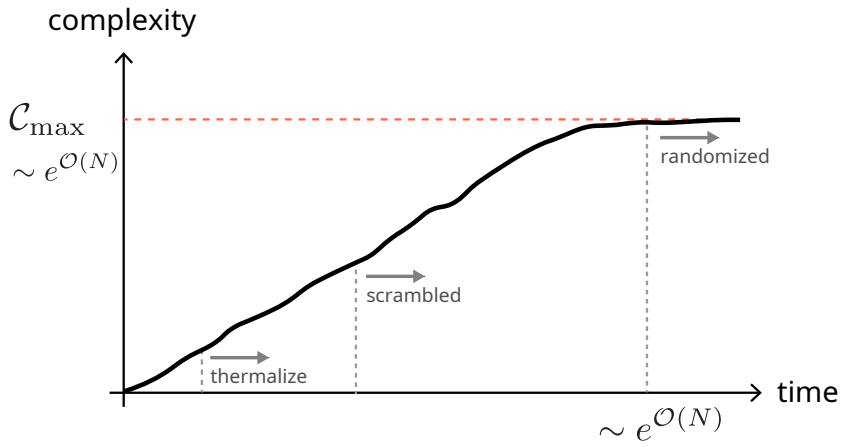

Fig. 6.2 Schematic of the expected complexity growth in a fully chaotic quantum system [230, 231]. The quantum circuit complexity is initially zero and increases linearly with time. After an exponentially long time, the complexity saturates at the maximum value $\mathcal{C}_{\max}$ within temporal fluctuations.

Local random quantum circuits are good toy models for chaotic quantum many-body dynamics. They are lattice systems for which the time evolution is given by randomly sampled unitary operators acting on neighboring sites. Random circuits have been extensively studied in the context of entanglement growth [232] and operator spreading [171]. Moreover, it is known that they form approximate unitary k-designs in polynomial time [196, 197]. Random circuits are also good toy models for studying the complexity growth because there is a specific connection between unitary k-designs and the complexity [188, 189, 197, 199]. Roughly speaking, approximate unitary k-designs have $\mathcal{O}(k)$ complexity [189, 197]. Quite recently, Brandão *et al.* [188] derived a rigorous lower bound of the complexity of local random circuits on the basis of the above fact. Their result supports a conjecture of the linear growth of the complexity of chaotic dynamics [229–231].

On the other hand, many-body dynamics generated by a time-independent Hamiltonian never form approximate unitary k-designs because of energy conservation [199] (see Sec. 7.1 for more details). However, chaotic dynamics are similar to pseudorandom dynamics (unitary designs) at least the lowest order complexity. Here by the lowest order complexity, we mean the complexity of unitary 1-designs. The average of an observable O over a unitary 1-design equals the uniform average of O in the Hilbert space. This argument closely resembles ergodicity (i.e., the long-time average equals the uniform average). We investigate this similarity more explicitly in Sec. 6.2.

The ETH is often regarded as a quantum counterpart of ergodicity. Thus, it is reasonable to consider that the ETH reflects the lowest order complexity of chaotic dynamics. On the other hand, we have relatively little knowledge of the higher-order complexity. While infor-

mation scrambling may be related to the second-order complexity because unitary 2-designs achieve perfect information scrambling, some unitary 1-designs (e.g., Pauli ensemble) are not a scrambler [199]. However, this argument does not fully explain the relationship between information scrambling and higher-order complexity. In fact, Huang *et al.* [233] proved, only using the conventional ETH (2.23), that the late-time value of the 4-point OTOC approaches to zero in the thermodynamic limit, which suggests that higher-order complexity might not be necessary, while sufficient, for information scrambling quantified by the OTOC.

To summarize, characterizing the higher-order order complexity of chaotic Hamiltonian dynamics is an important issue in quantum chaos but difficult. In the next section, we propose a new approach to this issue by considering the higher-order extension of the ETH.

6.2 k-ETH

6.2.1 Long time ensemble

We first show our setup and introduce the long-time ensemble (LTE) to deal with the typical behavior of the Hamiltonian dynamics at late times. The setup is almost the same as in the previous chapters: The system is on a lattice with N sites and isolated from environments. In this chapter, for simplicity, we suppose that the system does not have any symmetry and any few-body conserved quantities except for the total energy, and there is no degeneracy in the eigenenergies.

Because of energy conservation, the dynamics cannot mix states with different energies. We thus focus on the energy eigenstates within an energy shell $I_{E,\Delta E} := [E - \Delta E, E]$ with a given energy E and an energy width ΔE. The number of the energy eigenstates whose eigenenergies are in $I_{E,\Delta E}$ is denoted by $d := d_{E,\Delta E}$. Boltzmann's formula (5.14) implies that d increases exponentially with N. An eigenenergy in $I_{E,\Delta E}$ is denoted by E_i ($i = 1, \dots, d$), the corresponding energy eigenstate is denoted by $|E_i\rangle$, and a Hilbert space spanned by $\{|E_i\rangle : i = 1, \dots, d\}$ is denoted by $\mathcal{H} := \mathcal{H}_{E,\Delta E}$. We note that $\mathcal{H}$ is a subspace of the total Hilbert space of the many-body system. The Hamiltonian of the system is represented as $H = \sum_{i=1}^{d} E_i |E_i\rangle \langle E_i|$.

Our focus here is the late-time behavior of e^{-iHt}. We thus introduce the LTE $\mathsf{L} := \{e^{-iHt}\}_{t\in(0,\infty)}$ as an one-parameter ensemble satisfying

$$\mathbb{E}_{U\sim\mathsf{L}}[f(U)] = \lim_{\tau\to\infty} \frac{1}{\tau} \int_0^\tau f(e^{-iHt}) dt \tag{6.1}$$

for any function f. The right-hand side of the above is the long-time average of $f(e^{-iHt})$. In other words, the LTE represents uniformly sampling of e^{-iHt} from $t = 0$ to $t = \infty$.

To see the properties of the LTE, let us consider the corresponding 1-fold channel. From

the definition (6.1), the action of the 1-fold channel of the LTE for an operator $O \in \mathcal{B}(\mathcal{H})$ is given by

$$\Phi_{\mathsf{L}}^{(1)}(O) = \lim_{\tau\to\infty} \frac{1}{\tau} \int_0^\tau O(t)dt = \sum_i |E_i\rangle \langle E_i|O|E_i\rangle \langle E_i| \,, \tag{6.2}$$

where we used the no-degeneracy condition. This equality implies that $\Phi_{\mathsf{L}}^{(1)}$ is a completely dephasing channel in the energy eigenbasis.

By using the 1-fold channel, we revisit quantum ergodicity[*1], which can be regarded as a characterization of the lowest-order complexity of chaotic Hamiltonian dynamics. We define quantum ergodicity for a given operator $O \in \mathcal{B}(\mathcal{H})$ by

$$\Phi_{\mathsf{L}}^{(1)}(O) = \Phi_{\mathsf{H}}^{(1)}(O), \tag{6.3}$$

where H is the HRU. As seen from Eq. (6.2), the left-hand side of Eq. (6.3) is the long-time average of O in the Heisenberg picture. On the other hand, the right-hand side of Eq. (6.3) is the microcanonical average of O, which is given by

$$\Phi_{\mathsf{H}}^{(1)}(O) = \langle O\rangle_{\mathrm{MC}} I, \tag{6.4}$$

where $\langle O\rangle_{\mathrm{MC}} := d^{-1}\sum_i \langle E_i|O|E_i\rangle$, and I is the identity operator on $\mathcal{H}$ (see Appendix A for the derivation). That is, Eq. (6.3) states that the long-time average of O equals the microcanonical average for all initial states.

Furthermore, we can derive the conventional ETH as an equivalent representation of Eq. (6.3). By taking the average of the both sides of Eq. (6.3) in an energy eigenstate $|E_i\rangle$, we have

$$\langle E_i|O|E_i\rangle = \langle O\rangle_{\mathrm{MC}} \tag{6.5}$$

for all $i = 1, \ldots, d$, which is identically the ETH. Thus, we can regard the ETH as a quantum analog of ergodicity. We note that Eq. (6.5) is stronger than the definition of the ETH (2.23) given in Sec. 2.2, because the present definition does not allow any finite-size deviation.

6.2.2 Formulation of the k-ETH

Let us formulate the higher-order generalization of the ETH, which is named the k-ETH. There are two steps to obtain the explicit expression of the k-ETH. The first step is to formulate the higher-order extension of quantum ergodicity (6.3). The second step is to represent it in terms of the energy eigenbasis in the same manner as in Eq. (6.5).

[*1] We note that there are several formalisms of quantum ergodicity (see, e.g., Refs. [234, 235]).

As in the definition of unitary k-designs, we consider the k-replicated Hilbert space $\mathcal{H}^{\otimes k}$ and the k-fold channel, which is the main idea of the k-ETH. The natural extension of Eq. (6.3) to the k-replicated system is given by

$$\Phi_{\mathsf{L}}^{(k)}(O) = \Phi_{\mathsf{H}}^{(k)}(O) \tag{6.6}$$

for a given $O \in \mathcal{B}(\mathcal{H}^{\otimes k})$. We call this equality the *k-scrambling* for O. The k-scrambling for O implies that one cannot distinguish the LTE and the HRU by the measurement of O. As shown in Sec. 6.3, the k-scrambling for a specific operator is sufficient for the decay of the $2k$-point OTOC. We note that the k-scrambling for O (6.6) is quite similar to unitary k-designs (see Definition 4.1). However, they are different in the following point. The k-scrambling is an observable-dependent concept as well as the ETH, while a unitary k-design is an observable-independent concept because it concerns all operators in $\mathcal{B}(\mathcal{H}^{\otimes k})$ at the same time. We investigate the relationship among the k-ETH, the k-scrambling, and unitary k-designs in Chapter 7.

We next derive another representation of Eq. (6.6) by considering matrix elements in the energy eigenbasis. To derive a simple representation of the k-fold channel of the LTE, we impose the k-incommensurate condition [34, 236] on the Hamiltonian. We introduce an equivalence relation for $\boldsymbol{i} := (i_1, \ldots, i_k)$ and $\boldsymbol{j} := (j_1, \ldots, j_k)$: We denote $\boldsymbol{i} \sim \boldsymbol{j}$ if $(i_1, \ldots, i_k)$ is a permutation of $(j_1, \ldots, j_k)$ and denote $\boldsymbol{i} \nsim \boldsymbol{j}$ otherwise. Then, the k-incommensurate condition is defined as follows.

Assumption 3 (k-incommensurate condition)**.** $\sum_{m=1}^{k}(E_{i_m} - E_{j_m}) = 0$ *if and only if* $\boldsymbol{i} \sim \boldsymbol{j}$

This condition reproduces the no-degeneracy condition of eigenenergies for $k = 1$ and the nonresonant condition for $k = 2$. The k-incommensurate condition implies that the LTE is a diagonal-unitary k-design [198, 237–239], as discussed in detail in Sec. 7.3. The k-incommensurate condition is expected to hold in generic nonintegrable systems [34, 236].

From the k-incommensurate condition, we can show that

$$\Phi_{\mathsf{L}}^{(k)}(O) = \sum_{\boldsymbol{i}\sim\boldsymbol{j}} |E(\boldsymbol{i})\rangle \langle E(\boldsymbol{i})|O|E(\boldsymbol{j})\rangle \langle E(\boldsymbol{j})| \tag{6.7}$$

holds for any $O \in \mathcal{B}(\mathcal{H}^{\otimes k})$, where we write $|E(\boldsymbol{i})\rangle := |E_{i_1} \cdots E_{i_k}\rangle$. The derivation of Eq. (6.7) goes as follows. From the definition of the LTE, we have

$$\Phi_{\mathsf{L}}^{(k)}(O) = \sum_{\boldsymbol{i},\boldsymbol{j}} \lim_{T\to\infty} \frac{1}{T} \int_0^T dt \exp\left[it \left(\sum_{m=1}^{k} (E_{i_m} - E_{j_m}) \right) \right] |E(\boldsymbol{i})\rangle \langle E(\boldsymbol{i})|O|E(\boldsymbol{j})\rangle \langle E(\boldsymbol{j})| . \tag{6.8}$$

From the k-incommensurate condition, we have

$$\lim_{T\to\infty}\frac{1}{T}\int_0^T dt\exp\left[it\left(\sum_{m=1}^{k}(E_{i_m}-E_{j_m})\right)\right]=\begin{cases}1 & (\boldsymbol{i}\sim\boldsymbol{j})\\ 0 & (\boldsymbol{i}\not\sim\boldsymbol{j}).\end{cases} \tag{6.9}$$

Substituting this into Eq. (6.8), we obtain Eq. (6.7).

On the other hand, the k-fold channel of the HRU is given by

$$\Phi_{\mathsf{H}}^{(k)}(O)=\sum_{\pi,\tau\in S_k}\mathrm{Wg}_{\pi,\tau}(d)\mathrm{Tr}[OW_\tau]W_\pi. \tag{6.10}$$

Here, S_k is the symmetric group of k objects, and $W_\pi\in\mathcal{B}(\mathcal{H}^{\otimes k})$ is a permutation operator associated with $\pi\in S_k$, which acts on $\mathcal{H}^{\otimes k}$ as

$$W_\pi\left|i_1,i_2,\ldots,i_k\right\rangle=\left|i_{\pi(1)},i_{\pi(2)},\ldots,i_{\pi(k)}\right\rangle, \tag{6.11}$$

where $|i_1,i_2,\ldots,i_k\rangle$ represents the computational base of $\mathcal{H}^{\otimes k}$. The coefficient $\mathrm{Wg}_{\pi,\tau}(d)$ is the Weingarten matrix [240–242], which is a $k!\times k!$ matrix defined as the inverse of the matrix $Q_{\pi,\tau}(d):=\mathrm{Tr}[W_\pi W_\tau]$ whose legs are labeled by elements of the permutation group. We note that Eq. (6.10) is derived as a simple corollary of the Schur-Weyl duality [243]. See Appendix A for more details.

We now derive the explicit formula of the k-ETH for O. Substituting Eqs. (6.7) and (6.10) into Eq. (6.6) and comparing matrix elements in the energy eigenbasis, we obtain the following representation equivalent to the k-scrambling for O.

Definition 6.1 k-ETH for O

For any $\boldsymbol{i}=(i_1,\ldots,i_k)$ and $\boldsymbol{j}=(j_1,\ldots,j_k)$ with $\boldsymbol{i}\sim\boldsymbol{j}$,

$$\langle E(\boldsymbol{i})|O|E(\boldsymbol{j})\rangle=\sum_{\pi,\tau\in S_k}\delta_\pi(\boldsymbol{i},\boldsymbol{j})\mathrm{Wg}_{\pi,\tau}(d)\mathrm{Tr}[OW_\tau], \tag{6.12}$$

where $\delta_\pi(\boldsymbol{i},\boldsymbol{j}):=\delta_{i_1j_{\pi(1)}}\cdots\delta_{i_kj_{\pi(k)}}$.

This is the main result of this section. For $k=1$, Eq. (6.12) reduces to the ETH (6.5) (hereafter referred to as the 1-ETH). The 2-ETH reflects the second order of the complexity, and we will show the explicit expression of the 2-ETH later. In contrast to the 1-ETH, the k-ETH for $k\geq 2$ includes not only diagonal elements, but also off-diagonal elements of O. For $\boldsymbol{i}=\boldsymbol{j}=(i,i,\ldots,i)$, Eq. (6.12) reduces to

$$\langle E_i^{\otimes k}|O|E_i^{\otimes k}\rangle=\frac{1}{d(d+1)\cdots(d-k+1)}\sum_{\tau\in S_k}\mathrm{Tr}[OW_\tau], \tag{6.13}$$

where we used $\sum_{\pi\in S_k}\mathrm{Wg}_{\pi,\tau}(d)=d^{-1}(d+1)^{-1}\cdots(d-k+1)^{-1}$ [244]. Equation (6.13) can be obtained by the typicality argument, i.e., by a uniform random sampling of $|E_i\rangle$ from the

Hilbert space $\mathcal{H}$. On the other hand, the other equalities of the k-ETH cannot be derived in the same manner, and thus the k-ETH cannot reduce to the typicality argument.

The k-ETH (6.12) is not exactly satisfied in finite-size systems except for specific operators, as shown in Sec. 7.3. It raises a question whether the deviation from Eq. (6.12) vanishes in the thermodynamic limit (i.e., in the limit of $d \to \infty$). We consider a more general formalism of the k-ETH allowing finite-size deviations in Sec. 6.2.3.

We show the explicit form of the 2-ETH. By setting $k = 2$ in Eq. (6.12), we have the following expression of the 2-ETH for $O \in \mathcal{B}(\mathcal{H}^{\otimes 2})$:

$$\langle E_i E_i | O | E_i E_i \rangle = \frac{\mathrm{Tr}[O] + \mathrm{Tr}[OS]}{d(d+1)}, \tag{6.14}$$

$$\langle E_i E_j | O | E_i E_j \rangle = \frac{d\mathrm{Tr}[O] - \mathrm{Tr}[OS]}{d(d^2-1)} \qquad (i \neq j), \tag{6.15}$$

$$\langle E_i E_j | O | E_j E_i \rangle = \frac{-\mathrm{Tr}[O] + d\mathrm{Tr}[OS]}{d(d^2-1)} \qquad (i \neq j), \tag{6.16}$$

where S is the swap operator defined by

$$S \left| i \right\rangle \left| j \right\rangle = \left| j \right\rangle \left| i \right\rangle . \tag{6.17}$$

We note that Eqs. (6.14) and (6.15) are the conditions for the diagonal elements of O, while Eq. (6.16) is the condition for the off-diagonal elements of O.

There is another possible generalization of the ETH to the k-replicated system. We introduce a Hamiltonian of the k-replicated system as $H^{(k)} := H \otimes I^{\otimes(k-1)} + \cdots + I^{\otimes(k-1)} \otimes H$, implying that there is no interaction among the replicas. The (1-)ETH of $H^{(k)}$ for $O \in \mathcal{B}(\mathcal{H}^{\otimes k})$ is given by

$$\langle E(\boldsymbol{i}) | O | E(\boldsymbol{i}) \rangle = \frac{\mathrm{Tr}[O]}{d^k}. \tag{6.18}$$

Although this seems to be a natural generalization of the ETH to the k-replicated system, Eq. (6.12) and Eq. (6.18) are not equivalent in general. We argue that only the former is a proper generalization of the ETH. In fact, weak correlations among the energy eigenstates, which come from their orthogonality are taken into account in Eq. (6.12), but not in Eq. (6.18). This fact is crucial to understand the structure of the entanglement entropy of energy eigenstates.

So far, we have considered operators acting on the Hilbert space of the energy shell. However, we can extend the k-ETH to an operator acting on the entire Hilbert space of the system as follows. We denote a projection from the entire Hilbert space to $\mathcal{H}$ by P_{MC}. For an operator $\bar{O}$ acting on the k-replicas of the entire Hilbert space, we can define the projected operator by $P_{\mathrm{MC}}^{\otimes k} \bar{O} P_{\mathrm{MC}}^{\otimes k}$. Then, we define the k-ETH for $\bar{O}$ as the k-ETH for $P_{\mathrm{MC}}^{\otimes k} \bar{O} P_{\mathrm{MC}}^{\otimes k}$. We can neglect this projection procedure only for the case of $k = 1$.

6.2.3 Approximate k-ETH

As we mentioned before, the k-ETH is generally not true in a rigorous sense. Consequently, the validity of the k-ETH should be judged by whether Eq. (6.12) holds in the limit of $d \to \infty$. We now formulate an approximate version of the k-ETH in a similar manner to the 1-ETH. In Sec. 2.2, the measure quantifying the deviation from the exact 1-ETH is introduced by Eq. (2.22). We consider its straightforward extension to the k-ETH. The corresponding indicator of the k-ETH is defined by

$$I_k(O) := \max_{\boldsymbol{i} \sim \boldsymbol{j}} \left| \Delta^{(k)}_{\boldsymbol{i},\boldsymbol{j}}(O) \right|, \tag{6.19}$$

where $\Delta^{(k)}_{\boldsymbol{i},\boldsymbol{j}}(O)$ represents the difference between the both sides of Eq. (6.12), i.e.,

$$\Delta^{(k)}_{\boldsymbol{i},\boldsymbol{j}}(O) := \langle E(\boldsymbol{i})|O|E(\boldsymbol{j})\rangle - \sum_{\pi,\tau \in S_k} \delta_\pi(\boldsymbol{i},\boldsymbol{j}) \mathrm{Wg}_{\pi,\tau}(d) \mathrm{Tr}[OW_\tau]. \tag{6.20}$$

We note that $I_k(O) = 0$ holds if and only if Eq. (6.12) holds for all $\boldsymbol{i}, \boldsymbol{j}$ with $\boldsymbol{i} \sim \boldsymbol{j}$. In the same manner as the approximate 1-ETH (2.23), we define the approximate k-ETH for O by $\lim_{d\to\infty} I_k(O) = 0$. On the other hand, for finite d, we define the exact k-ETH for O by $I_k(O) = 0$.

The indicator $I_k(O)$ is equivalent to the maximum norm of $\Delta^{(k)}(O) := \Phi^{(k)}_{\mathsf{L}}(O) - \Phi^{(k)}_{\mathsf{H}}(O) \in \mathcal{B}(\mathcal{H}^{\otimes k})$. Thus, $I_k(O)$ can be regarded as the finite-size error of the k-scrambling (6.6) for O. The approximate version of the k-scrambling can be defined in the same manner as the k-ETH. Moreover, there is another possible choice of a norm of $\Delta^{(k)}(O)$, such as the Schatten norm and the vector norm [154], while these norms do not recover the standard definition of the approximate 1-ETH (2.23) in general. Thus, we only consider the maximum norm in this thesis. However, the maximum norm might be inappropriate to characterize the higher-order complexity as shown in Sec. 6.2.4 and Sec. 6.3, because it is weaker than other norms.

6.2.4 Tensor-product form operator

As a special case, we consider an operator with the tensor-product form: $O = A^{\otimes k}$ with $A \in \mathcal{B}(\mathcal{H})$. As shown in Sec. 6.3, this type of operators naturally appears in the $2k$-point OTOC. In this case, we can simplify the k-ETH as follows. By decomposing a permutation τ into the product of cyclic permutations, we have

$$\mathrm{Tr}[A^{\otimes k} W_\tau] = \prod_{m=1}^{c(\tau)} \mathrm{Tr}[A^{l_m(\tau)}], \tag{6.21}$$

where we denote the number of cycles in the decomposition by $c(\tau)$ and the length of the mth-longest cycle by $l_m(\tau)$. Thus, the k-ETH for $O = A^{\otimes k}$ is given by

$$A_{i_1 j_1} \cdots A_{i_k j_k} = \sum_{\pi,\tau \in S_k} \delta_\pi(\boldsymbol{i},\boldsymbol{j}) \mathrm{Wg}_{\pi,\tau}(d) \prod_{m=1}^{c(\tau)} \mathrm{Tr}[A^{l_m(\tau)}] \tag{6.22}$$

with $A_{ij} := \langle E_i|A|E_j\rangle$.

We remark that several properties of the product of k matrix elements in chaotic systems were already studied in Ref. [245]. They mainly focused on the products of matrix elements in the cyclic order, i.e., $A_{i_1 i_2} A_{i_2 i_3} \cdots A_{i_k i_1}$, but not the products in a general order. Instead, their argument is not limited to the matrix elements inside the energy shell. Thus, their result is complementary to our result (6.22).

For $k = 2$, Eq. (6.22) is simplified as follows:

$$A_{ii} A_{ii} = \langle A \rangle_{\mathrm{MC}}^2 + \frac{\langle A^2 \rangle_{\mathrm{MC}} - \langle A \rangle_{\mathrm{MC}}^2}{d+1}, \tag{6.23}$$

$$A_{ii} A_{jj} = \langle A \rangle_{\mathrm{MC}}^2 - \frac{\langle A^2 \rangle_{\mathrm{MC}} - \langle A \rangle_{\mathrm{MC}}^2}{d^2-1} \qquad (i \neq j), \tag{6.24}$$

$$A_{ij} A_{ji} = \frac{d(\langle A^2 \rangle_{\mathrm{MC}} - \langle A \rangle_{\mathrm{MC}}^2)}{d^2-1} \qquad (i \neq j), \tag{6.25}$$

where we used $\mathrm{Tr}[A] = d \langle A \rangle_{\mathrm{MC}}$ and $\mathrm{Tr}[A^2] = d \langle A^2 \rangle_{\mathrm{MC}}$. These expressions were already known in random matrix theory [48, 246]. If Eq. (6.23) holds, the variance $\Delta(A)^2$ of the diagonal matrix elements of A considered in Sec. 2.3 is calculated as

$$\Delta(A)^2 = \frac{1}{d} \sum_i (A_{ii} A_{ii} - \langle A \rangle_{\mathrm{MC}}^2) = \frac{1}{d} \sum_i \frac{\langle A^2 \rangle_{\mathrm{MC}} - \langle A \rangle_{\mathrm{MC}}^2}{d+1} = \frac{\langle A^2 \rangle_{\mathrm{MC}} - \langle A \rangle_{\mathrm{MC}}^2}{d+1}. \tag{6.26}$$

This leads to $\Delta(A)^2 \propto d^{-1}$, which is consistent with the d^{-1} scaling of $\Delta(A)^2$ in nonintegrable systems (see Sec. 2.4).

We can easily see that the exact 2-ETH for $A^{\otimes 2}$ is not compatible with the exact 1-ETH (6.5) from the fact that the left-hand side of Eq. (6.23) becomes $A_{ii} A_{ii} = \langle A \rangle_{\mathrm{MC}}^2$ from the exact 1-ETH for A. This is not a contradiction because neither the exact 2-ETH nor the exact 1-ETH holds in general. On the other hand, they can be compatible in an approximate sense, as seen from the following analysis.

We analyze the asymptotic behavior of the right-hand side of Eq. (6.22) for large d. Here, we assume that $\langle A^l \rangle_{\mathrm{MC}} = \mathcal{O}(1)$ for all $l = 1, 2, \ldots, k$, which is expected to be true for a local operator. Under the above assumption, we have

$$\sum_{\pi,\tau \in S_k} \delta_\pi(\boldsymbol{i},\boldsymbol{j}) \mathrm{Wg}_{\pi,\tau}(d) \prod_{m=1}^{c(\tau)} \mathrm{Tr}[A^{l_m(\tau)}] = \begin{cases} \langle A \rangle_{\mathrm{MC}}^k + \mathcal{O}(d^{-1}) & \text{for} \quad \boldsymbol{i} = \boldsymbol{j} \\ \mathcal{O}(d^{-1}) & \text{for} \quad \boldsymbol{i} \neq \boldsymbol{j}. \end{cases} \tag{6.27}$$

Thus, Eq. (6.22) implies that

$$A_{i_1 j_1} \cdots A_{i_k j_k} = \begin{cases} \langle A \rangle_{\mathrm{MC}}^k + \mathcal{O}(d^{-1}) & \text{for} \quad \boldsymbol{i} = \boldsymbol{j} \\ \mathcal{O}(d^{-1}) & \text{for} \quad \boldsymbol{i} \neq \boldsymbol{j}. \end{cases} \tag{6.28}$$

For $k \geq 2$, this equality implies that $A_{ii} = \langle A \rangle_{\mathrm{MC}} + \mathcal{O}(d^{-1})$ and $A_{ij} = \mathcal{O}(d^{-1/2})$ for $i \neq j$. The former leads to the approximate 1-ETH (2.23) for A, and the latter leads to the off-diagonal ETH (2.26) for A. In this sense, the approximate k-ETH for $A^{\otimes k}$ is not a new relation and compatible with the approximate 1-ETH. The approximate k-ETH for $A^{\otimes k}$ follows from the approximate 1-ETH (2.23) and the off-diagonal ETH (2.26).

We provide the deviation of Eq. (6.27). From the assumption, we have

$$\prod_{m=1}^{c(\tau)} \mathrm{Tr}[A^{l_m(\tau)}] = d^{c(\tau)} \prod_{m=1}^{c(\tau)} \langle A^{l_m(\tau)} \rangle_{\mathrm{MC}} = \mathcal{O}(d^{c(\tau)}). \tag{6.29}$$

We use the following asymptotic form of the Weingarten matrix:

$$\mathrm{Wg}_{\pi,\tau}(d) = \mathcal{O}(d^{-2k-1+c(\pi\tau)}), \tag{6.30}$$

(see Appendix A). By combining Eqs. (6.29) and (6.30), we have

$$\sum_{\tau \in S_k} \mathrm{Wg}_{\pi,\tau}(d) \prod_{m=1}^{c(\tau)} \mathrm{Tr}[A^{l_m(\tau)}] = \sum_{\tau \in S_k} \mathcal{O}(d^{-2k+c(\pi\tau)+c(\tau)}) = \mathcal{O}(d^{-k+c(\pi)}), \tag{6.31}$$

where we used $c(\pi\tau) \leq k + c(\pi) - c(\tau)$ [247]. From $c(I) = k$ and $c(\pi) \leq k-1$ for $\pi \neq I$, we have

$$\sum_{\tau \in S_k} \mathrm{Wg}_{\pi,\tau}(d) \prod_{m=1}^{c(\tau)} \mathrm{Tr}[A^{l_m(\tau)}] = \begin{cases} \mathcal{O}(1) & \text{for} \quad \pi = I \\ \mathcal{O}(d^{-1}) & \text{for} \quad \pi \neq I. \end{cases} \tag{6.32}$$

Because $\delta_I(\boldsymbol{i}, \boldsymbol{j}) = 1$ is equivalent to $\boldsymbol{i} = \boldsymbol{j}$, we obtain

$$\sum_{\pi,\tau \in S_k} \delta_\pi(\boldsymbol{i}, \boldsymbol{j}) \mathrm{Wg}_{\pi,\tau}(d) \prod_{m=1}^{c(\tau)} \mathrm{Tr}[A^{l_m(\tau)}] = \begin{cases} \mathcal{O}(1) & \text{for} \quad \boldsymbol{i} = \boldsymbol{j} \\ \mathcal{O}(d^{-1}) & \text{for} \quad \boldsymbol{i} \neq \boldsymbol{j}. \end{cases} \tag{6.33}$$

Finally, we derive the explicit form of $\mathcal{O}(1)$ terms. For $\boldsymbol{i} = \boldsymbol{j}$, we have

$$\sum_{\pi,\tau \in S_k} \delta_\pi(\boldsymbol{i}, \boldsymbol{j}) \mathrm{Wg}_{\pi,\tau}(d) \prod_{m=1}^{c(\tau)} \mathrm{Tr}[A^{l_m(\tau)}] = \frac{1}{d(d+1)\cdots(d-k+1)} \sum_{\tau \in S_k} \prod_{m=1}^{c(\tau)} \mathrm{Tr}[A^{l_m(\tau)}] \tag{6.34}$$

$$= \langle A \rangle_{\mathrm{MC}}^k + \mathcal{O}(d^{-1}), \tag{6.35}$$

where we used $\sum_{\pi \in S_k} \mathrm{Wg}_{\pi,\tau}(d) = d^{-1}(d+1)^{-1} \cdots (d-k+1)^{-1}$ [244].

6.3 Relationship between the k-ETH and the OTOC

In this section, we show that the k-ETH for $A^{\otimes k}$ (6.22) determines the late-time value of the $2k$-point OTOC (4.23). In particular, we show that the long-time average of the $2k$-point OTOC equals the HRU average if the exact k-ETH holds for $A^{\otimes k}$.

6.3.1 Exact decay of the $2k$-point OTOC

Let us consider the long-time average of the $2k$-point OTOC, which is given by

$$F_{\mathsf{L}}^{(2k)}(\boldsymbol{A},\boldsymbol{B}) := \mathbb{E}_{U\sim\mathsf{L}}\left[\mathrm{Tr}\left\{(U^\dagger A_k U)B_k\cdots(U^\dagger A_1 U)B_1\rho\right\}\right] \tag{6.36}$$

$$= \lim_{\tau\to\infty}\frac{1}{\tau}\int_0^\tau \mathrm{Tr}[A_k(t)B_k(0)\cdots A_1(t)B_1(0)\rho]dt \tag{6.37}$$

with $A_1,\ldots,A_k,B_1,\ldots,B_k\in\mathcal{B}(\mathcal{H})$. For simplicity, we consider the case of $A_1=\cdots=A_k=:A$, $B_1=\cdots=B_k=:B$, and $\rho=\rho_{\mathrm{MC}}:=P_{\mathrm{MC}}/d$, i.e.,

$$F_{\mathsf{L}}^{(2k)}(\boldsymbol{A},\boldsymbol{B}) = \mathbb{E}_{U\sim\mathsf{L}}\left[d^{-1}\mathrm{Tr}\left\{(U^\dagger AU)B\cdots(U^\dagger AU)B\right\}\right]. \tag{6.38}$$

Again, we remark that all the operators now act on the Hilbert space of the energy shell, but not on the entire Hilbert space of the many-body system. In the entire Hilbert space, Eq. (6.38) is represented as

$$F_{\mathsf{L}}^{(2k)}(\boldsymbol{A},\boldsymbol{B}) = \mathbb{E}_{U\sim\mathsf{L}}\left[\mathrm{Tr}\left\{(U^\dagger \bar{A}U)\rho_{\mathrm{MC}}^{1/2k}\bar{B}\rho_{\mathrm{MC}}^{1/2k}\cdots(U^\dagger\bar{A}U)\rho_{\mathrm{MC}}^{1/2k}\bar{B}\rho_{\mathrm{MC}}^{1/2k}\right\}\right], \tag{6.39}$$

where $\bar{A}$ and $\bar{B}$ are operators acting on the entire Hilbert space such that $P_{\mathrm{MC}}\bar{A}P_{\mathrm{MC}}=A$ and $P_{\mathrm{MC}}\bar{B}P_{\mathrm{MC}}=B$. The right-hand side of Eq. (6.39) is very similar to the regularization of the OTOC in field theories [61,248,249]. This regularization is important to remove the effect of other energy scales. If there is no regularization, the long-time average of the OTOC can deviate from the HRU average even in fully chaotic systems. In fact, Ref. [233] shows that, for the non-regularized (4-point) OTOC with traceless operators, the Haar random average decays exponentially with the system size, while the long-time average decays polynomially with system size on the basis of a result of Ref. [80].

We go back to representation (6.38). By considering the k-replicated Hilbert space, we can rewrite the trace of the product of k operators as

$$\mathrm{Tr}[A_1\cdots A_k] = \mathrm{Tr}[(A_1\otimes\cdots\otimes A_k)W_{\mathrm{cyc}}], \tag{6.40}$$

where W_{cyc} is the cyclic permutation operator (see Fig. 6.3 for a graphical representation). By using this relation, we can rewrite the long-time average of the $2k$-point OTOC as follows [199]:

$$F_{\mathsf{L}}^{(2k)}(\boldsymbol{A},\boldsymbol{B}) = d^{-1}\mathrm{Tr}\left[\Phi_{\mathsf{L}}^{(k)}(A^{\otimes k})B^{\otimes k}W_{\mathrm{cyc}}\right]. \tag{6.41}$$

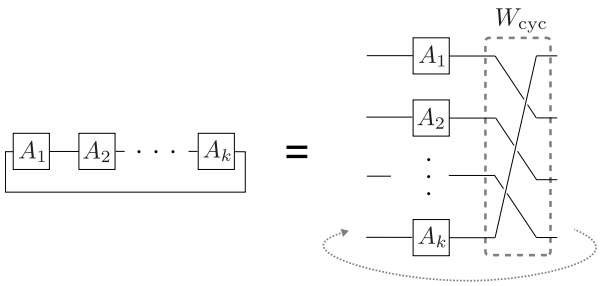

Fig. 6.3 Graphical representation of Eq. (6.40), where we impose the periodic boundary condition in the right-hand side. The closed diagram indicates taking the trace.

This representation of the $2k$-point OTOC by the k-fold channel is true not just for the LTE but also for any ensembles. As an immediate consequence of Eq. (6.41), if the k-scrambling (6.6) holds exactly for $A^{\otimes k}$, we obtain

$$F_{\mathsf{L}}^{(2k)}(\boldsymbol{A},\boldsymbol{B}) = F_{\mathsf{H}}^{(2k)}(\boldsymbol{A},\boldsymbol{B}), \tag{6.42}$$

where $F_{\mathsf{H}}^{(2k)}(\boldsymbol{A},\boldsymbol{B})$ is the Haar random average of the $2k$-point OTOC. Equation (6.42) represents the exact decay (relaxation) of the $2k$-point OTOC to the HRU average. In this sense, our definition of the k-scrambling (6.6) represents the kth-order extension of (operator) scrambling. From the equivalence between the k-scrambling and the k-ETH, Eq. (6.42) is also achieved from the exact k-ETH for $A^{\otimes k}$. On the other hand, Eq. (6.42) does not necessarily imply the k-scrambling (6.6) or the k-ETH (6.12) for $A^{\otimes k}$.

6.3.2 Approximate decay of the $2k$-point OTOC

We next consider the approximate decay of the OTOC, as the k-ETH holds only approximately for finite-size systems. Note that there is no generally accepted definition of the approximate decay of the OTOC. We here use the following naive definition: The approximate decay of the $2k$-point OTOC to the HRU average is defined as

$$\lim_{d\to\infty} \left| F_{\mathsf{L}}^{(2k)}(\boldsymbol{A},\boldsymbol{B}) - F_{\mathsf{H}}^{(2k)}(\boldsymbol{A},\boldsymbol{B}) \right| = 0. \tag{6.43}$$

This definition seems to be natural, but might be insufficient to characterize the higher-oder complexity. In fact, for $k = 2$, Huang *et al.* [233] showed that Eq. (6.43) is achieved if the approximate 1-ETH and off-diagonal ETH are satisfied for A and B. This is reasonable because the approximate 2-ETH for $A^{\otimes 2}$ follows from the approximate 1-ETH and off-diagonal ETH for A as shown in Sec. 6.2.4. On the other hand, it is not clear whether Eq. (6.43) is achieved only from the approximate k-ETH for $A^{\otimes k}$ and $B^{\otimes k}$. In this sense, the relaxation of the $2k$-point OTOC to a small value is not straightforwardly related to the higher-order complexity of the Hamiltonian dynamics.

6.4 Eigenstate entanglement entropy

In this section, we investigate the k-REE of energy eigenstates in light of the k-ETH. The k-REE characterizes the complexity of a quantum state. In fact, we cannot efficiently approximate states in one-dimensional systems by matrix product states if the k-REE of them obey the volume law for $k \geq 1$ [250, 251].

6.4.1 k-ETH for the partial cyclic permutation operator

We first introduce the partial cyclic permutation (PCP) operator to define the k-REE. The PCP operator allows us to study the k-REE of the energy eigenstates from the k-ETH. We assume that the system consists of N qubits. That is, each site of the lattice has a two dimensional Hilbert space. As in Sec. 2.5, the single replica system is partitioned into two subsystems X and $\bar{X}$ containing n and $N-n$ qubits, respectively. The dimension of the Hilbert space on X is denoted by $d_X := 2^n$.

For $k \geq 2$, we define the PCP operator C_X supported on X as a cyclic permutation among k replicas of X. The action of C_X is given by

$$C_X \left|x_1 y_1, x_2 y_2, \ldots, x_k y_k\right\rangle = \left|x_2 y_1, x_3 y_2, \ldots, x_1 y_k\right\rangle, \tag{6.44}$$

where $|x_i\rangle$ and $|y_i\rangle$ $(i = 1, \ldots, k)$ are the computational bases of the Hilbert spaces of X and $\bar{X}$, respectively. We note that C_X is unitary but not Hermitian for $k \geq 3$. The k-REE is defined as the kth-Rényi entropy of the reduced density operator [120]. For the special case of $k = 2, 3, \ldots$, the k-REE of $|\psi\rangle$ can be expressed as

$$R^{(k)}(X) := \frac{1}{1-k} \log \langle \psi^{\otimes k} | C_X | \psi^{\otimes k} \rangle . \tag{6.45}$$

Because this representation connects the k-REE with the expectation value of C_X, we can employ the k-ETH for C_X to study the k-REE of individual energy eigenstates. Importantly, C_X cannot be written in the tensor-product form $A^{\otimes k}$, which implies that the approximate k-ETH of C_X does not reduce to the conventional ETH.

Let us consider the k-ETH for C_X. Because C_X is defined as an operator acting on the entire Hilbert space, not in the energy shell $\mathcal{H}^{\otimes k}$, we project C_X to the energy shell $\mathcal{H}^{\otimes k}$. The projected PCP operator $\tilde{C}_X \in \mathcal{B}(\mathcal{H}^{\otimes k})$ is defined by $\tilde{C}_X := P_{\mathrm{MC}}^{\otimes k} C_X P_{\mathrm{MC}}^{\otimes k}$. Then, the k-ETH for C_X is given by

$$\langle E(\boldsymbol{i}) | C_X | E(\boldsymbol{j}) \rangle = \sum_{\pi, \tau \in S_k} \delta_\pi(\boldsymbol{i}, \boldsymbol{j}) \mathrm{Wg}_{\pi,\tau}(d) \mathrm{Tr}[\tilde{C}_X W_\tau], \tag{6.46}$$

for $\boldsymbol{i} \sim \boldsymbol{j}$. We rewrite $\mathrm{Tr}[\tilde{C}_X W_\tau]$ as

$$\mathrm{Tr}[\tilde{C}_X W_\tau] = d^k \mathrm{Tr}[C_X W_\tau \rho_{\mathrm{MC}}^{\otimes k}]. \tag{6.47}$$

The right-hand side of the above is interpreted as the expectation value of $C_X W_\tau$ in the k-replicated microcanonical state $\rho_{\rm MC}^{\otimes k}$ except for a factor d^k. A quantity $\mathrm{Tr}[C_X W_\tau \rho_{\rm MC}^{\otimes k}]$ is a specific case of the entanglement feature [252], which provides more detail information about entanglement properties than entanglement entropies.

We remark that Eq. (6.46) is related to the k-REE of the energy eigenstates only for the case of $\boldsymbol{i} = \boldsymbol{j} = (i, \ldots, i)$, while the other cases are irrelevant to the k-REE. As shown in Sec. 6.5, Eq. (6.46), including the case of $\boldsymbol{i} \neq \boldsymbol{j}$, is closely related to the OSEE. In the following, we investigate the k-REE of individual energy eigenstates by using Eq. (6.46).

6.4.2 2-REE

Let us consider the simplest case of $k = 2$. The PCP operator for $k = 2$ is specifically called the partial swap operator and denoted by S_X whose action is defined by $S_X |x_1 y_1, x_2 y_2\rangle = |x_2 y_1, x_1 y_2\rangle$. To derive a simple expression of the 2-ETH for S_X, we use the following relations

$$\mathrm{Tr}[\tilde{S}_X] = d^2 \mathrm{Tr}[S_X \rho_{\rm MC}^{\otimes 2}] = d^2 e^{-R_{\rm MC}^{(2)}(X)}, \tag{6.48}$$

$$\mathrm{Tr}[\tilde{S}_X S] = d^2 \mathrm{Tr}[S_{\bar{X}} \rho_{\rm MC}^{\otimes 2}] = d^2 e^{-R_{\rm MC}^{(2)}(\bar{X})}, \tag{6.49}$$

where $R_{\rm MC}^{(2)}(X)$ is the second Rényi entropy of the reduced microcanonical state $\rho_{\rm MC}^X := \mathrm{Tr}_{\bar{X}}[\rho_{\rm MC}]$, which is given by $R_{\rm MC}^{(2)}(X) := -\log \mathrm{Tr}[(\rho_{\rm MC}^X)^2]$. As investigated later, we expect that $R_{\rm MC}^{(2)}(X)$ linearly grows with the subsystem size. Then, Eq. (6.46) reduces to

$$\langle E_i E_i | S_X | E_i E_i \rangle = \frac{d}{d+1} \left(e^{-R_{\rm MC}^{(2)}(X)} + e^{-R_{\rm MC}^{(2)}(\bar{X})} \right), \tag{6.50}$$

$$\langle E_i E_j | S_X | E_i E_j \rangle = \frac{d^2}{d^2-1} \left(e^{-R_{\rm MC}^{(2)}(X)} - e^{-R_{\rm MC}^{(2)}(\bar{X})}/d \right), \tag{6.51}$$

$$\langle E_i E_j | S_X | E_j E_i \rangle = \frac{d^2}{d^2-1} \left(e^{-R_{\rm MC}^{(2)}(\bar{X})} - e^{-R_{\rm MC}^{(2)}(X)}/d \right). \tag{6.52}$$

These are the 2-ETH for S_X, and Eq. (6.50) is symmetric with respect to the exchange of X and $\bar{X}$, but Eqs. (6.51) and (6.52) are not symmetric. When the number of qubits in X is far fewer than that in $\bar{X}$ ($n \ll N - n$), then $R_{\rm MC}^{(2)}(X) \ll R_{\rm MC}^{(2)}(\bar{X})$ holds. In this case, the second terms on the right-hand sides of Eqs. (6.50) and (6.51) are negligible compared to the first terms. We thus have

$$\langle E_i E_i | S_X | E_i E_i \rangle \approx e^{-R_{\rm MC}^{(2)}(X)}, \tag{6.53}$$

$$\langle E_i E_j | S_X | E_i E_j \rangle \approx e^{-R_{\rm MC}^{(2)}(X)}, \tag{6.54}$$

$$\langle E_i E_j | S_X | E_j E_i \rangle \approx 0, \tag{6.55}$$

for $n \ll N$. These imply that the values of the diagonal elements of S_X are about the same for all i, j, while the off-diagonal elements of S_X vanish in the limit of $d \to \infty$. These behavior

are similar to the case of $A^{\otimes 2}$ (see Eqs. (6.23)-(6.25)). On the other hand, when the sizes of X and $\bar{X}$ are comparable, i.e., $n = N/2$, Eqs. (6.23)-(6.25) are approximated as

$$\langle E_i E_i | S_X | E_i E_i \rangle \approx 2e^{-R^{(2)}_{\mathrm{MC}}(X)}, \tag{6.56}$$

$$\langle E_i E_j | S_X | E_i E_j \rangle \approx 2e^{-R^{(2)}_{\mathrm{MC}}(X)}, \tag{6.57}$$

$$\langle E_i E_j | S_X | E_j E_i \rangle \approx e^{-R^{(2)}_{\mathrm{MC}}(X)}, \tag{6.58}$$

where we used $R^{(2)}_{\mathrm{MC}}(X) = R^{(2)}_{\mathrm{MC}}(\bar{X})$. The coefficient of 2 in the right-hand sides of Eqs. (6.56) and (6.57) corresponds to the Page correction of the 2-REE as revealed later.

Before deriving the Page curve, we take a look at the extensivity of $R^{(2)}_{\mathrm{MC}}(X)$. In the case of $n = N$, we have $R^{(2)}_{\mathrm{MC}}(X) = -\log \mathrm{Tr}[\rho^2_{\mathrm{MC}}] = \log d$, which implies that $R^{(2)}_{\mathrm{MC}}(X)$ equals the thermodynamic entropy of the entire system. As an extension of this, we expect that the value of $R^{(2)}_{\mathrm{MC}}(X)$ is approximated as the thermodynamic entropy of subsystem for $1 \ll n < N$. This observation leads the extensivity of $R^{(2)}_{\mathrm{MC}}(X)$. The extensivity can also be understood in a different way. If subsystem X is far smaller than the entire system, and the interaction between X and $\bar{X}$ is negligible, we have $\rho^X_{\mathrm{MC}} \approx e^{-\beta H_X}/\mathrm{Tr}[e^{-\beta H_X}]$, where H_X is the Hamiltonian truncated to X. If the above approximation is true, we obtain $R^{(2)}_{\mathrm{MC}}(X) \approx -\log \mathrm{Tr}[e^{-2\beta H_X}] + 2\log \mathrm{Tr}[e^{-\beta H_X}]$. Since $\mathrm{Tr}[e^{-2\beta H_X}]$ and $\log \mathrm{Tr}[e^{-\beta H_X}]$ are extensive quantities, we conclude that $R^{(2)}_{\mathrm{MC}}(X)$ is extensive for $n \ll N$.

We next derive the finite-temperature extension of the Page curve from Eq. (6.50). Considering the logarithm of Eq. (6.50) and the definition of the 2-REE, we obtain

$$R^{(2)}_i(X) = R^{(2)}_{\mathrm{th}}(X) := R^{(2)}_{\mathrm{MC}}(X) - \log \frac{1 + e^{R^{(2)}_{\mathrm{MC}}(X) - R^{(2)}_{\mathrm{MC}}(\bar{X})}}{1 + 1/d}, \tag{6.59}$$

where $R^{(2)}_{\mathrm{th}}(X)$ takes the same form as proposals of the finite-temperature extensions of the Page curve based on random thermal pure quantum states [134–136]. In fact, our formula (6.59) can be regarded as the finite-temperature Page curve in the following sense. The first term of $R^{(2)}_{\mathrm{th}}(X)$ grows linearly with the subsystem-size and is near the maximum value of the second Rényi entropy under the energy constraint. The second term of $R^{(2)}_{\mathrm{th}}(X)$ is negligible for $n \ll N$ but becomes $\log 2$ at $n = N/2$. This subsystem-size dependence is the same as the Page correction of the 2-REE.

More explicitly, Eq. (6.59) recovers the Page curve, if the microcanonical state is approximated as the maximally mixed state of the entire Hilbert space: $\rho_{\mathrm{MC}} \approx I/2^N$. In this case, we have $R^{(2)}_{\mathrm{MC}}(X) \approx n \log 2$ and $R^{(2)}_{\mathrm{MC}}(\bar{X}) \approx (N - n)\log 2$. Thus, $R^{(2)}_{\mathrm{th}}(X)$ is approximated as

$$R^{(2)}_{\mathrm{th}}(X) \approx n \log 2 - \log(1 + 2^{2n-N}), \tag{6.60}$$

which is equivalent to the Page curve of the 2-REE [129]. Therefore, our formula (6.59) can be regarded as a natural extension of the Page curve to the finite-temperature pure states.

Moreover, we show a direct connection to a universal formula of the 2-REE proposed in Refs [134, 135]. Their formula for a pure state at inverse temperature β is written as

$$R_{\rm th}^{(2)}(X) = n \log a(\beta) - \log(1 + a(\beta)^{-N+2n}) + \log K(\beta), \tag{6.61}$$

where $a(\beta)$ and $K(\beta)$ are constants depending only on β. We assume that $R_{\rm th}^{(2)}(X)$ is extensive, i.e., there exist n-independent constants $1 \leq w(u) \leq 2$ and $\kappa(u) \geq 0$ such that

$$R_{\rm MC}^{(2)}(X) = n \log w(u) + \kappa(u), \tag{6.62}$$

where u is the energy density of the thermal pure state. From the equivalence of ensembles [86, 220], this is provable for $n \ll N$ if we take u equal to the energy density at infinite temperature. By substituting Eq. (6.62) into Eq. (6.59), we have

$$R_{\rm th}^{(2)}(X) \approx n \log w(u) - \log(1 + w(u)^{-N+2n}). \tag{6.63}$$

Because the energy density u can be represented as a function of the inverse temperature β except for phase transition points, we can rewrite the above equality as a function of the inverse temperature:

$$R_{\rm th}^{(2)}(X) \approx n \log w(\beta) - \log(1 + w(\beta)^{-N+2n}), \tag{6.64}$$

which equals the right-hand side of Eq. (6.61) by setting $a(\beta) = w(\beta)$ and $\log K(\beta) \approx 0$.

6.4.3 k-REE

We generalize the foregoing results to the case of $k \geq 3$. For $\boldsymbol{i} = \boldsymbol{j} = (i, \ldots, i)$, Eq. (6.46) reduces to

$$\langle E_i^{\otimes k} | C_X | E_i^{\otimes k} \rangle = \frac{d^{k-1}}{(d+1)\cdots(d+k-1)} \sum_{\tau \in S_k} {\rm Tr}[C_X W_\tau \rho_{\rm MC}^{\otimes k}] \approx \sum_{\tau \in S_k} {\rm Tr}[C_X W_\tau \rho_{\rm MC}^{\otimes k}]. \tag{6.65}$$

The term concerning $\tau = I$ in the summation of the right-hand side can be written as

$${\rm Tr}[C_X \rho_{\rm MC}^{\otimes k}] = e^{-(k-1)R_{\rm MC}^{(k)}(X)}, \tag{6.66}$$

where $R_{\rm MC}^{(k)}(X) := (1-k)^{-1} \log {\rm Tr}[C_X \rho_{\rm MC}^{\otimes k}]$ is the kth-Rényi entropy of the reduced microcanonical state. This term gives the leading contribution to the k-REE for $d \gg 1$. By taking the logarithm of Eq. (6.65), we have

$$R_i^{(k)}(X) \approx R_{\rm th}^{(k)}(X) := R_{\rm MC}^{(k)}(X) - \gamma_X^{(k)}, \tag{6.67}$$

where

$$\gamma_X^{(k)} := \frac{1}{k-1} \log \left(e^{(k-1)R_{\rm MC}^{(k)}(X)} \sum_{\tau \in S_k} {\rm Tr}[C_X W_\tau \rho_{\rm MC}^{\otimes k}] \right). \tag{6.68}$$

In the same sense as Eq. (6.59), Eq. (6.67) can be regarded as the finite-temperature extensions of the Page curve of the k-REE. The first term of $R_{\rm th}^{(k)}(X)$, i.e., $R_{\rm MC}^{(k)}(X)$ is a straightforward extension of $R_{\rm th}^{(2)}(X)$ and represents the thermal behavior. On the other hand, the second term of $R_{\rm th}^{(k)}(X)$, i.e., $\gamma_X^{(k)}$ is the higher-order Page correction. For $k=3$, Eq. (6.67) reduces to

$$R_{\rm th}^{(3)}(X) = R_{\rm MC}^{(3)}(X) - \gamma_X^{(3)}, \tag{6.69}$$

$$\gamma_X^{(3)} = \frac{1}{2}\log\Big\{1 + e^{2R_{\rm MC}^{(3)}(X)-2R_{\rm MC}^{(3)}(\bar{X})} + 3e^{2R_{\rm MC}^{(3)}(X)}{\rm Tr}[\rho_{\rm MC}(\rho_{\rm MC}^{X}\otimes\rho_{\rm MC}^{\bar{X}})] + e^{2R_{\rm MC}^{(3)}(X)}{\rm Tr}[C_X C_{\bar{X}}^{-1}\rho_{\rm MC}^{\otimes 3}]\Big\}. \tag{6.70}$$

Again, Eq. (6.69) has the same form as the finite-temperature Page curve studied in Refs. [134–136].

Finally, we comment on the 1-REE $R^{(1)}(X) := -{\rm Tr}[\rho_X \log \rho_X]$, which cannot be written in the form of the average of any state-independent operator, as opposed to the case of $k \geq 2$. Accordingly, the 1-ETH does not provide the finite-temperature Page curve of the 1-REE. However, we can obtain the 1-REE by taking the limit of $k \to 1$ in Eq. (6.67). In this sense, we can say that the finite-temperature Page curve of the 1-REE follows from the $(1+\epsilon)$-ETH with a small number $\epsilon > 0$. In addition, the following lower bound on the 1-REE immediately follows from the 2-ETH for S_X:

$$R_i^{(1)}(X) \geq R_i^{(2)}(X) = R_{\rm th}^{(2)}(X) \tag{6.71}$$

implying that $R_i^{(1)}(X)$ takes a nearly maximum value for $n \ll N$.

6.5 Operator space entanglement entropy (OSEE)

In this section, we introduce the OSEE, which is an extension of the entanglement entropy to an operator. We formulate the OSEE counterpart of the finite-temperature Page curve in parallel to the k-REE. The k-ETH for the PCP operator leads to the finite-temperature Page curve for the OSEE of the LTE.

6.5.1 Definition of the k-OSEE

We introduce the OSEE by mapping the operator into the quantum state in the extended Hilbert space. For simplicity, we first consider the case where $\mathcal{H}$ equals the entire Hilbert space. The mapping is based on the fact that the operator space $\mathcal{B}(\mathcal{H})$ is a d^2-dimensional Hilbert space. Any operator $O \in \mathcal{B}(\mathcal{H})$ can be mapped to a state $|O\rangle$ in the extended Hilbert space $\mathcal{H}^{\otimes 2}$ by

$$|O\rangle := (O\otimes I)\,|I\rangle\,, \tag{6.72}$$

where $|I\rangle$ is a maximally entangled state between two replicas:

$$|I\rangle := \frac{1}{d^{1/2}} \sum_{i=1}^{d} |i\rangle \otimes |i\rangle \,. \tag{6.73}$$

This mapping is known as the channel-state duality (the Choi-Jamiołkowski isomorphism) [253, 254]. The inner product of states $|O_1\rangle$ and $|O_2\rangle$ equals the Hilbert-Schmidt inner product of operators O_1 and O_2:

$$\langle O_1|O_2\rangle = \frac{1}{d}\mathrm{Tr}[O_1^\dagger O_2]. \tag{6.74}$$

We define the k-OSEE of an unitary operator $U \in \mathcal{U}(\mathcal{H})$ as the k-REE of the corresponding state $|U\rangle$ [255, 256]. Let us see more explicitly the definition of the k-OSEE. We divide each replica into two subsystems and denote subsystems of one replica by X and $\bar{X}$ and that of the other replica by Y and $\bar{Y}$. The k-OSEE for a subsystem XY is represented as

$$R_U^{(k)}(X,Y) := \frac{1}{1-k} \log \mathrm{Tr}\left[(\rho_{XY}^U)^k\right], \tag{6.75}$$

where ρ_{XY}^U is the reduced density operator of $|U\rangle$ on a subsystem XY. The k-OSEE has similar properties to the k-OSEE, such as

$$0 \le R_U^{(k)}(X,Y) \le \log d_X d_Y. \tag{6.76}$$

The k-OSEE characterizes the complexity as well as the k-REE. In fact, U can be efficiently approximated by a matrix product operator if $R_U^{(k)}(X,Y) = \mathcal{O}(\log N)$ for any $0 < k < 1$, while the approximation becomes inefficient if $R_U^{(k)}(X,Y) = \mathcal{O}(N)$ for $k \ge 1$ [250, 251]. Moreover, the k-OSEE quantifies scrambled information [57, 257–260], because the specific type of the operator-averaged $2k$-point OTOC is equivalent to the k-OSEE [168, 199].

If k is an integer and $k \ge 2$, the k-OSEE can be written as

$$R_U^{(k)}(X,Y) = \frac{1}{1-k} \log \frac{\mathrm{Tr}\left[C_X^{-1} U^{\dagger\otimes k} C_Y U^{\otimes k}\right]}{d^k}, \tag{6.77}$$

where C_X and C_Y are the PCP operators (6.44). Motivated by this representation, the k-OSEE of an ensemble ν is introduced by

$$R_\nu^{(k)}(X,Y) := \frac{1}{1-k} \log \frac{\mathrm{Tr}\left[C_X^{-1} \Phi_\nu^{(k)}(C_Y)\right]}{d^k}. \tag{6.78}$$

We remark that $R_\nu^{(k)}(X,Y)$ is not equivalent to the ensemble average of $R_U^{(k)}(X,Y)$.

6.5.2 Explicit form of the Page curve

As a natural extension of the Page curve of the k-REE, we introduce the Page curve of the k-OSEE as the k-OSEE of the HRU:

$$R_{\mathsf{H}}^{(k)}(X,Y) := \frac{1}{1-k}\log\frac{\mathrm{Tr}\left[C_X^{-1}\Phi_{\mathsf{H}}^{(k)}(C_Y)\right]}{d^k}. \tag{6.79}$$

The explicit expression of the Page curve of the k-OSEE [257, 258, 261] is given by

$$R_{\mathsf{H}}^{(k)}(X,Y) = \log d_X d_Y - \gamma_{X,Y}^{(k)}, \tag{6.80}$$

where

$$\gamma_{X,Y}^{(k)} := \frac{1}{k-1}\log\left(\sum_{\pi\in S_k} d^{-2k+2c(\pi)}(d_X d_Y)^{c(\pi\pi_{\mathrm{cyc}})-c(\pi)+k-1}\right). \tag{6.81}$$

Equation (6.80) is analogous to the Page curve of the k-REE as follows. The first term on the right-hand side of Eq. (6.80) equals the maximum value of the k-OSEE. It can be rewritten as $\log d_X d_Y = (m+n)\log 2$, where m and n are the number of qubits in X and Y, respectively. Therefore, the first term implies the volume law of the k-OSEE. On the other hand, $\gamma_{X,Y}^{(k)}$ is the subleading terms and can be regarded as the Page correction. The Page correction takes the maximum value at $m = n = N/2$. In particular, the maximum value converges to $\log\frac{(2k)!}{k!(k+1)!}$ in the limit of $d\to\infty$ [258]. For the simplest case of $k=2$, the Page curve is given by

$$R_{\mathsf{H}}^{(2)}(X,Y) = (m+n)\log 2 - \log\left(1+\frac{1-2^{2m}-2^{2n}+2^{2(m+n)}}{2^{2N}-1}\right), \tag{6.82}$$

$$\approx (m+n)\log 2 - \log\left(1+2^{2(m+n-N)}\right) \quad \text{for } N\gg 1. \tag{6.83}$$

We note that this can be obtained from Eq. (6.60) by replacing $n\to m+n$ and $N\to 2N$.

We next derive the finite-temperature extension of Eq. (6.80) by considering the case where $\mathcal{H}$ is a strict subspace of the entire Hilbert space corresponding to the energy shell. As in Sec. 6.4, we consider the projected PCP operator $\tilde{C}_X$. The finite-temperature Page curve of the k-OSEE is formally defined by

$$R_{\mathrm{th}}^{(k)}(X,Y) := \frac{1}{1-k}\log\frac{\mathrm{Tr}\left[\tilde{C}_X^{-1}\Phi_{\mathsf{H}}^{(k)}(\tilde{C}_Y)\right]}{d^k}. \tag{6.84}$$

In order to see its property, we derive a more explicit expression for the case of $k=2$ and $d\gg 1$. From Eqs. (6.48) and (6.49), we obtain

$$d^{-2}\mathrm{Tr}\left[\tilde{S}_X\Phi_{\mathsf{H}}^{(2)}(\tilde{S}_Y)\right] \approx e^{-R_{\mathrm{MC}}^{(2)}(X)-R_{\mathrm{MC}}^{(2)}(Y)} + e^{-R_{\mathrm{MC}}^{(2)}(\bar{X})-R_{\mathrm{MC}}^{(2)}(\bar{Y})}. \tag{6.85}$$

Taking the logarithm on the both sides, we obtain the following representation of the 2-OSEE:

$$R^{(2)}_{\rm th}(X,Y) \approx R^{(2)}_{\rm MC}(X) + R^{(2)}_{\rm MC}(Y) - \log\left(1 + e^{R^{(2)}_{\rm MC}(X)+R^{(2)}_{\rm MC}(Y)-R^{(2)}_{\rm MC}(\bar{X})-R^{(2)}_{\rm MC}(\bar{Y})}\right). \tag{6.86}$$

The leading contributions of the finite-temperature Page curve comes from the second Rényi entropy of the reduced microcanonical state, which is the same as the case of the k-REE. The third term on the right-hand side of Eq. (6.86) is a subleading correction and can be regarded as the finite-temperature Page correction. The finite-temperature Page correction takes the maximum value $\log 2$ at $m = n = N/2$. Moreover, Eq. (6.86) recovers the (infinite-temperature) Page curve (6.83) if four terms $R^{(2)}_{\rm MC}(X), R^{(2)}_{\rm MC}(\bar{X}), R^{(2)}_{\rm MC}(Y)$, and $R^{(2)}_{\rm MC}(\bar{Y})$ achieve the maximum of the subsystem entropy, i.e., $R^{(2)}_{\rm MC}(X) \approx m\log 2, R^{(2)}_{\rm MC}(\bar{X}) \approx (N-m)\log 2, R^{(2)}_{\rm MC}(Y) \approx n\log 2$, and $R^{(2)}_{\rm MC}(\bar{Y}) \approx (N-m)\log 2$. Therefore, we can say that $R^{(2)}_{\rm th}(X,Y)$ is the finite-temperature Page curve of the 2-OSEE. In fact, we can show that $R^{(2)}_{\rm th}(X,Y)$ follows the universal formula (6.61) as follows. From the assumption (6.62), we have

$$R^{(2)}_{\rm th}(X,Y) \approx (m+n)\log w(u) - \log\left(1 + w(u)^{2(m+n-N)}\right). \tag{6.87}$$

By rewriting $w(u)$ as a function of the inverse temperature in the same manner as in Sec. 6.4.2 and replacing $n+m \to n$ and $2N \to N$, we recovers the universal formula (6.61).

6.5.3 Relationship with the k-ETH

We next clarify the relationship between the k-ETH and the Page curve of the k-OSEE. If the exact k-ETH for the PCP operator is satisfied, we have $\Phi^{(k)}_{\rm L}(\tilde{C}_Y) = \Phi^{(k)}_{\rm H}(\tilde{C}_Y)$ and thus

$$R^{(k)}_{\rm L}(X,Y) = R^{(k)}_{\rm th}(X,Y), \tag{6.88}$$

where $R^{(k)}_{\rm L}(X,Y)$ is the k-OSEE of the LTE. Therefore, we can conclude that the k-ETH for the PCP operator leads not only to the Page curve of the k-REE of energy eigenstates but also to the Page curve of the k-OSEE.

To investigate implications of the 2-ETH, let us reconsider the 2-ETH for S_X in terms of the 2-OSEE. We show that Eqs. (6.51) and (6.52) are crucial to achieve the Page curve of the 2-OSEE in contrast to the case of the 2-REE. To see this, we consider the order of the contributions to the 2-OSEE. The 2-OSEE is proportional to $d^{-2}{\rm Tr}\left[\tilde{S}_X\Phi^{(2)}_{\rm L}(\tilde{S}_Y)\right]$, and it is divided as

$$\begin{aligned} d^{-2}{\rm Tr}\left[\tilde{S}_X\Phi^{(2)}_{\rm L}(\tilde{S}_Y)\right] &= d^{-2}\sum_i \langle E_iE_i|\tilde{S}_X|E_iE_i\rangle\langle E_iE_i|\tilde{S}_Y|E_iE_i\rangle \\ &\quad + d^{-2}\sum_{i\neq j} \langle E_iE_j|\tilde{S}_X|E_iE_j\rangle\langle E_iE_j|\tilde{S}_Y|E_jE_i\rangle \\ &\quad + d^{-2}\sum_{i\neq j} \langle E_iE_j|\tilde{S}_X|E_jE_i\rangle\langle E_iE_j|\tilde{S}_Y|E_iE_j\rangle. \end{aligned} \tag{6.89}$$

We note that the first terms on the right-hand is evaluated by Eqs. (6.50), while the second and the third terms are evaluated by a combination of Eqs. (6.51) and (6.52). In fact, for $d \gg 1$, we can show that

$$\text{first term} \approx 0, \tag{6.90}$$

$$\text{second term} \approx e^{-R^{(2)}_{\mathrm{MC}}(X)-R^{(2)}_{\mathrm{MC}}(\bar{Y})}, \tag{6.91}$$

$$\text{third term} \approx e^{-R^{(2)}_{\mathrm{MC}}(\bar{X})-R^{(2)}_{\mathrm{MC}}(Y)}. \tag{6.92}$$

These equalities imply that only the second and the third terms contribute to the 2-OSEE. This is reasonable because the summation in the first term of Eq. (6.89) runs over d matrix elements, while the summations in the second and third terms run over d^2-d matrix elements. Moreover, we can see that the leading contribution comes from Eq. (6.51) if $m, n \ll N$, while it comes from both Eq. (6.51) and Eq. (6.52) if $m = n = N/2$. Therefore, the implications of the 2-ETH for the partial swap operator is phrased as follows: Eq. (6.50) implies both the volume law and the Page correction of the 2-REE of individual energy eigenstates, Eq. (6.51) implies the volume law of the 2-OSEE for the LTE, and Eq. (6.52) implies the finite-temperature Page correction of the 2-OSEE for the LTE.

Finally, we comment on previous numerical studies investigating the 1-OSEE of the time evolution operator e^{-iHt} of various integrable and nonintegrable models. References [57, 261] have shown that the 1-OSEE of the time evolution operator relaxes to the HRU value in nonintegrable systems, while it does not saturate at the HRU value in noninteracting and interacting integrable systems. These findings look reasonable from the viewpoint of the 2-ETH for S_X: the 1-OSEE saturates at the HRU value if the 2-ETH for S_X is satisfied. This relationship can be shown as follows. We expect that $R^{(2)}_U(X,Y) \approx R^{(2)}_{\mathsf{L}}(X,Y)$ holds at late times, and we have $R^{(2)}_{\mathsf{L}}(X,Y) \approx R^{(2)}_{\mathsf{H}}(X,Y)$, if the 2-ETH is true for S_X. On the other hand, $R^{(1)}_U(X,Y) \leq R^{(2)}_U(X,Y)$ follows from a standard property of the Rényi entropy. By combining these fact, we have $R^{(1)}_U(X,Y) \gtrsim R^{(2)}_{\mathsf{H}}(X,Y)$, which is the desired result. Therefore, previous numerical results suggest that the 2-ETH for S_X is only valid in nonintegrable systems. This is also consistent with our argument based on numerical calculations presented in Sec. 6.6.

6.6 Numerical verification of the 2-ETH

In this section, we numerically investigate the validity of the approximate 2-ETH. We show that, for both $A^{\otimes 2}$ and S_X, the 2-ETH is approximately satisfied in the nonintegrable parameter region of the spin-1/2 XXZ ladder model.

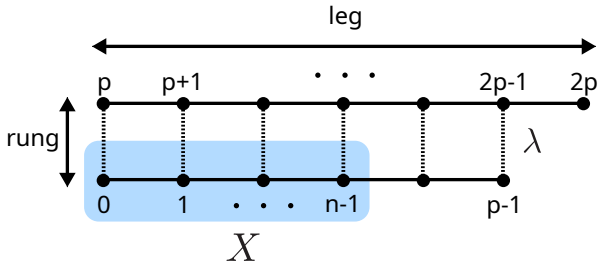

Fig. 6.4 The structure of the ladder of our model (6.93). The sites in a short (long) chain are labeled as $0, 1, \ldots, p-1$ $(p, p+1, \ldots, 2p)$. The coupling strength between two chains is denoted by λ.

6.6.1 Setup and method

We study the one-dimensional spin-1/2 XXZ ladder model, introduced in Ref. [104]. In order to break the reflection symmetry, we consider a ladder composed of short and long open chains whose lengths are p and $p+1$, respectively (see Fig. 6.4) and denote the total number of sites by $N := 2p+1$. The Hamiltonian of our model is given by

$$H_{\mathrm{XXZ}} := \sum_{i=0}^{p-2} h_{i,i+1} + \sum_{i=p}^{2p-1} h_{i,i+1} + \lambda \sum_{i=0}^{p-1} h_{i,i+p}, \tag{6.93}$$

where the XXZ coupling $h_{i,j}$ is given by

$$h_{i,j} := X_i X_j + Y_i Y_j + \Delta Z_i Z_j, \tag{6.94}$$

and X_i, Y_i, Z_i represent the Pauli operators of a spin located at site i. Because the total number of up-spins $N_\uparrow := \sum_{i=1}^{N} (Z_i+1)/2$ is a conserved quantity, we focus on the energy eigenstates of H_{XXZ} within a sector of $N_\uparrow = p$. In the following calculation, we fix the anisotropic parameter as $\lambda = 0.8$ as in Ref. [104]. The model is nonintegrable except for a specific point $\lambda = 0$ and satisfies the approximate 1-ETH and the off-diagonal ETH in the nonintegrable region [104].

We investigate the system-size (the total number of sites) dependence of the indicator of the approximate 2-ETH $I_2(O)$ introduced in Sec. 6.2.3. In our calculation, we adopt the following procedure in the same manner as Refs. [99, 104]. We use thicker and thinner energy shells to overcome the smallness of the number of states in the energy shell. To reduce statistical errors, we sample all the energy eigenstates in a thicker energy shell, which is given by $[E-\Delta E, E]$ with $\Delta E = N\delta$ and an N-independent constant $\delta > 0$. The number of energy eigenstates in the thicker shell is denoted by d. On the other hand, in the calculation of the microcanonical average in $I_2(O)$, we use a thinner energy shell defined as follows, in order to take account of the energy changing. A thinner energy shell for calculation of $\Delta^{(2)}_{ij,ij}(O)$ and $\Delta^{(2)}_{ij,ji}(O)$ is given by $[E_{ij} - \delta_{\mathrm{mc}}, E_{ij}]$ with $E_{ij} := (E_i + E_j)/2$. Here, the energy width of the thinner energy shell

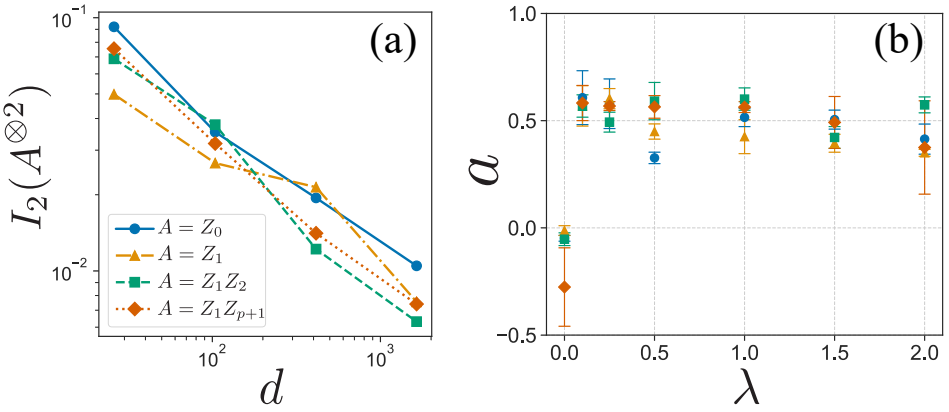

Fig. 6.5 (a) Log-log plot of $I_2(A^{\otimes 2})$ vs d with $\lambda = 1.0$ (nonintegrable). $I_2(A^{\otimes 2})$ tends to zero and scales polynomially with d for all four observables. (b) The fitting result a of $I_2(A^{\otimes 2}) = \mathcal{O}(d^{-a})$ is plotted against the nonintegrability parameter λ. In the integrable case ($\lambda = 0$), the exponent a takes a value near 0 for Z_0, Z_1, and Z_1Z_2 and a negative value for Z_1Z_{p+1}. In the nonintegrable cases ($\lambda \neq 0$), the exponent a takes a value near 0.5. In both panels, the observable A is set to Z_0, Z_1, Z_1Z_2, and Z_1Z_{p+1}. Reproduced from Fig. 4 of [226].

$\delta_{\rm mc}$ is independent of the system-size N. In our numerical calculations, the parameters of the energy shells are fixed as $E = 0$ (the energy at infinite temperature), $\delta = 0.02$, and $\delta_{\rm mc} = 0.1$.

6.6.2 Tensor product operator

We first investigate the validity of the 2-ETH for the tensor-product form operator $O = A^{\otimes 2}$ with a few-body operator A. We consider four operators, Z_0, Z_1, Z_1Z_2 and Z_1Z_{p+1} for a single replica operator A and calculate $I_2(A^{\otimes 2})$ by changing the system size as $N = 11, 13, 15, 17$.

The d-dependence of $I_2(A^{\otimes 2})$ with $\lambda = 1.0$ (nonintegrable) is shown in Fig. 6.5 (a). We clearly see that $I_2(A^{\otimes 2})$ decays polynomially with d for all four observables. Thus, we conclude that the approximate 2-ETH is true for all of those observables. This result is reasonable because the XXZ ladder model (6.93) satisfies the approximate 1-ETH and the off-diagonal ETH [104, 105].

We next carry out the fitting to study the d-dependence of $I_2(A^{\otimes 2})$ in more detail. We numerically fit $\log I_2(A^{\otimes 2})$ with a fitting function $f(d) := -a \log d + b$ with two fitting parameters a and b. Figure 6.5 (b) shows the values of a for the several values of λ. At $\lambda = 0$ (integrable), the exponent a is not positive within the numerical error, which implies the violation of the approximate 2-ETH. This is consistent with the fact that the XXZ ladder model (6.93) does not satisfy the approximate 1-ETH and the off-diagonal ETH at the integrable point [104]. On the other hand, in nonintegrable cases, the exponent a is approximately 0.5 regardless of

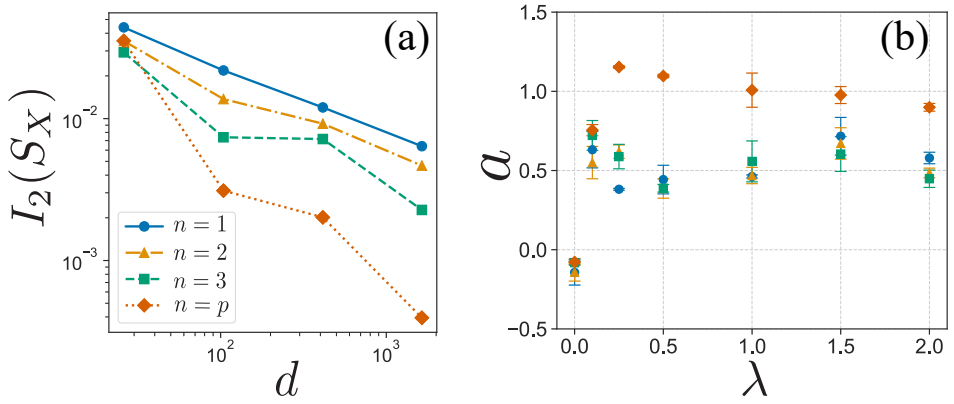

Fig. 6.6 (a) Log-log plot of $I_2(S_X)$ vs d with $\lambda = 1.0$ (nonintegrable). Similar to Fig. 6.5 (a), $I_2(S_X)$ tends to zero and scales polynomially with d in all cases. (b) The fitting result a of $I_2(S_X) = \mathcal{O}(d^{-a})$ is plotted against the nonintegrability parameter λ. In the integrable case ($\lambda = 0$), the exponent a takes a slightly negative value for all choices of the subsystem size. In nonintegrable cases ($\lambda \neq 0$), the exponent a takes a value near 0.5 for $n = 1, 2, 3$ (local) and a value near 1.0 for $n = p$ (nonlocal). In both panels, X is taken as in Fig. 6.4, and the subsystem size is set to $n = 1, 2, 3, p$. Reproduced from Fig. 5 of [226].

the observable. This result implies that the 2-ETH for $A^{\otimes 2}$ holds only at the leading order. In other words, a nontrivial higher-order correction of the 2-ETH is not found for $A^{\otimes 2}$.

6.6.3 Partial swap operator

We next investigate the validity of the 2-ETH for the partial swap operator S_X. We set subsystem X as illustrated in Fig. 6.4 and denote the number of spins in X by n. Figure 6.6 shows the d-dependence of the indicator $I_2(S_X)$ with $\lambda = 1$ (nonintegrable) for four subsystem sizes $n = 1, 2, 3, p$. In the case of $n = p$, X corresponds to the shorter chain, which grows linearly with the entire system size. As in the case of $O = A^{\otimes 2}$, $I_2(S_X)$ decays polynomially with d, which implies that the approximate 2-ETH for S_X holds regardless of locality of X. The validity of the 2-ETH also implies that the 2-REE takes a value near the maximum for all the energy eigenstates.

As in Sec. 6.6.2, we fit $\log I_2(S_X)$ with a fitting function $f(d) = -a \log d + b$. Figure 6.6 shows the λ-dependence of the exponent a for $I_2(S_X)$. As is the case for $A^{\otimes 2}$, the exponent a takes a nonpositive value in the integrable case ($\lambda = 0$), while takes a positive value in the nonintegrable cases ($\lambda \neq 0$). This result implies that the approximate 2-ETH for S_X holds only in the nonintegrable case and, a low-entanglement energy eigenstate exists in the integrable case.

Moreover, the exponent a takes a different value depending on the locality of X in the

nonintegrable cases. For $n = 1, 2, 3$ (local region), the exponent a is near 0.5, which is the same as in the case of $A^{\otimes 2}$. This correspondence can be explained as follows. The partial swap operator can be represented as

$$S_X = \frac{1}{d_X} \sum_{i=1}^{d_X^2} A_i^{\otimes 2}, \tag{6.95}$$

where the summation runs over all the Pauli operators supported on X, including the many-body Pauli operators. If X is local, the number of the terms in the summation does not grow with d. Thus, the d-dependence of $I_2(S_X)$ is the same as that of $I_2(A_i^{\otimes 2})$.

In contrast to the case of local regions, the exponent a is approximately one for $n = p$. Because the summation on the right-hand side of Eq. (6.95) grows with d in this case, the argument below Eq. (6.95) cannot be applied. Moreover, the d^{-1} scaling implies that the 2-REE of the energy eigenstate follows the (infinite-temperature) Page curve (6.60). In our numerical setup with $n = p$, the 2-ETH corresponding to the 2-REE is given by

$$\langle E_i E_i | S_X | E_i E_i \rangle \approx 2d^{-1/2}, \tag{6.96}$$

where we used an approximation $R_{\mathrm{MC}}^{(2)}(X) \approx \log d^{1/2}$. We note again that the factor of 2 in front of $d^{-1/2}$ is crucial for the Page correction. The d^{-1} scaling of $I_2(S_X)$ implies that $\langle E_i E_i | S_X | E_i E_i \rangle = 2d^{-1/2} + \mathcal{O}(d^{-1})$ holds, and thus the 2-REE of the corresponding eigenstate contains the Page correction. Because the Page correction cannot be explained from the approximate 1-ETH, this result implies that three is a nontrivial contribution of the 2-ETH in the case of the nonlocal partial swap operator.

We remark that we used the following random vector technique in numerical calculations of the trace over $\mathcal{H}^{\otimes 2}$ to reduce the computation time. From the mathematically rigorous argument of typicality [132], the trace of $O \in \mathcal{B}(\mathcal{H}^{\otimes 2})$ is well approximated by $d^2 \langle \psi | O | \psi \rangle$, where $|\psi\rangle$ is a pure state uniformly sampled from $\mathcal{H}^{\otimes 2}$. We thus used $d^2 \langle \psi | O | \psi \rangle$ instead of directly calculating the trace.

6.6.4 Summary of numerical results

We present Table 6.1 to summarize our results in this section. From Figs. 6.5 and 6.6, we conclude that the approximate 2-ETHs for $A^{\otimes 2}$ and S_X are not satisfied in the integrable case because the exponent a does not take a positive value. This is consistent with the fact that the approximate 1-ETH is violated in the integrable case. The next natural question is whether typical energy eigenstates satisfy the 2-ETH, i.e., the weak 2-ETH. We can prove the weak 2-ETH for a local operator from the weak 1-ETH and the weak off-diagonal ETH, while that for a nonlocal partial swap is not obtained in a straightforward way. Thus, the numerical

Table 6.1 Summary of the fitting exponent a defined through $I_2(O) = \mathcal{O}(d^{-a})$. The approximate 2-ETH for $A^{\otimes 2}$ and S_X is valid only in the nonintegrable cases.

	$A^{\otimes 2}$	S_X	
	local	local	nonlocal
Integrable	~ 0	~ 0	~ 0
Nonintegrable	~ 0.5	~ 0.5	~ 1

verification of the weak 2-ETH for a nonlocal partial swap is important, while, unfortunately that is not clear from the numerical calculation.

On the other hand, the approximate 2-ETH is valid for all considered operators in the nonintegrable cases. In particular, we found the quantitative difference of the exponent a between local and nonlocal operators: $a \sim 0.5$ for local operators and $a \sim 1$ for a nonlocal partial swap. The former implies the absence of the nontrivial correction from the 2-ETH, while the latter implies the presence of that corresponding to the Page correction.

6.7 Summary

In this chapter, we have formulated the k-ETH (6.12) and investigated its properties by using quantum-information theoretic techniques. The k-ETH characterizes the hierarchical structure of quantum chaos: The 1-ETH represents the conventional ETH, which is consistent with our expectation that thermalization describes the lowest complexity of chaotic many-body dynamics. For $k \geq 2$, the k-ETH leads to the finite-temperature Page curve for the k-REE of individual energy eigenstates and that for the k-OSEE of the LTE. These results imply that the eigenstate Page curve describes the higher-order complexity.

To check the validity of the above scenario in a finite-size system, we have formulated an approximation of the k-ETH by using the max-norm (6.19). Using this formulation, we have provided the numerical evidence that the 2-ETH approximately holds in the nonintegrable cases while not in the integrable case (see Table 6.1). These results imply that scrambling and the entanglement structure crucially depend on the integrability, as well as thermalization. Specifically, for the nonlocal operator swapping a half of the entire system, we found that the finite-size deviation from the 2-ETH is proportional to d^{-1} in the nonintegrable cases, which is the evidence of the presence of the Page correction.

As mentioned in Sec. 6.2, the k-ETH is related but not equivalent to unitary k-designs. We consider the details of this relationship in the next chapter. Similar to the fact that unitary k-designs are sufficient for the kth-order information scrambling, the exact k-ETH for

tensor-product form operator implies the relaxation of the $2k$-point OTOC to the HRU value. However, we have pointed out that a naive definition of the approximate decay of the $2k$-point OTOC does not work well to characterize the higher-order complexity at least in the cases of $k = 2$ [233]. The reason for the failure of the naive argument is that the approximate k-ETH for $A^{\otimes k}$ follows from the approximate 1-ETH and off-diagonal ETH for A. It is an important issue to establish a more meaningful formulation of the approximate decay of the OTOC and the approximate k-ETH.

The hierarchical appearance of chaotic behavior shown in Fig 6.2 is an essential aspect of chaotic many-body dynamics as well as the late-time chaotic behavior investigated in this chapter. The k-ETH is expected to give insights into the mechanism of such the structure. In fact, several studies [245, 262, 263] have established essential connections between the Srednicki's ETH ansatsz (2.29) and the early time operator growth.

Chapter 7

Partial unitary design

In this chapter, we reconsider the relationship among the k-scrambling (6.6), the k-ETH (6.12) and unitary k-designs and propose a generalization of unitary k-designs to give an information-theoretic view on the pseudorandomness of chaotic Hamiltonian dynamics. In Sec. 7.1, we first point out that the long-time ensemble (LTE) does not achieve a unitary k-design because of energy conservation. At the same time, however, the LTE can still be almost indistinguishable from the Haar random unitary (HRU) as long as one only observes a limited class of observables. In Sec. 7.2, we formulate such pseudorandomness of ensembles as *partial* unitary (PU) k-designs. We also introduce the set of k-scrambled operators, which is the maximum set of operators that makes an ensemble a PU k-design. In Sec. 7.3, we give the explicit expressions of the set of k-scrambled operators for specific ensembles. Furthermore, we specify the linear space of operators satisfying the exact k-ETH.

7.1 Basic idea

As already mentioned in Sec. 6.2, the LTE does not form a unitary k-design, which means that the exact k-ETH (6.12) is not satisfied for some operators. We now explain how this fact can be seen as a natural consequence of energy conservation. Because the time-evolution operator e^{-iHt} is diagonal in the energy eigenbasis of H for any t, it cannot randomize the occupation probabilities of the energy eigenstates. This can be seen more clearly by considering the projection to an energy eigenstate $P_i := |E_i\rangle \langle E_i|$. By energy conservation, P_i is invariant

under the action of the 1-fold channel of the LTE, while the HRU randomizes P_i as seen from Eq. (6.10):

$$\Phi_{\mathsf{L}}^{(1)}(P_i) = P_i \neq \frac{I}{d} = \Phi_{\mathsf{H}}^{(1)}(P_i). \tag{7.1}$$

Thus, the 1-scrambling (i.e., quantum ergodicity) for P_i is not satisfied, and the LTE is not even a unitary 1-design.

However, we expect that chaotic dynamics and the HRU have a common feature in the following sense. The important point here is that, in practice, one only has incomplete accessibility to the system and cannot measure all the observables. Since the number of linearly independent observables of many-body systems increases exponentially with the system size, we need an exponentially large number of measurements to know all the details of dynamics. On the other hand, our main concern is about few-body observables. The number of $\mathcal{O}(1)$-body operators grows only polynomially with the system size. Moreover, in practical experimental setups [13, 17], one only can measure few-body observables and cannot access highly nonlocal and many-body observables. In general, one cannot distinguish chaotic dynamics and the HRU just by measuring such the limited class of observables (see Fig. 7.1). Or to put it the other way round, the behavior of observables outside the accessible class can deviate from that of the HRU, which allows the dynamics itself not to be unitary designs. As for the preceding argument, it will be hard to directly measure the occupation of a single energy eigenstate in the experiment, because the projection operator P_i is highly nonlocal. We also note that this situation is the same as the case of the second law, which has been discussed in Sec. 5.1. In that case, cyclic operations, instead of observables, are limited to accessible operations.

Thus, we need to consider *partial randomness* (i.e., randomness only on accessible observables) to bridge a gap between chaotic Hamiltonian dynamics and the HRU. This observation brings us to the concept of partial unitary designs only on the set of accessible observables, which will be formalized in the next subsection.

7.2 PU k-design

7.2.1 Definition of PU k-designs

We now formulate PU k-designs. Let us fix an arbitrary subset of $\mathcal{B}(\mathcal{H}^{\otimes k})$, which is not necessarily a linear space and written as $\mathcal{A}$. The subset $\mathcal{A}$ represents the set of accessible operators. Then, PU k-designs are defined as ensembles of unitaries that act like unitary k-designs at least on $\mathcal{A}$.

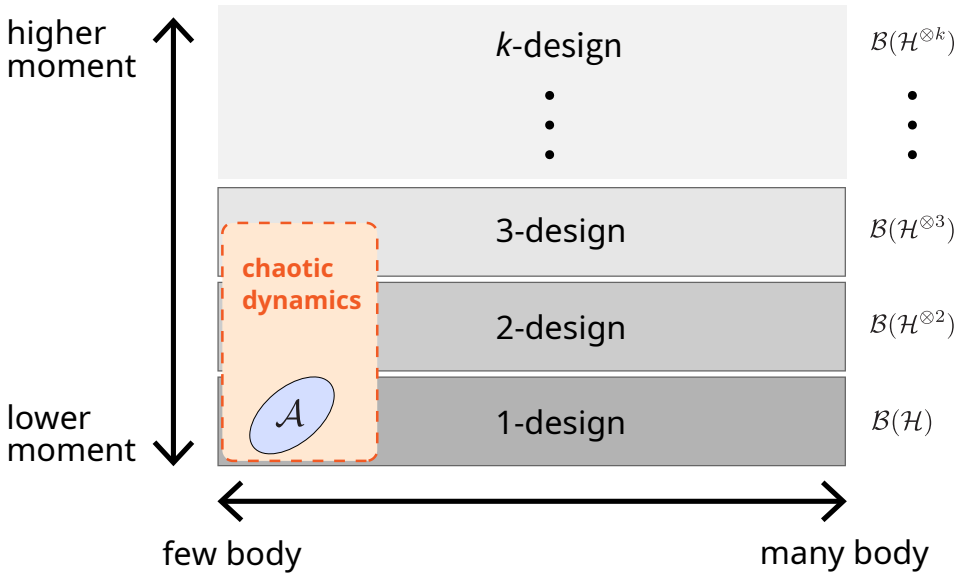

Fig. 7.1 Schematic illustration of the relationship between unitary k-designs and chaotic dynamics. $\mathcal{A}$ represents the set of accessible operators.

Definition 7.1 Partial unitary k-design

An ensemble ν is a PU k-design on $\mathcal{A} \subset \mathcal{B}(\mathcal{H}^{\otimes k})$ if

$$\Phi_{\nu}^{(k)}(O) = \Phi_{\mathsf{H}}^{(k)}(O) \tag{7.2}$$

holds for any $O \in \mathcal{A}$.

The definition of PU k-designs can be phrased as the k-scrambling (6.6) for all the accessible operators. If ν is a PU k-design on $\mathcal{A}$, ν is also a PU k-design on any subset of $\mathcal{A}$. However, the converse of this property is not true in general. If we can access all the observable, i.e., $\mathcal{A} = \mathcal{B}(\mathcal{H}^{\otimes k})$, PU k-designs reduces to the conventional unitary k-designs (see Definition 4.1).

7.2.2 k-scrambled observables

We next consider the maximum subset of $\mathcal{B}(\mathcal{H}^{\otimes k})$, written as $\mathcal{M}_{\nu}^{(k)}$, such that the ensemble ν becomes a PU k-design, namely, the full set of the k-scrambled operators by ν. As shown below, this set quantifies the randomness of a given ensemble. We define $\mathcal{M}_{\nu}^{(k)} \subset \mathcal{B}(\mathcal{H}^{\otimes k})$ by

$$\mathcal{M}_{\nu}^{(k)} := \{O \in \mathcal{B}(\mathcal{H}^{\otimes k}) : \Phi_{\nu}^{(k)}(O) = \Phi_{\mathsf{H}}^{(k)}(O)\}. \tag{7.3}$$

In other words, $\mathcal{M}_{\nu}^{(k)}$ is the kernel of the channel $\Delta_{\nu}^{(k)} := \Phi_{\nu}^{(k)} - \Phi_{\mathsf{H}}^{(k)}$. By definition, $\mathcal{M}_{\nu}^{(k)}$ is a linear space. That is, for any $O_1, O_2 \in \mathcal{M}_{\nu}^{(k)}$ and $c_1, c_2 \in \mathbb{C}$, $c_1 O_1 + c_2 O_2 \in \mathcal{M}_{\nu}^{(k)}$ holds. We give some examples of $\mathcal{M}_{\nu}^{(k)}$ in Sec. 7.3. In particular, we show an explicit expression of

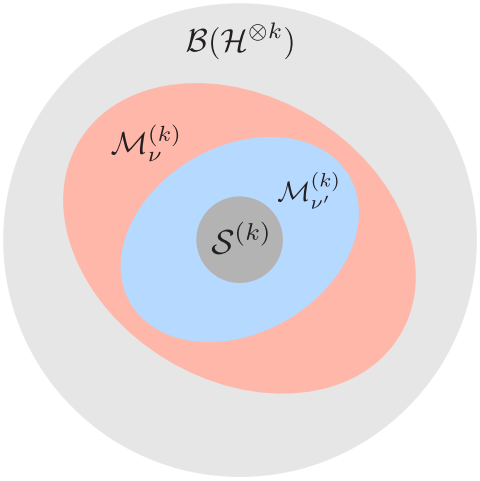

Fig. 7.2 Schematic of relations (7.4) and (7.7). $\mathcal{S}^{(k)}$ represents the set of the k-scrambled operators for a single unitary ensemble (i.e., the minimally random ensemble) and is placed at the center . If $\mathcal{M}_{\nu}^{(k)}$ includes $\mathcal{M}_{\nu'}^{(k)}$, ν can be regarded as more random than ν'

the k-scrambled operators for the LTE, which equals the complete set of operators satisfying the exact k-ETH (6.12). The set of the k-scrambled observables $\mathcal{M}_{\nu}^{(k)}$ also provides a simple representation of the definition of PU k-design as follows: ν is a PU k-design on a given set $\mathcal{A}$ if and only if $\mathcal{A} \subset \mathcal{M}_{\nu}^{(k)}$.

Moreover, $\mathcal{M}_{\nu}^{(k)}$ allows us to represent the hierarchical structure of randomness. An ensemble ν can be regarded as more random than another ensemble ν' if the former is indistinguishable from the HRU for a broader class of operators than the latter:

$$\mathcal{M}_{\nu'}^{(k)} \subset \mathcal{M}_{\nu}^{(k)} \tag{7.4}$$

holds for all k. This subset relation gives a preorder relation on ensembles of unitaries. Furthermore, the dimension of $\mathcal{M}_{\nu}^{(k)}$ as a linear space gives a simple necessary condition of Eq. (7.4): If Eq. (7.4) is satisfied, we have

$$\dim(\mathcal{M}_{\nu'}^{(k)}) \leq \dim(\mathcal{M}_{\nu}^{(k)}). \tag{7.5}$$

We remark that the subset relation does not give the total order, i.e., there exist ensembles such that neither $\mathcal{M}_{\nu'}^{(k)} \subset \mathcal{M}_{\nu}^{(k)}$ nor $\mathcal{M}_{\nu'}^{(k)} \supset \mathcal{M}_{\nu}^{(k)}$ is satisfied, but the order of dimensions gives the total order over ensembles of unitaries.

It is obvious that $\mathcal{M}_{\nu}^{(k)} = \mathcal{M}_{\mathsf{H}}^{(k)} = \mathcal{B}(\mathcal{H}^{\otimes k})$ holds if and only if ν is a unitary k-design. This implies that unitary k-designs are the maximally random ensembles at the level of kth order. On the other hand, the identity ensemble $\nu_{\mathrm{id}} := \{I\}$, where the identity operator I arises with probability one, is a minimally random. As shown in Sec. 7.3, the set of k-scrambled

observables of ν_{id} is a linear combination of the permutation operators on k replicas:

$$\mathcal{M}_{\nu_{\mathrm{id}}}^{(k)} = \mathcal{S}^{(k)} := \mathrm{span}\left\{W_\pi : \pi \in S_k\right\}, \tag{7.6}$$

where $\mathrm{span}\{\cdots\}$ denotes the operator space linearly spanned by $\{\cdots\}$. Since the cardinality of S_k is $k!$, the dimension of $\mathcal{M}_{\nu_{\mathrm{id}}}^{(k)}$ is $k!$. We note that the following relation holds for any ensemble ν:

$$\mathcal{S}^{(k)} = \mathcal{M}_{\nu_{\mathrm{id}}}^{(k)} \subset \mathcal{M}_{\nu}^{(k)} \subset \mathcal{M}_{\mathsf{H}}^{(k)} = \mathcal{B}(\mathcal{H}^{\otimes k}). \tag{7.7}$$

Here, $\mathcal{M}_{\nu}^{(k)} = \mathcal{S}^{(k)}$ is satisfied only if ν contains only a single unitary, and $\mathcal{M}_{\nu}^{(k)} = \mathcal{B}(\mathcal{H}^{\otimes k})$ is satisfied only if ν is a unitary k-design. The relation (7.7) leads to the following inequality of the dimension:

$$k! \leq \dim(\mathcal{M}_{\nu}^{(k)}) \leq d^k. \tag{7.8}$$

Therefore, we can say that ν has a nearly maximal randomness if $\dim(\mathcal{M}_{\nu}^{(k)}) \approx d^k$ and a nearly minimal randomness if $\dim(\mathcal{M}_{\nu}^{(k)}) \approx k!$.

We can also show the following expression:

$$\mathcal{M}_{\nu}^{(k)} = \mathrm{Ker}(\Phi_{\nu}^{(k)}) \oplus \mathcal{S}^{(k)}, \tag{7.9}$$

where $\mathrm{Ker}(\Phi_{\nu}^{(k)})$ represents the kernel of $\Phi_{\nu}^{(k)}$, i.e., $\mathrm{Ker}(\Phi_{\nu}^{(k)}) := \{O \in \mathcal{B}(\mathcal{H}^{\otimes k}) : \Phi_{\nu}^{(k)}(O) = 0\}$. Thus, we can say that the kth randomness of ν is characterized by $\mathrm{Ker}(\Phi_{\nu}^{(k)})$. Equation (7.9) follows from the fact that $\mathcal{S}^{(k)}$ is invariant under the action of the k-fold channel of any ensemble, and $\mathcal{S}^{(k)}$ is the image of the k-fold channel of the HRU. See also Fig. 7.3 for a schematic. Equation (7.9) also implies

$$\dim(\mathcal{M}_{\nu}^{(k)}) = k! + \dim[\mathrm{Ker}(\Phi_{\nu}^{(k)})]. \tag{7.10}$$

7.3 Examples

We provide an explicit expression of the set of the k-scrambled operators for several ensembles that are not full unitary designs.

7.3.1 Single unitary ensemble

The first example is the simplest ensemble containing only a a single unitary operator $U \in \mathcal{U}(\mathcal{H})$. We denote a single unitary ensemble by $\nu_U := \{U\}$, where U arises with probability one. We note that the identity ensemble is a particular case of a single unitary ensemble ν_U with $U = I$. As an immediate consequence of Eq. (7.9) and $\mathrm{Ker}(\Phi_{\nu_U}^{(k)}) = 0$, we have

$$\mathcal{M}_{\nu_U}^{(k)} = \mathcal{S}^{(k)}. \tag{7.11}$$

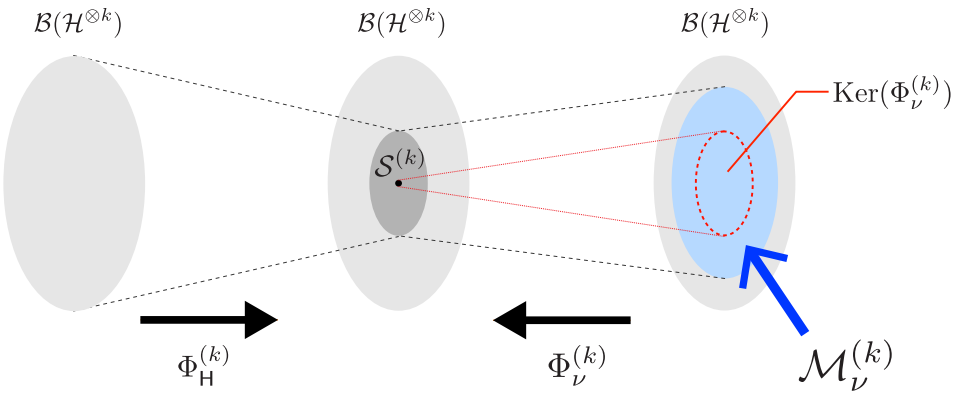

Fig. 7.3 Schematic of Eq. (7.9). The image of the k-fold channel of the HRU is equivalent to $\mathcal{S}^{(k)}$. The region surrounded by the red circle represents the kernel of the k-fold channel of ν, and the blue region represents the set of the k-scrambled operators of ν, which is mapped to $\mathcal{S}^{(k)}$ by $\Phi_\nu^{(k)}$.

and $\dim(\mathcal{M}_{\nu_U}^{(k)}) = k!$. These results imply that ν_U has the minimum randomness.

7.3.2 Random diagonal-unitary ensemble

We next consider the ensemble of random diagonal-unitaries [198, 237, 238], which is defined as follows. We fix an orthonormal basis $J := \{|j\rangle\}_{j\in\{1,\dots,d\}}$ of $\mathcal{H}$ and define a random diagonal-unitary in the basis J by

$$U_{\mathrm{diag}} = \sum_{j=1}^{d} e^{i\phi_j} |j\rangle\langle j|, \tag{7.12}$$

where $\phi_1, \dots, \phi_d$ are drawn uniformly and independently from $[-\pi, \pi]$. The ensemble of random diagonal-unitaries in the basis J is denoted by D_J. The k-fold channel of a random diagonal-unitary ensemble D_J is given by

$$\Phi_{\mathsf{D}_J}^{(k)}(O) = \int_{-\pi}^{\pi} \prod_{j=1}^{d} \frac{d\phi_j}{2\pi} \sum_{\boldsymbol{j},\boldsymbol{j}'} e^{-i\sum_{i=1}^{k}(\phi_{j_i} - \phi_{j'_i})} |\boldsymbol{j}\rangle\langle\boldsymbol{j}|O|\boldsymbol{j}'\rangle\langle\boldsymbol{j}'| \tag{7.13}$$

$$= \sum_{\boldsymbol{j}\sim\boldsymbol{j}'} |\boldsymbol{j}\rangle\langle\boldsymbol{j}|O|\boldsymbol{j}'\rangle\langle\boldsymbol{j}'|. \tag{7.14}$$

Therefore, the kernel of $\Phi_{\mathsf{D}_J}^{(k)}$ is given by

$$\mathrm{Ker}(\Phi_{\mathsf{D}_J}^{(k)}) = \mathrm{span}\{|\boldsymbol{j}\rangle\langle\boldsymbol{j}'| : \pi \in S_k, \boldsymbol{j} \not\sim \boldsymbol{j}'\}. \tag{7.15}$$

From this and Eq. (7.9), the set of the k-scrambled operators for D_J is given by

$$\mathcal{M}_{\mathsf{D}_J}^{(k)} = \mathrm{span}\{W_\pi, |\boldsymbol{j}\rangle\langle\boldsymbol{j}'| : \pi \in S_k, \boldsymbol{j} \not\sim \boldsymbol{j}'\}. \tag{7.16}$$

We next specify the complete set of observables that satisfy the exact k-ETH (6.12) from the correspondence between the LTE and the diagonal ensemble. As in Sec. 6.2, we assume the k-incommensurate condition (Assumption 3). We denote the energy eigenbasis by $E := \{|E_i\rangle\}_{\in\{1,\dots,d\}}$. By comparing Eq. (6.7) and Eq. (7.14), we obtain

$$\Phi_{\mathsf{L}}^{(k)}(O) = \Phi_{\mathsf{D}_E}^{(k)}(O) \tag{7.17}$$

for any $O \in \mathcal{B}(\mathcal{H}^{\otimes k})$. Therefore, the LTE is indistinguishable from random diagonal-unitaries in the energy eigenbasis as long as one looks at the action of the k-fold channel, which is referred to as a diagonal-unitary k-design in E. Applying the result of random diagonal-unitaries (7.16), we obtain the following explicit expression of the k-scrambled operators for the LTE:

$$\mathcal{M}_{\mathsf{L}}^{(k)} = \mathcal{M}_{\mathsf{D}_E}^{(k)} = \mathrm{span}\{W_\pi, |E(\boldsymbol{i})\rangle\langle E(\boldsymbol{i}')| : \pi \in S_k, \boldsymbol{i} \not\sim \boldsymbol{i}'\}. \tag{7.18}$$

This set is equivalent to the set of operators satisfying the exact k-ETH (6.12).

7.3.3 Pauli ensemble

The third example is the Pauli ensemble, which is a unitary 1-design, but not a 2-design [190]. We denote the set of tensor products of Pauli operators acting on each qubit (Pauli chains) by

$$\mathcal{P} := \{\sigma_1 \otimes \cdots \otimes \sigma_N : \sigma_n = I,\ X,\ Y,\ Z\}. \tag{7.19}$$

$\mathcal{P}$ forms a basis of $\mathcal{B}(\mathcal{H})$. The uniform ensemble over $\mathcal{P}$ is called the Pauli ensemble and denoted by P. From the completeness of $\mathcal{P}$, we can show $\Phi_{\mathsf{P}}^{(1)}(O) = \dfrac{I}{d}\mathrm{Tr}[O]$. Therefore, we have

$$\mathcal{M}_{\mathsf{P}}^{(1)} = \mathcal{B}(\mathcal{H}). \tag{7.20}$$

On the other hand, the set of the 2-scrambled operators by P is given by

$$\mathcal{M}_{\mathsf{P}}^{(2)} = \mathrm{span}\{W_\pi, P_l \otimes P_m \in \mathcal{P}_N^{\otimes 2} : \pi \in S_2, l \neq m\}. \tag{7.21}$$

Therefore, the Pauli ensemble is not a unitary 2-design. In contrast to the fact that $\dim(\mathcal{M}_{\nu_U}^{(k)}) = 2$ holds for a single unitary ensemble, we have $\dim(\mathcal{M}_{\mathsf{P}}^{(2)}) = d^4 - d^2 + 2$ for the Pauli ensemble. Because it is close to the maximum value d^4, we can say that the Pauli ensemble is much closer to a full unitary 2-design than a single unitary ensemble.

Equation (7.21) can be derived as follows. We first calculate the 2-fold channel of P. Any nontrivial Pauli operator $P_l \in \mathcal{P}(P_l \neq I)$ commutes with a half of the operators in $\mathcal{P}$, while

anti-commutes with the others. Accordingly, we introduce a Boolean-valued function

$$F(l,m) := \begin{cases} 0 & \text{for } P_l P_m = P_l P_m \\ 1 & \text{for } P_l P_m = -P_m P_l. \end{cases} \tag{7.22}$$

This function satisfies

$$\frac{1}{d^2}\sum_j (-1)^{F(j,l)+F(j,m)} = \delta_{lm} \tag{7.23}$$

for any l and m. Because $\mathcal{P}$ is an orthonormal basis of the operator space $\mathcal{B}(\mathcal{H})$, any operator $O \in \mathcal{B}(\mathcal{H}^{\otimes 2})$ is represented as $O = \sum_{l,m} \langle P_l \otimes P_m | O \rangle \, P_l \otimes P_m$. By using these facts, we can calculate the action of the 2-fold channel of P as follows:

$$\Phi_{\mathsf{P}}^{(2)}(O) = \frac{1}{d^2}\sum_{j,l,m} \langle P_l \otimes P_m | O \rangle \, (P_j P_l P_j) \otimes (P_j P_m P_j) \tag{7.24}$$

$$= \frac{1}{d^2}\sum_{j,l,m} \langle P_l \otimes P_m | O \rangle \, (-1)^{F(j,l)+F(j,m)} P_l \otimes P_m \tag{7.25}$$

$$= \sum_l \langle P_l \otimes P_l | O \rangle \, P_l \otimes P_l. \tag{7.26}$$

Therefore, the kernel of $\Phi_{\mathsf{P}}^{(2)}$ is given by

$$\mathrm{Ker}(\Phi_{\mathsf{P}}^{(2)}) = \mathrm{span}\{P_l \otimes P_m \in \mathcal{P}_N^{\otimes 2} : l \neq m\}. \tag{7.27}$$

Then, Eq. (7.21) is follows from Eq. (7.9).

Chapter 8

Conclusions and future perspectives

8.1 Conclusions

In this thesis, we have studied the fundamental properties of chaotic dynamics in isolated quantum many-body systems. In particular, we have addressed two questions: (i) how the second law of thermodynamics emerges from purely quantum dynamics and (ii) why chaotic many-body systems share various common features, such as thermalization, information scrambling, and the universal structure of entanglement. The eigenstate thermalization hypothesis (ETH) connects the properties of energy eigenstates with those of statistical ensembles. Although the ETH has been mainly studied in the context of thermalization, it is reasonable to expect that the ETH plays a key role in the mechanism of the second law. Thus, it is important to confirm the validity of the second law at the level of individual energy eigenstates for establishing the foundation of statistical mechanics. Moreover, because the ETH is one of the significant features of quantum chaos, it may also be relevant for understanding universal features of chaotic dynamics beyond the conventional statistical mechanics. Our studies have clarified that the ETH and its extension are essential to understand not only the foundation of statistical mechanics but also the origin of various chaotic features.

In Chapter 5, we have investigated the possibility of work extraction from a single energy eigenstate and the role of the ETH. We have numerically calculated average work extraction from individual energy eigenstates of the quantum Ising model by cyclic quenches and have shown a clear difference between the integrable case and the nonintegrable cases (Fig. 5.2). To obtain a more quantitative result, we have focused on the system-size dependence of the number of work-extractable eigenstates (Fig. 5.4). As a result, we have found that no one can extract a macroscopic amount of work from an energy eigenstate in the nonintegrable cases,

which implies that the second law is valid for all the energy eigenstates. On the other hand, the number of work-extractable eigenstates does not vanish in the integrable case. With an analytical argument and a numerical verification (Fig. 5.5), we have argued that these numerical results can be understood from the ETH for a nonlocal many-body observable. Moreover, we have proved a rigorous upper bound (5.16) of the ratio of work-extractable eigenstates, implying that one cannot extract work from most finite-temperature eigenstates. This bound is true even in integrable systems as long as the Boltzmann entropy is extensive. Our result suggests that the second law, as well as thermalization, is true at the level of individual energy eigenstates for nonintegrable many-body systems.

In Chapter 6, we have addressed the unification of various features of quantum chaos by introducing the k-ETH (Definition 6.1). The formulation of the k-ETH is based on a quantum information-theoretic notion of statistical pseudorandomness, namely unitary k-designs. The lowest-order ETH (i.e., the 1-ETH) is identical to the conventional ETH and thus characterizes quantum ergodicity. Specifically, we have focused on two types of operators acting on the k-replicated Hilbert space: one is the tensor-product form operator $A^{\otimes k}$, and the other is the subsystem-permuting operator C_X. The former is related to the out-of-time-ordered correlator (OTOC), and the latter is related to the entanglement entropy. We have proved that, if the k-ETH for $A^{\otimes k}$ holds exactly, the corresponding $2k$-point OTOC relaxes to the exact value of the Haar random average. On the other hand, the k-ETH for C_X implies that the kth-Rényi entanglement entropy of an energy eigenstate and its extension to the operator space obey the finite-temperature extension of the Page curve. We would like to emphasize that the Page correction intrinsically originates from the k-ETH and cannot be explained by the conventional ETH (the 1-ETH). Furthermore, we numerically verified that the 2-ETHs for $A^{\otimes 2}$ and C_X approximately hold in the nonintegrable cases, but do not in the integrable case (Figs. 6.5 and 6.6). These results imply that the k-ETH provides a unified view on quantum many-body chaos.

In Chapter 7, to further study the information-theoretic structure behind the k-ETH, we have proposed a partial unitary (PU) k-design (Definition 7.1) and proved its basic properties. A PU k-design is a new type of approximation of random unitaries, in which one focuses on a limited class of operators. Conventional unitary k-designs can be regarded as a special case of PU k-designs where one focuses on all the operators acting on the k-replicated Hilbert space. Moreover, we have shown that the set of the k-scrambled operators (i.e., the maximum set that makes an ensemble a PU k-design) quantifies the randomness of ensembles that are not completely unitary k-designs. We have also derived the explicit forms of the set of the k-scrambled operators for specific ensembles. As a by-product, we have specified operators satisfying the exact k-ETH (7.18).

8.2 Future perspectives

As the epilogue, we discuss a few future perspectives. First, we note that there is no general and rigorous mathematical proof of the ETH (2.23). Proving the ETH and our extensions of the ETH is a most important future problem. The nonintegrability of the system is required to satisfy the ETH, but it is not all. In fact, some many-body systems, such as many-body localized (MBL) systems [102, 222, 223] and quantum many-body scar (QMBS) systems [264–266], are not integrable but do not satisfy the ETH. Many researchers expect that the random matrix-like behavior of a chaotic Hamiltonian inside its energy shell is related to the mechanism of the ETH [35, 246, 267, 268]. However, some systems [98, 99, 269, 270] do not completely obey the finite-size scaling of the variance of the eigenstate expectation values predicted from random matrix theory, nevertheless they undoubtedly satisfy the ETH in the thermodynamic limit. The reason for the failure of the finite-size scaling of the random matrix predictions would lie in the fact that realistic Hamiltonians have additional structure, such as the locality, and thus cannot be fully random. The k-ETH and PU k-designs might give an insight into such incomplete randomness.

The second open question is how the circuit complexity of quantum dynamics grows with time. The complexity growth is crucial to understand quantum many-body chaos and has also been investigated in the context of the holographic duality [271, 272, 272]. However, as mentioned in Sec. 6.1, it is not very easy to estimate the complexity of many-body Hamiltonian dynamics as well as quantum circuits. Recently, Brown and Susskind [230, 231] conjectured that the quantum circuit complexity of highly chaotic dynamics grows linearly for an exponentially long time and fluctuates around the maximum value once it reaches the maximum (see Fig. 6.2). A very recent work [188] has shown a fascinating result based on unitary k-designs: Random quantum circuits are expected to form approximate unitary k-designs in $\mathcal{O}(k)$ depth. In fact, this expectation has been proved in the limit of large local dimension [273]. Because the complexity of a unitary k-design is bounded from below by $\mathcal{O}(k)$, the complexity of random quantum circuits with T depth is $\mathcal{O}(T)$, i.e., the linear growth of the complexity. In the above analysis, forming unitary k-designs is crucial to estimate the complexity of an ensemble, and thus it is not applicable to an ensemble which is not a unitary design. By using PU k-designs, it might be possible to generalize the above analysis to less random dynamics. The first step for achieving this would be to derive the bound of the complexity of PU k-designs.

Third, we anticipate the experimental studies of the second law and the higher-order complexity of quantum many-body dynamics. As reviewed in Sec. 1.3, the recent development of experimental technologies has made it possible to realize isolated quantum many-body systems. In fact, not only thermalization but also the entanglement entropy [274, 275] and the 4-point OTOC [276, 277] have been observed in experiments. In addition, unitary 2-designs

have been constructed by using nuclear magnetic resonance (NMR) systems [278, 279], but the system size is very limited. Compared to unitary designs, PU designs requires much less controllability to realize. Thus, we expect that one can realize PU designs in large quantum systems.

Appendix A

Review of the Weingarten calculus

In this Appendix, we provide a brief review of the Weingarten calculus, which is a crucial tool to calculate the average over the Haar random unitary (HRU). In Sec. A.1, we derive the explicit representation of the k-fold channel of the HRU (6.10) by using the Weingarten matrix. In Sec. A.2, we introduce the Weingarten function [240–242] and investigate its properties to calculate the Weingarten matrix.

A.1 k-fold channel of the HRU

We first prove the following expression of the k-fold channel of the HRU used to derive the k-ETH in Sec. 6.2:

$$\Phi_{\mathsf{H}}^{(k)}(O) = \sum_{\pi,\tau\in S_k} \mathrm{Wg}_{\pi,\tau}(d)\mathrm{Tr}[OW_\tau]W_\pi, \tag{A.1}$$

where $O \in \mathcal{B}(\mathcal{H}^{\otimes k})$, and the Weingarten matrix $\mathrm{Wg}_{\pi,\tau}(d)$ is the inverse of the matrix $Q_{\pi,\tau}(d) := \mathrm{Tr}[W_\pi W_\tau]$. The main tool of the proof is the Schur-Weyl duality [243], which connects the irreducible representation of the unitary group $\mathcal{U}(\mathcal{H})$ and the symmetric group S_k. The Schur-Weyl duality states that $O \in \mathcal{B}(\mathcal{H}^{\otimes k})$ satisfies $[O, U^{\otimes k}] = 0$ for any $U \in \mathcal{U}(\mathcal{H})$ if and only if O is a linear combination of the permutation operators.

We prove Eq. (A.1). From the unitary invariance of the Haar measure, we have

$$U^{\dagger\otimes k}\Phi_{\mathsf{H}}^{(k)}(O)U^{\otimes k} = \Phi_{\mathsf{H}}^{(k)}(O) \tag{A.2}$$

for any $U \in \mathcal{U}(\mathcal{H})$. From the Schur-Weyl duality, $\Phi_{\mathsf{H}}^{(k)}(O)$ can be written as

$$\Phi_{\mathsf{H}}^{(k)}(O) = \sum_{\pi \in S_k} c_\pi(O) W_\pi \tag{A.3}$$

with $c_\pi(O) \in \mathbb{C}$. Because $\Phi_{\mathsf{H}}^{(k)}$ is a linear map on $\mathcal{B}(\mathcal{H}^{\otimes k})$, c_π is also a linear map on $\mathcal{B}(\mathcal{H}^{\otimes k})$ and thus can be represented as

$$c_\pi(O) = \mathrm{Tr}[C_\pi O] \tag{A.4}$$

with an appropriate choice of operator $C_\pi \in \mathcal{B}(\mathcal{H}^{\otimes k})$. From Eq. (A.2), we can show that $[C_\pi, U^{\otimes k}] = 0$ for any $U \in \mathcal{U}(\mathcal{H})$. Applying the Schur-Weyl duality again, we have

$$C_\pi = \sum_{\tau \in S_k} c_{\pi,\tau} W_\tau \tag{A.5}$$

with $c_{\pi,\tau} \in \mathbb{C}$. Therefore, the k-fold channel of the HRU is written as

$$\Phi_{\mathsf{H}}^{(k)}(O) = \sum_{\pi,\tau \in S_k} c_{\pi,\tau} \mathrm{Tr}[O W_\tau] W_\pi. \tag{A.6}$$

On the other hand, from the definition of the k-fold channel, $\Phi_{\mathsf{H}}^{(k)}(W_\pi) = W_\sigma$ holds for all $\sigma \in S_k$. We thus have

$$W_\sigma = \sum_{\pi,\tau \in S_k} c_{\pi,\tau} \mathrm{Tr}[W_\sigma W_\tau] W_\pi, \tag{A.7}$$

which implies that $c_{\pi,\tau}$ is a matrix element of the inverse matrix of $Q_{\sigma,\tau} = \mathrm{Tr}[W_\sigma W_\tau]$. Therefore, $c_{\pi,\tau}$ is a matrix element of the Weingarten matrix. This completes the proof.

By using results in Sec. A.2, we have the following representations of the k-fold channel of the HRU for small k:

- $k = 1$

$$\Phi_{\mathsf{H}}^{(1)}(O) = \frac{\mathrm{Tr}[O]}{d} I. \tag{A.8}$$

- $k = 2$

$$\Phi_{\mathsf{H}}^{(2)}(O) = \frac{d\mathrm{Tr}[O] - \mathrm{Tr}[SO]}{d(d^2-1)} I^{\otimes 2} + \frac{d\mathrm{Tr}[SO] - \mathrm{Tr}[O]}{d(d^2-1)} S. \tag{A.9}$$

A.2 Weingarten function

We need the explicit values of the matrix elements of the Weingarten matrix to derive Eqs. (A.8) and (A.9). As shown in the following, we can obtain them by using the mathematical results of Refs. [240–242].

A.2.1 Definition of the Weingarten function

We here consider the HRU average of the degree k monomials of matrix elements. The exact expression of the average is given by

$$\mathbb{E}_{U\sim\mathsf{H}}\left[U_{i_1j_1}\cdots U_{i_kj_k}U^*_{i'_1j'_1}\cdots U^*_{i'_kj'_k}\right]=\sum_{\pi,\tau\in S_k}\mathrm{Wg}(d,\pi^{-1}\tau)\delta_\pi(\boldsymbol{i},\boldsymbol{i}')\delta_\tau(\boldsymbol{j},\boldsymbol{j}'), \tag{A.10}$$

where $\delta_\pi(\boldsymbol{i},\boldsymbol{i}'):=\prod_{m=1}^k\delta_{i_mi'_{\pi(m)}}$, and $\mathrm{Wg}(d,\sigma)$ is a function on the symmetric group S_k called the (unitary) Weingarten function [240–242]. We note that Eq. (A.10) is equivalent to Eq. (A.1), and the Weingarten matrix $\mathrm{Wg}_{\pi,\tau}(d)$ is written as

$$\mathrm{Wg}_{\pi,\tau}(d)=\mathrm{Wg}(d,\pi\tau). \tag{A.11}$$

Thus, we analyze the properties of the Weingarten function $\mathrm{Wg}(d,\sigma)$ instead of the Weingarten matrix $\mathrm{Wg}_{\pi,\tau}(d)$.

By using the tool of representation theory of the symmetric group S_k [243], we show a more explicit representation of $\mathrm{Wg}(d,\sigma)$. The conjugacy class of S_k is determined by the cycle types of permutations. The cycle type of $\sigma\in S_k$ is a list of the lengths of the disjoint cycles appeared in the cycle decomposition of σ, and denoted as $(l_1,l_2,\ldots,l_c)$ with $l_1\geq\cdots\geq l_c\geq 1$, where $c=c(\sigma)$ is the number of the cycles, and $l_m=l_m(\sigma)$ is the length of the mth cycle. We say that $\lambda=(\lambda_1,\ldots,\lambda_r)\in\mathbb{Z}^r$ is a partition of k and write $\lambda\vdash k$ if $\lambda_1\geq\cdots\geq\lambda_r\geq 1$ and $\sum_{i=1}^r\lambda_i=k$ hold. The cycle type of a permutation is also a partition of integer k. Because the number of the irreducible representations of a finite group equals the number of its conjugacy class, the irreducible representation of S_k can be labeled by a partition of integer k. Then, the Weingarten function $\mathrm{Wg}(d,\sigma)$ is represented as

$$\mathrm{Wg}(d,\sigma)=\frac{1}{k!}\sum_{\lambda\vdash k}\frac{\chi^\lambda(I)\chi^\lambda(\sigma)}{C_\lambda(d)}, \tag{A.12}$$

where $C_\lambda(d):=\prod_{i=1}^{r(\lambda)}\prod_{j=1}^{\lambda_i}(d+j-i)$, $\chi^\lambda(\sigma)$ is the character corresponding to an irreducible representation of S_k labeled by λ, and the summation runs over all partitions of k [241, 242]. Moreover, the Weingarten function $\mathrm{Wg}(d,\sigma)$ depends only on the cycle type of σ because a character takes a constant value on each conjugacy class. There is a combinatorial method to calculate the characters of S_k [280]. Thus, we can numerically calculate the Weingarten function $\mathrm{Wg}(d,\sigma)$ [281, 282].

We give the values of the Weingarten function for $k=1,2,3$:

- $k=1$

$$\mathrm{Wg}(d,(1))=\frac{1}{d}. \tag{A.13}$$

- $k = 2$

$$\mathrm{Wg}(d, (1,1)) = \frac{1}{d^2-1}, \quad \mathrm{Wg}(d, (2)) = -\frac{1}{d(d^2-1)}. \tag{A.14}$$

- $k = 3$

$$\begin{aligned} \mathrm{Wg}(d, (1,1,1)) &= \frac{d^2-2}{d(d^2-1)(d^2-4)}, \quad \mathrm{Wg}(d, (2,1)) = -\frac{1}{(d^2-1)(d^2-4)} \\ \mathrm{Wg}(d, (3)) &= \frac{2}{d(d^2-1)(d^2-4)}. \end{aligned} \tag{A.15}$$

A.2.2 Asymptotic behavior of the Weingarten function

Finally, we investigate the asymptotic behavior of the Weingarten function in large d. We introduce the Möbius function on S_k by

$$\mathrm{Moeb}(\sigma) := \prod_{m=1}^{c(\sigma)} (-1)^{l_m(\sigma)} \mathrm{Cat}_{l_m(\sigma)}, \tag{A.16}$$

where $(l_1, l_2, \ldots, l_c)$ is the cycle type of σ, and Cat_n is the nth Catalan number, defined by $\mathrm{Cat}_n := 2n!/(n!(n+1)!)$. Then, the Weingarten function has the following asymptotic form [241, 242]:

$$\mathrm{Wg}(d, \sigma) = \mathrm{Moeb}(\sigma) d^{-2k+c(\sigma)} + \mathcal{O}(d^{-2k-2+c(\sigma)}). \tag{A.17}$$

As a corollary, we have the asymptotic form of the Weingarten matrix:

$$\mathrm{Wg}_{\pi,\tau}(d) = \mathrm{Moeb}(\pi\tau) d^{-2k+c(\pi\tau)} + \mathcal{O}(d^{-2k-2+c(\pi\tau)}), \tag{A.18}$$

which leads to Eq. (6.30).

Acknowledgements

I am very grateful to my supervisor, Prof. Takahiro Sagawa for fruitful discussion, valuable advice, and kind support during the five years of my graduate course. He suggested the main topic in this thesis as the research in my Ph.D. course: the foundation of statistical mechanics in isolated quantum systems. He also spent a lot of time for improving my papers as well as this thesis. I sincerely thank my collaborator, Dr. Eiki Iyoda for valuable advice on numerical calculations and discussion on many topics related to my study. In particular, I acknowledge his numerical verification of the k-ETH presented in Chapter 6 and comments on this thesis. I would like to thank other collaborators, Mr. Shotaro Baba and Mr. Yosuke Mitsuhashi for valuable discussion on thermalization and the second law. Moreover, I am deeply grateful to Mr. Kazuki Yamaga for explaining his outstanding work and discussion on the second law. I am very much grateful to my thesis committee: Naoto Nagaosa, Yasunobu Nakamura, Masato Koashi, and Keisuke Fujii for helpful feedback on this thesis. I would like to thank Prof. Jae Dong Noh, Prof. Shinichi Sasa, Prof. Naomichi Hatano, Prof. Keiji Saito, Dr. Masaki Tezuka, Dr. Takashi Mori, Dr. Naoto Shiraishi, Dr. Aki Kutvonen, Dr. Yuto Ashida, and Mr. Shunsuke Nakamura for helpful comments. I also thank Mrs. Sachiko Seto for supporting me with paperwork. Finally, I greatly acknowledge the finial support by Research Fellowships of Japan Society for the Promotion of Science (JSPS) for Young Scientists and JSPS KAKENHI Grant No. JP17J06875.

Bibliography

[1] H. Tasaki, *Statistical Mechanics I (in Japanese)* (Baifukan, Tokyo, 2008).

[2] J. von. Neumann, Z. Phys. **57**, 30 (1929).

[3] J. von. Neumann and R. Tumulka, Eur. Phys. J. H **35**, 201 (2010).

[4] C. C. Moore, Proc. Natl. Acad. Sci. USA **112**, 7 (2015).

[5] Y. G. Sinai, Russ. Math. Surv. **25**, 137 (1970).

[6] L. Markus and K. R. Meyer, Mem. Am. Math. Soc. 144 (1974).

[7] E. Fermi, P. Pasta, and S. Ulam, *Studies of nonlinear problems*, Tech. Rep., (1955).

[8] J. L. Lebowitz, Physica A **194**, 1 (1993).

[9] H. Tasaki, J. Stat. Phys. **163**, 937 (2016).

[10] D. Lazarovici and P. Reichert, Erkenntnis **80**, 689 (2015).

[11] S. Goldstein, D. A. Huse, J. L. Lebowitz, and R. Tumulka, Annalen der Physik **529**, 7 (2017).

[12] I. Bloch, J. Dalibard, and W. Zwerger, Rev. Mod. Phys. **80**, 885 (2008).

[13] C. Gross and I. Bloch, Science **357**, 995 (2017).

[14] D. Leibfried, R. Blatt, C. Monroe, and D. Wineland, Rev. Mod. Phys. **75**, 281 (2003).

[15] R. Blatt and C. F. Roos, Nat. Phys. **8**, 277 (2012).

[16] J. Clarke and F. K. Wilhelm, Nature **453**, 1031 (2008).

[17] G. Wendin, Rep. Prog. Phys. **80**, 106001 (2017).

[18] S. Trotzky, Y.-A. Chen, A. Flesch, I. P. McCulloch, U. Schollwöck, J. Eisert, and I. Bloch, Nat. Phys. **8**, 325 (2012).

[19] J. P. Ronzheimer, M. Schreiber, S. Braun, S. S. Hodgman, S. Langer, I. P. McCulloch, F. Heidrich-Meisner, I. Bloch, and U. Schneider, Phys. Rev. Lett. **110**, 205301 (2013).

[20] G. Clos, D. Porras, U. Warring, and T. Schaetz, Phys. Rev. Lett. **117**, 170401 (2016).

[21] C. Neill, P. Roushan, M. Fang, Y. Chen, M. Kolodrubetz, Z. Chen, A. Megrant, R. Barends, B. Campbell, B. Chiaro, A. Dunsworth, E. Jeffrey, J. Kelly, J. Mutus, P. J. J. O'Malley, C. Quintana, D. Sank, A. Vainsencher, J. Wenner, T. C. White, A. Polkovnikov, and J. M. Martinis, Nat. Phys. **12**, 1037 (2016).

[22] G. Kucsko, S. Choi, J. Choi, P. C. Maurer, H. Sumiya, S. Onoda, J. Isoya, F. Jelezko,

E. Demler, N. Y. Yao, and M. D. Lukin, Phys. Rev. Lett. **121**, 023601 (2018).
[23] C. Kollath, A. M. Läuchli, and E. Altman, Phys. Rev. Lett. **98**, 180601 (2007).
[24] M. Cramer, A. Flesch, I. P. McCulloch, U. Schollwöck, and J. Eisert, Phys. Rev. Lett. **101**, 063001 (2008).
[25] A. Flesch, M. Cramer, I. P. McCulloch, U. Schollwöck, and J. Eisert, Phys. Rev. A **78**, 033608 (2008).
[26] G. Roux, Phys. Rev. A **79**, 021608 (2009).
[27] S. Sorg, L. Vidmar, L. Pollet, and F. Heidrich-Meisner, Phys. Rev. A **90**, 033606 (2014).
[28] M. Rigol, V. Dunjko, and M. Olshanii, Nature **452**, 854 (2008).
[29] M. Rigol, Phys. Rev. Lett. **103**, 100403 (2009).
[30] M. Rigol and L. F. Santos, Phys. Rev. A **82**, 011604 (2010).
[31] M. Rigol, Phys. Rev. Lett. **112**, 170601 (2014).
[32] M. Srednicki, Phys. Rev. E **50**, 888 (1994).
[33] M. Srednicki, J. Phys. A: Math. Gen. **29** L75 (1996).
[34] M. Srednicki, J. Phys. A: Math. Gen. **32**, 1163 (1999).
[35] L. D'Alessio, Y. Kafri, A. Polkovnikov, and M. Rigol, Adv. Phys. **65**, 239 (2016).
[36] M. V. Berry, J. Phys. A: Math. Gen. **10**, 2083 (1977).
[37] A. Peres, Phys. Rev. A **30**, 504 (1984).
[38] R. V. Jensen and R. Shankar, Phys. Rev. Lett. **54**, 1879 (1985).
[39] M. Feingold and A. Peres, Phys. Rev. A **34**, 591 (1986).
[40] J. M. Deutsch, Phys. Rev. A **43**, 2046 (1991).
[41] H. Tasaki, Phys. Rev. Lett. **80**, 1373 (1998).
[42] S. H. Strogatz, *Nonlinear Dynamics and Chaos: With Applications to Physics, Biology, Chemistry, and Engineering* (Westview Press, Cambridge, 2000).
[43] T.-Y. Li and J. A. Yorke, Am. Math. Monthly **82**, 985 (1975).
[44] Y. Oono, *The Nonlinear World: Conceptual Analysis and Phenomenology* (Springer 2012).
[45] M. Berry, Physica Scripta **40**, 335 (1989).
[46] I. S. Gomez, M. Losada, and O. Lombardi, Entropy **19** (2017).
[47] O. Bohigas, M. J. Giannoni, and C. Schmit, Phys. Rev. Lett. **52**, 1 (1984).
[48] T. A. Brody, J. Flores, J. B. French, P. A. Mello, A. Pandey, and S. S. M. Wong, Rev. Mod. Phys. **53**, 385 (1981).
[49] M. V. Berry and M. Tabor, Proc. R. Soc. London **356**, 375 (1977).
[50] B. Swingle, Nat Phys. **14**, 988 (2018).
[51] V. Jahnke, Adv. High Energy Phys. **2019** (2019).
[52] D. N. Page, Phys. Rev. Lett. **71**, 3743 (1993).
[53] P. Hayden and J. Preskill, J. High Energy Phys. 09 (2007) 120.

[54] Y. Sekino and L. Susskind, J. High Energy Phys. 10 (2008) 065.
[55] N. Lashkari, D. Stanford, M. Hastings, T. Osborne, and P. Hayden, J. High Energy Phys. 04 (2013) 022.
[56] E. Iyoda and T. Sagawa, Phys. Rev. A **97**, 042330 (2018).
[57] O. Schnaack, S. Paeckel, S. R. Manmana, S. Kehrein, and M. Schmitt, arXiv:1808.05646.
[58] P. Bordia, F. Alet, and P. Hosur, Phys. Rev. A **97**, 030103 (2018).
[59] V. Alba and P. Calabrese, Phys. Rev. B **100**, 115150 (2019).
[60] A. Larkin and Y. Ovchinnikov, Sov. Phys. JETP **28**, 1200 (1969).
[61] J. Maldacena, S. H. Shenker, and D. Stanford, J. High Energy Phys. 08 (2016) 106.
[62] A. Kitaev, *Hidden correlations in the Hawking radiation and thermal noise Presentation at KITP*, (2015).
[63] Y. Masuyama, K. Funo, Y. Murashita, A. Noguchi, S. Kono, Y. Tabuchi, R. Yamazaki, M. Ueda and Y. Nakamura, Nat. Commun. **9**, 1291 (2018).
[64] U. Schollwöck, Rev. Mod. Phys. **77**, 259 (2005).
[65] T. Kinoshita, T. Wenger, and D. S. Weiss, Nature **440**, 900 (2006).
[66] E. H. Lieb and W. Liniger, Phys. Rev. **130**, 1605 (1963).
[67] M. Rigol, A. Muramatsu, and M. Olshanii, Phys. Rev. A **74**, 053616 (2006).
[68] M. Rigol, V. Dunjko, V. Yurovsky, and M. Olshanii, Phys. Rev. Lett. **98**, 050405 (2007).
[69] P. Bocchieri and A. Loinger, Phys. Rev. **107**, 337 (1957).
[70] L. S. Schulman, Phys. Rev. A **18**, 2379 (1978).
[71] C. Gogolin and J. Eisert, Rep. Prog. Phys.**79**, 056001 (2016).
[72] T. Mori, T. N. Ikeda, E. Kaminishi, and M. Ueda, J. Phys. B **51** 112001 (2018).
[73] P. Reimann, Phys. Rev. Lett. **101**, 190403 (2008).
[74] N. Linden, S. Popescu, A. J. Short, and A. Winter, Phys. Rev. E **79**, 061103 (2009).
[75] P. Reimann, New J. Phys. **12**, 055027 (2010).
[76] A. J. Short, New J. Phys. **13**, 053009 (2011).
[77] A. J. Short and T. C. Farrelly, New J. Phys. **14**, 013063 (2012).
[78] P. Reimann and M. Kastner, New J. Phys. **14**, 043020 (2012).
[79] T. Morimae, Phys. Rev. A **81**, 022304 (2010).
[80] I. Arad, T. Kuwahara, and Z. Landau, J. Stat. Mech. (2016) 33301.
[81] T. Kuwahara, J. Stat. Mech. 053103 (2016).
[82] A. Anshu, New J. Phys. **18**, 083011 (2016).
[83] B. Dakić and M. Radonjić, Phys. Rev. Lett. **119**, 090401 (2017).
[84] T. N. Ikeda and M. Ueda, Phys. Rev. E **92**, 020102 (2015).
[85] G. Biroli, C. Kollath, and A. M. Läuchli, Phys. Rev. Lett. **105**, 250401 (2010).
[86] H. Tasaki, J. Stat. Phys. **172**, 905 (2018).
[87] T. Kuwahara and K. Saito, arXiv:1906.10872.

[88] V. Alba, Phys. Rev. B **91**, 155123 (2015).
[89] E. Iyoda, K. Kaneko, and T. Sagawa, Phys. Rev. Lett. **119**, 100601 (2017).
[90] T. Mori, arXiv:1609.09776.
[91] Y. Ogata, Commun. Math. Phys. **296**, 35 (2010).
[92] H. Kim, T. N. Ikeda, and D. A. Huse, Phys. Rev. E **90**, 052105 (2014).
[93] J. R. Garrison and T. Grover, Phys. Rev. X **8**, 021026 (2018).
[94] A. Dymarsky, N. Lashkari, and H. Liu, Phys. Rev. E **97**, 012140 (2018).
[95] K. R. Fratus and M. Srednicki, Phys. Rev. E **92**, 040103 (2016).
[96] R. Mondaini, K. R. Fratus, M. Srednicki, and M. Rigol, Phys. Rev. E **93**, 032104 (2016).
[97] R. Mondaini and M. Rigol, Phys. Rev. E **96**, 012157 (2017).
[98] R. Steinigeweg, J. Herbrych, and P. Prelovšek, Phys. Rev. E **87**, 012118 (2013).
[99] T. Yoshizawa, E. Iyoda, and T. Sagawa, Phys. Rev. Lett. **120**, 200604 (2018).
[100] J. Richter, J. Gemmer, and R. Steinigeweg, Phys. Rev. B **99**, 155130 (2019).
[101] T. LeBlond, K. Mallayya, L. Vidmar, and M. Rigol, arXiv:1909.09654.
[102] A. Pal and D. A. Huse, Phys. Rev. B **82**, 174411 (2010).
[103] D. J. Luitz, Phys. Rev. B **93**, 134201 (2016).
[104] W. Beugeling, R. Moessner, and M. Haque, Phys. Rev. E **89**, 042112 (2014).
[105] W. Beugeling, R. Moessner, and M. Haque, Phys. Rev. E **91**, 012144 (2015).
[106] R. Steinigeweg, A. Khodja, H. Niemeyer, C. Gogolin, and J. Gemmer, Phys. Rev. Lett. **112**, 012120 (2014).
[107] Z. Lan and S. Powell, Phys. Rev. B **96**, 115140 (2017).
[108] S. Genway,A. F. Ho, and D. K. K. Lee, Phys. Rev. A **86**, 023609 (2012).
[109] R. Mondaini and M. Rigol, Phys. Rev. A **92**, 041601 (2015).
[110] M. Rigol, Phys. Rev. A **80**, 053607 (2009).
[111] M. Rigol and M. Srednicki, Phys. Rev. Lett. **108**, 110601 (2012).
[112] C. Neuenhahn and F. Marquardt, Phys. Rev. E, **85**, 060101 (2012).
[113] D. Jansen, J. Stolpp, L. Vidmar, and F. Heidrich-Meisner, Phys. Rev. B **99**, 155130 (2019).
[114] J. Sonner and M. Vielma, J. High Energy Phys. 11 (2017) 149.
[115] M. Haque and P. A. McClarty, Phys. Rev. B **100**, 115122 (2019).
[116] N. Hunter-Jones, J. Liu, and Y. Zhou, J. High Energy Phys. 02 (2018) 142.
[117] G. Roux, Phys. Rev. A **81**, 053604 (2010).
[118] L. F. Santos and M. Rigol, Phys. Rev. E **82**, 031130 (2010).
[119] E. Khatami, G. Pupillo, M. Srednicki, and M. Rigol, Phys. Rev. Lett. **111**, 050403 (2013).
[120] R. Horodecki, P. Horodecki, M. Horodecki, and K. Horodecki, Rev. Mod. Phys. **81**, 865 (2009).

[121] N. Laflorencie, Physics Reports **646**, 1 (2016).
[122] T. Nishioka, S. Ryu, and T. Takayanagi, J. Phys.: Math. Theo. **42**, 504008 (2009).
[123] J. Eisert, M. Cramer, and M. B. Plenio, Rev. Mod. Phys. **82**, 277 (2010).
[124] M. B. Hastings, J. Stat. Mech. P08024 (2007).
[125] I. Arad, Z. Landau, U. Vazirani, and T. Vidick, Commun. Math. Phys. **356**, 65 (2017).
[126] R. Movassagh and P. W. Shor, Proc. Natl. Acad. Sci. USA **113**, 13278 (2016).
[127] P. Calabrese and J. Cardy, J. Stat. Mech. P04010 (2004).
[128] P. Calabrese and J. Cardy, J. Phys.: Math. Theo. **42**, 504005 (2009).
[129] D. N. Page, Phys. Rev. Lett. **71**, 1291 (1993).
[130] S. K. Foong and S. Kanno, Phys. Rev. Lett. **72**, 1148 (1994).
[131] J. Sánchez-Ruiz, Phys. Rev. E **52**, 5653 (1995).
[132] S. Popescu, A. J. Short, and A. Winter, Nat Phys. **2**, 754 (2006).
[133] A. Sugita, Nonlinear Phenomena in Complex Systems **10**, 192 (2006).
[134] Y. O. Nakagawa, M. Watanabe, H. Fujita, and S. Sugiura, Nat. Commun. **9**, 1635 (2018).
[135] H. Fujita, Y. O. Nakagawa, S. Sugiura, and M. Watanabe, J. High Energy Phys. (2018) 112.
[136] T. C. Lu and T. Grover, Phys. Rev. E **99**, 032111 (2019).
[137] S. Sugiura and A. Shimizu, Phys. Rev. Lett. **111**, 010401 (2013).
[138] J. M. Deutsch, New J. Phys. **12**, 075021 (2010).
[139] V. Čápek and D. P. Sheehan, *Challenges to the Second Law of Thermodynamics* (Springer, 2005).
[140] A. E. Allahverdyan and T. M. Nieuwenhuizen, Physica A **305**, 542 (2002).
[141] T. Sagawa, *Second Law-like Inequalitites with Quantum Relative Entropy: An Introduction,in Lectures on Quantum Computing, Thermodynamics and Statistical Physics*, Kinki University Series on Quantum Computing, Vol. 8, edited by M. Nakahara (World Scientific, New Jersey, 2013).
[142] C. Jarzynski, Phys. Rev. Lett. **78**, 2690 (1997).
[143] J. Kurchan, arXiv:0007360.
[144] H. Tasaki, arXiv:0009244.
[145] M. Hayashi and H. Tajima, Phys. Rev. A **95**, 032132 (2017).
[146] H. Tasaki, Phys. Rev. Lett. **116**, 170402 (2016).
[147] W. Pusz and S. L. Woronowicz, Commun. Math. Phys. **58**, 273 (1978).
[148] A. Lenard, J. Stat. Phys. **19**, 575 (1978).
[149] A. E. Allahverdyan, R. Balian, and T. M. Nieuwenhuizen, Euro. Lett. **67**, 565 (2004).
[150] R. Alicki and M. Fannes, Phys. Rev. E **87**, 042123 (2013).
[151] R. Alicki and R. Kosloff, arXiv:1801.08314.

[152] G. De Palma, A. Mari, S. Lloyd, and V. Giovannetti, Phys. Rev. A **93**, 062328 (2016).
[153] M. Perarnau-Llobet, K. V. Hovhannisyan, M. Huber, P. Skrzypczyk, J. Tura, and A. Acín Phys. Rev. E **92**, 042147 (2015).
[154] R. Bhatia, *Matrix Analysis* (Springer, New York, 1997).
[155] G. H. Hardy, J. E. Littlewood, G. Pólya, *Inequalities* (Cambridge university press, 1952).
[156] S. H. Shenker and D. Stanford, J. High Energy Phys. 03 (2014) 067.
[157] S. H. Shenker and D. Stanford, J. High Energy Phys. 12 (2014) 046.
[158] S. H. Shenker and D. Stanford, J. High Energy Phys. 05 (2015) 132.
[159] D. A. Roberts, D. Stanford, and L. Susskind, J. High Energy Phys. 03 (2015) 051.
[160] D. A. Roberts and D. Stanford, Phys. Rev. Lett. **115**, 131603 (2015).
[161] A. L. Fitzpatrick and J. Kaplan, J. High Energy Phys. 05 (2016) 070.
[162] J. De Boer, E. Llabrés, J. F. Pedraza, and D. Vegh, Phys. Rev. Lett. **120**, 1 (2018).
[163] M. Heyl, F. Pollmann, and B. Dóra, Phys. Rev. Lett. **121**, 16801 (2018).
[164] Q. Wang and F. Pérez-Bernal, arXiv:1812.01920.
[165] C. B. Dağ, K. Sun, and L. M. Duan, Phys. Rev. Lett. **123**, 140602 (2019).
[166] C. B. Dağ, L. M. Duan, and K. Sun, arXiv:1906.05241.
[167] A. Bohrdt, C. B. Mendl, M. Endres, and M. Knap, New J. Phys. **19**, 063001 (2017).
[168] P. Hosur, X. L. Qi, D. A. Roberts, and B. Yoshida, J. High Energy Phys. 02 (2016) 004.
[169] B. Swingle and D. Chowdhury, Phys. Rev. B **95**, 060201 (2017).
[170] X. Chen and T. Zhou, arXiv:1804.08655.
[171] A. Nahum, S. Vijay, and J. Haah, Phys. Rev. X **8**, 21014 (2018).
[172] D. E. Parker, X. Cao, A. Avdoshkin, T. Scaffidi, and E. Altman, Phys. Rev. X **9**, 41017 (2019).
[173] G. M. Zaslavsky, Physics Reports **80**, 157 (1981).
[174] D. P. DiVincenzo, D. W. Leung, and B. M. Terhal, IEEE Trans. Inf. Theory **48**, 580 (2002).
[175] J. Emerson, Y. S. Weinstein, M. Saraceno, S. Lloyd, and D. G. Cory, Science **302**, 2098 (2003).
[176] P. Hayden, D. Leung, P. W. Shor, and A. Winter, Commun. Math. Phys. **250**, 371 (2004).
[177] C. H. Bennett, P. Hayden, D. W. Leung, P. W. Shor, and A. Winter, IEEE Trans. Inf. Theory **51**, 56 (2005).
[178] F.G.S.L. Brandão, P. Ćwikliński, M. Horodecki, P. Horodecki, J. K. Korbicz, and M.Mozrzymas, Phys. Rev. E **86**, 031101 (2012).
[179] L. Masanes, A. J. Roncaglia, and A. Acín, Phys. Rev. E **87**, 032137 (2013).
[180] S. Goldstein, T. Hara, and H. Tasaki, New J. Phys. **17**, 045002 (2015).
[181] P. Reimann, Nat. Commun.**7**, 10821 (2016).

[182] L. del Rio, A. Hutter, R. Renner, and S. Wehner, Phys. Rev. E **94**, 022104 (2016).
[183] E. Knill, arXiv:9508006.
[184] C. Dankert, R. Cleve, J. Emerson, and E. Livine, Phys. Rev. A**80**, 012304 (2009).
[185] J. Naor and M. Naor, SIAM J. Comp. **22**, 838 (1993).
[186] Z. Ji, Y. K. Liu, and F. Song, *Pseudorandom quantum states*, in Advances in Cryptology CRYPTO 2018, p. 126. (Springer, 2018).
[187] A. Bouland, B. Fefferman, and U. Vazirani, arXiv:1910.14646.
[188] F. G. S. L. Brandão, W. Chemissany, N. Hunter-Jones, R. Kueng, and J. Preskill, arXiv:1912.04297.
[189] D. Gross, K. Audenaert, and J. Eisert, J. Math. Phys. **48** (2007).
[190] R. A. Low, arXiv:1006.5227.
[191] Z. Webb, arXiv:1510.02769.
[192] H. Zhu, Phys. Rev. A **96**, 062336 (2017).
[193] R. M. Guralnick and P. H. Tiep, Representation Theory **9**, 138 (2005).
[194] E. Bannai, G. Navarro, N. Rizo, and P. H. Tiep, arXiv:1810.02507.
[195] M. B. Hastings and A. W. Harrow, Quantum Inf. Comput. **9**, 336 (2009).
[196] F. G. Brandão, A. W. Harrow, and M. Horodecki, Phys. Rev. Lett. **116**, 170502 (2016).
[197] F. G. Brandão, A. W. Harrow, and M. Horodecki, Commun. Math. Phys. **346**, 397 (2016).
[198] Y. Nakata, C. Hirche, M. Koashi, and A. Winter, Phys. Rev. X **7**, 021006 (2017).
[199] D. A. Roberts and B. Yoshida, J. High Energy Phys. 04 (2017) 121.
[200] A. J. Scott, J. Phys.: Math. Theo. **41**, 055308 (2008).
[201] K. Kaneko, E. Iyoda, and T. Sagawa, Phys. Rev. E **99**, 032128 (2019).
[202] T. N. Ikeda, N. Sakumichi, A. Polkovnikov, and M. Ueda, Ann. Phys. **354**, 338 (2015).
[203] S. Goldstein, T. Hara, and H. Tasaki, arXiv:1303.6393.
[204] M. Perarnau-Llobet, K. V. Hovhannisyan, M. Huber, P. Skrzypczyk, N. Brunner, and A. Acín, Phys. Rev. X **5**, 041011 (2015).
[205] M. Frey, K. Funo, and M. Hotta, Phys. Rev. E **90**, 012127 (2014).
[206] T. Mori, J. Phys.: Math. Theo. **49**, 444003 (2016).
[207] F. Jin, R. Steinigeweg, H. De Raedt, K. Michielsen, M. Campisi, and J. Gemmer Phys. Rev. E **94**, 012125 (2016).
[208] D. Schmidtke, L. Knipschild, M. Campisi, R. Steinigeweg, and J. Gemmer, Phys. Rev. E **98**, 012123 (2018).
[209] K. Kaneko, E. Iyoda, and T. Sagawa, Phys. Rev. E **96**, 062148 (2017) (2017).
[210] M. Esposito, U. Harbola, and S. Mukamel, Rev. Mod. Phys. **81**, 1665 (2009).
[211] M. Campisi, P. Hänggi, and P. Talkner, Rev. Mod. Phys. **83**, 771 (2011).
[212] M. B. Hastings, arXiv:1008.5137.

[213] H. Tajima, N. Shiraishi, and K. Saito, arXiv:1906.04076.

[214] R. Takagi and H. Tajima, arXiv:1909.01336.

[215] P. Medley, D. M. Weld, H. Miyake, D. E. Pritchard, and W. Ketterle, Phys. Rev. Lett. **106**, 195301 (2011).

[216] S. Braun J. P. Ronzheimer, M. Schreiber, S. S. Hodgman, T. Rom, I. Bloch, and U. Schneider, Science **339**, 52 (2013).

[217] J. Simon, W. S. Bakr, R. Ma, M. E. Tai, P. M. Preiss, and M. Greiner, Nature **472**, 307 (2011).

[218] P. Schauss, Quantum Science and Technology **3**, 023001 (2018).

[219] P. R. Zangara, A. D. Dente, E. J. Torres-Herrera, H. M. Pastawski, A. Iucci, and L. F. Santos, Phys. Rev. E **88**, 032913 (2013).

[220] D. W. Wood and D. Ruelle, *Statistical Mechanics: Rigorous Results* (World Scientific, 1990).

[221] H. Touchette, Physics Reports **478**, 1 (2009).

[222] R. Nandkishore and D. A. Huse, Ann. Rev. Cond. Matt. Phys. **6**, 15 (2015).

[223] D. A. Abanin, E. Altman, I. Bloch, and M. Serbyn, Rev. Mod. Phys. **91**, 21001 (2019).

[224] F. C. Binder, S. Vinjanampathy, K. Modi, and J. Goold, New J. Phys. **17**, 075015 (2015).

[225] F. Campaioli, F. A. Pollock, F. C. Binder, L. Céleri, J. Goold, S. Vinjanampathy, and K. Modi, Phys. Rev. Lett. **118**, 150601 (2017).

[226] K. Kaneko, E. Iyoda, and T. Sagawa, arXiv:1911.10755.

[227] M. A. Nielsen and I. Chuang, *Quantum Computation and Quantum Information* (Cambridge University Press, 2002).

[228] S. Aaronson, arXiv:1607.05256.

[229] L. Susskind, Fortsch. Phys. **64**, 49 (2016).

[230] A. R. Brown, L. Susskind, and Y. Zhao, Phys. Rev. D **95**, 045010 (2017).

[231] A. R. Brown and L. Susskind, Phys. Rev. D **97**, 86015 (2018).

[232] A. Nahum, J. Ruhman, S. Vijay, and J. Haah, Phys. Rev. X **7**, 031016 (2017).

[233] Y. Huang, F. G. Brandão, and Y. L. Zhang, Phys. Rev. Lett. **123**, 10601 (2019).

[234] S. Zelditch, arXiv:0503026.

[235] L. C. Venuti and L. Liu, arXiv:1904.02336.

[236] S. Goldstein, J. L. Lebowitz, R. Tumulka, and N. Zanghì, J. Stat. Phys. **125**, 1193 (2006).

[237] Y. Nakata, P. S. Turner, and M. Murao, Phys. Rev. A **86**, 012301 (2012).

[238] Y. Nakata, M. Koashi, and M. Murao, New J. Phys. **16**, 053043 (2014).

[239] Y. Nakata, C. Hirche, C. Morgan, and A. Winter, J. Math. Phys. **58**, 052203 (2017).

[240] D. Weingarten, J. Math. Phys.**19**, 999 (1978).

[241] B. Collins, Int. Math. Res. Not. **17**, 953 (2003).
[242] B. Collins and P. Śniady, Commun. Math. Phys. **264**, 773 (2006).
[243] R. Goodman and N. R. Wallach, *Representations and Invariants of the Classical Groups* (Cambridge University Press, 2000).
[244] Y. Gu, *Moments of random matrices and weingarten functions*, M.Sc. thesis, Queen's University, Ontario, Canada (2013).
[245] L. Foini and J. Kurchan, Phys. Rev. E **99**, 42139 (2019).
[246] R. Hamazaki and M. Ueda, Phys. Rev. E **99**, 42116 (2019).
[247] S. Goldstein, T. Hara, and H. Tasaki, arXiv:1402.3380.
[248] N. Tsuji, T. Shitara, and M. Ueda, Phys. Rev. E **98**, 012216 (2018).
[249] A. Romero-Bermúdez, K. Schalm, and V. Scopelliti, J. High Energy Phys. 07 (2019) 107.
[250] F. Verstraete and J. I. Cirac, Phys. Rev. B **73**, 094423 (2006).
[251] N. Schuch, M. M. Wolf, F. Verstraete, and J. I. Cirac, Phys. Rev. Lett. **100**, 030504 (2008).
[252] Y. Z. You and Y. Gu, Phys. Rev. B **98**, 014309 (2018).
[253] M. D. Choi, Linear Algebra and Its Applications **10**, 285 (1975).
[254] A. Jamiołkowski, Reports on Mathematical Physics **3**, 275 (1972).
[255] P. Zanardi, Phys. Rev. A **63**, 040304 (2001).
[256] T. Prosen and I. Pižorn, Phys. Rev. A **76**, 032316 (2007).
[257] Z. W. Liu, S. Lloyd, E. Y. Zhu, and H. Zhu, Phys. Rev. Lett. **120**, 130502 (2018).
[258] Z. W. Liu, S. Lloyd, E. Zhu, and H. Zhu, J. High Energy Phys. 07 (2018) 041
[259] J. Dubail, J. Phys.: Math. Theo. **50**, 234001 (2017).
[260] S. Nakamura, E. Iyoda, T. Deguchi, and T. Sagawa, Phys. Rev. B **99**, 224305 (2019).
[261] T. Zhou and D. J. Luitz, Phys. Rev. B **95**, 094206 (2017).
[262] A. Chan, A. De Luca, and J. T. Chalker, Phys. Rev. Lett. **122**, 220601 (2019).
[263] C. Murthy and M. Srednicki, Phys. REv. Lett. **122**, 230606 (2019).
[264] H. Bernien, S. Schwartz, A. Keesling, H. Levine, A. Omran, H. Pichler, S. Choi, A. S. Zibrov, M. Endres, M. Greiner, V. Vuletic, and M. D. Lukin, Nature **551**, 579 (2017).
[265] C. J. Turner, A. A. Michailidis, D. A. Abanin, M. Serbyn, and Z. Papić, Nat Phys. **14**, 745 (2018).
[266] C. J. Turner, A. A. Michailidis, D. A. Abanin, M. Serbyn, and Z. Papić, Phys. Rev. B **94**, 155134 (2018).
[267] C. Nation and D. Porras, New J. Phys. **20**, 103003 (2018).
[268] I. M. Khaymovich, M. Haque, and P. A. McClarty, Phys. Rev. Lett. **122**, 70601 (2019).
[269] R. Hamazaki and M. Ueda, Phys. Rev. Lett. **120**, 80603 (2018).
[270] M. Mierzejewski and L. Vidmar, arXiv:1908.08569.

[271] D. Stanford and L. Susskind, Phys. Rev. D **90**, 126007 (2014).

[272] A. R. Brown, D. A. Roberts, L. Susskind, B. Swingle, and Y. Zhao, Phys. Rev. D **93**, 191301 (2016).

[273] N. Hunter-Jones, arXiv:1905.12053.

[274] R. Islam, R. Ma, P. M. Preiss, M. Eric Tai, A. Lukin, M. Rispoli, and M. Greiner, Nature **528**, 77 (2015).

[275] A. M. Kaufman, M. E. Tai, A. Lukin, M. Rispoli, R. Schittko, P. M. Preiss, and M. Greiner, Science **353**, 794 (2016).

[276] M. Garttner, J. G. Bohnet, A. Safavi-Naini, M. L. Wall, J. J. Bollinger, and A. M. Rey, Nat Phys. **13**, 781 (2017).

[277] J. Li, R. Fan, H. Wang, B. Ye, B. Zeng, H. Zhai, X. Peng, and J. Du, Phys. Rev. X **7**, 031011 (2017).

[278] C. A. Ryan, M. Laforest, and R. Laflamme, New J. Phys. **11** (2009).

[279] J. Li, Z. Luo, T. Xin, H. Wang, D. Kribs, D. Lu, B. Zeng, R. Laflamme, Phys. Rev. Lett. **123**, 30502 (2019).

[280] D. Bernstein, J. Symb. Comp. **37**, 727 (2004).

[281] Z. Puchała and J. A. Miszczak, Bulletin of the Polish Academy of Sciences: Technical Sciences **65**, 21 (2017).

[282] M. Fukuda, R. König, and I. Nechita, J. Phys.: Math. Theo. **52**, 425303 (2019).